

Summer 8-19-2016

Synthesis and Development of Long-Acting Abacavir Prodrug Nanoformulations

Dhirender Singh
University of Nebraska Medical Center

Tell us how you used this information in this [short survey](#).

Follow this and additional works at: <https://digitalcommons.unmc.edu/etd>

 Part of the [Pharmaceutical Preparations Commons](#), and the [Virus Diseases Commons](#)

Recommended Citation

Singh, Dhirender, "Synthesis and Development of Long-Acting Abacavir Prodrug Nanoformulations" (2016). *Theses & Dissertations*. 140.

<https://digitalcommons.unmc.edu/etd/140>

This Dissertation is brought to you for free and open access by the Graduate Studies at DigitalCommons@UNMC. It has been accepted for inclusion in Theses & Dissertations by an authorized administrator of DigitalCommons@UNMC. For more information, please contact digitalcommons@unmc.edu.

**SYNTHESIS AND DEVELOPMENT OF LONG-ACTING
ABACAVIR PRODRUG NANOFORMULATIONS**

by

Dhirender Singh

A DISSERTATION

Presented to the Faculty of the Graduate School in the University of
Nebraska Medical Center in Partial Fulfillment of the Requirements
for the Degree of Doctor of Philosophy

Department of Pharmaceutical Science

Under the Supervision of Dr. Howard E. Gendelman

University of Nebraska Medical Center, Omaha, Nebraska

August 2016

Supervisory Committee:

Howard E. Gendelman, M.D.

Ram Mahato, Ph.D

JoEllyn M. McMillan, Ph.D.

David Oupicky, Ph.D

SYNTHESIS AND DEVELOPMENT OF LONG-ACTING ABACAVIR PRODRUG NANOFORMULATIONS

Dhirender Singh, Ph.D.

University of Nebraska Medical Center, 2016

Supervisor: Howard E Gendelman, M.D.

Over the past decade, work from our laboratory has demonstrated the potential of targeted nanoformulated antiretroviral therapy (nanoART) to produce sustained high plasma and tissue drug concentrations for weeks following a single intramuscular (IM) administration that can suppress ongoing viral replication and mitigate dose associated viral resistance. While progress has occurred towards developing long-acting nanoformulations for protease and nonnucleoside reverse transcriptase (RT) inhibitors, development of nanoformulations of hydrophilic nucleoside RT inhibitor drugs have remained elusive. Abacavir (ABC); a hydrophilic molecule exhibited limited utilities to develop into long-acting nanoformulation platform. Furthermore, inefficient conversion of ABC to its biological active metabolites; carbovir triphosphate jeopardizes its therapeutic index. Thus, improving bioavailability and the therapeutic index of the ABC is urgently needed. To this end, a phosphoramidate prodrug of ABC (PABC), and a myristoylated prdrug of ABC (MABC) was synthesized to improve the therapeutic index of its native hydrophilic counterpart.

The notion of PABC synthesis was to increase intracellular nucleoside 5'-O- triphosphate levels by bypassing rate-limiting monophosphorylation of the parent drug. We reasoned that long-acting PABC nanoformulations could

improve ABC's Pharmacokinetic (PK) and pharmacodynamics (PD). Herein, PABC was successfully synthesized and characterized by ¹H-NMR and FTIR spectroscopy. PABC was incorporated into a PLGA-lipid nanoformulation. *In vitro* and *in vivo* viral efficacy of PABC and PABC encased nanoformulation were evaluated in human monocytes derived macrophages (MDM) and Hu-PBL reconstituted NSG mice respectively. Concomitantly, a platform was constructed to convert the hydrophilic ABC into a hydrophobic derivative through esterification at 5'-OH position of ABC (MABC). MABC was loaded with high concentration into a polymer and decorated with appropriate targeting ligands for improvement in biodistribution, half-life and antiretroviral efficacy. Antiretroviral activity, uptake, retention and cellular trafficking of both the pro-drug and MABC encased in poloxamer nanoformulations were assessed in MDM. Drug PK was evaluated over 14 days for ABC and nanoformulated MABC after intramuscular injection in Balb/c mice.

ACKNOWLEDGEMENT

First and foremost, I would like to express my sincere gratitude to my parents; Lal Singh Chauhan and Bimlesh Devi, my wife Seema Singh, and my daughter Aayushi Singh, for what I am today. Their constant support and encouragement are always an inspiration, and have been reflected in the success of my life. Next, I would like to thank my graduate mentor Dr. Howard E. Gendelman for his constant support and guidance. I am extremely obliged to him for accepting me to be a part of his lab, while I was in deep trouble. His unique personality and flair to the science has influenced my research career to no end. Dr. Gendelman has taught me the true meaning of scientific research, patience, perseverance and how to bloom during hard times. His dedication, thoroughness, and eye for perfection have inspired me immensely and his example will serve for life in whatever I do or pursue.

Next, I would like to express my sincere gratitude to Dr. Benson Edagwa for being there as a pillar of strength and support whenever I needed it most. A lot would have not been possible without his valuable suggestions and inputs throughout the process. He taught me numerous qualities that would be reflected as a good scientist throughout my scientific career, however cannot find any qualifying words to thank him for believing in me during the hard part of process.

I would also like to sincerely thank my committee members Dr. JoEllyn McMillan, Dr. Ram Mahato and Dr. David Oupicky for their valuable inputs, suggestions and guidance during my graduate training here at UNMC. Their feedback helped in shaping this thesis. I specially thank Dr. JoEllyn McMillan for

her continuous support and for fostering my research skills (technical and scientific) and for all her suggestions and guidance during my studies

I also thank Dr. Pavan Puligujja and James Hilaire for their expert advice and lively discussions about my career throughout the course of this project. I am also greatly indebted to Dr. Nagsen Gautam, Diana Palandri and Dr. Yazen Alnouti for the support I needed for bioanalysis.

I would also like to thank Dr. Tatiana Bronich for her guidance as graduate mentor during my temporary stay in her lab. I would like to thank all the college of Pharmacy core facility staff for teaching me the fundamentals of pharmaceutical sciences, and drug delivery. Also, I am thankful to all members in the UNMC animal facility for their extreme cooperation with my research studies. I specially thank the UNMC Graduate studies office and department of pharmacology and college of pharmacy for providing me the financial support for my graduate studies.

I will cherish all the delightful moments that I had with my lab mates over the last five years. I would like to specially thank my friends I would also like to thank Dr. Pavan Pulligujja, James Hilaire, Nathan Smith, Brady Sillman, Bhavesh Kevadiya, Tian Zhou, Zhiyi Lin, Hang Su, Dong Wei, Dr. Andrea Skinner, Mary Banoub, Denise Cobb, Vivek Agrahari, Monalisha Elango, and Ibrahim Ibrahim for all their constant support and encouragement throughout my PhD program. I would like to special thanks to James Hilaire, Brady Sillman and Dr. Pavan Puligujja for help on animal sacrifice, and Diana Palandri for UPLC analysis.

Special Thanks to Dr. Arainga Ramirez for helping me on some of the complex biological analysis.

I would like to thank PEN department secretaries Theresa Grutel, Leticia Tran, Kim Morrison, Robin Taylor, Na Ly for all the administrative help during my studies here at UNMC. I like to specially thank Lana Reichardt from department of Pharmacology and Winter Katina from college of Pharmacy for all administrative support.

Finally, I would like to thank my family and all the members, past and present, of Dr. Gendelman's lab. I appreciate everyone who has constantly supported, encouraged and motivated me during my graduate studies. Thank you.

Dhirender Singh

Department of Pharmaceutical Sciences, and

Department of pharmacology

University of Nebraska Medical Center

August 2016

TABLE OF CONTENTS

CHAPTER 1.OVERVIEW AND STATEMENT OF THE PROBLEMS	1
1.1 THE HUMAN IMMUNODEFICIENCY VIRUS (HIV): STRUCTURE AND LIFE CYCLE	2
1.2 THE HIV PANDEMICS.....	4
1.3 CLINICAL MANIFESTATIONS.....	5
1.4 ANTIRETROVIRAL THERAPY (ART).....	7
1.5 HIV RESERVOIR; A CHALLENGE IN HIV ERADICATION	11
1.5.1. Cellular Reservoir	11
1.5.2 Anatomical Reservoir.....	14
1.6 EFFORTS TOWARDS THE ERADICATION OF HIV-1 RESERVOIRS ..	15
1.6.1 Macrophage-Mediated Drug Delivery: A Promising Approach In Latent Virus Eradication	17
1.6.2 Design Consideration of Cell-Mediated Drug Delivery Construct	18
1.6.2.4 Drug depot at site of interest from the macrophages	22
1.7 DESIGN CONSIDERATION OF NANOMEDICINE FOR EFFICIENT CELL-CARRIERS.....	24
1.7.1 Shape, Size and Surface Charge of Nanocarriers.....	24
1.7.2 Drug Loading and Encapsulation Efficiency	26
1.7.3 Drug Release.....	27

1.8 ANIMAL MODEL OF HIV	28
1.8.1 Human-Peripheral Blood Lymphocytes (Hu-Pbl) Reconstituted Mice..	28
1.9. SIGNIFICANCE OF THE PROJECT	29
1.10 REFERENCES.....	38
CHAPTER 2. HYPOTHESIS AND SPECIFICS AIMS.....	47
2.1. HYPOTHESES.....	48
Specific Aim 1: Synthesis, Characterization and Nanoformulation of Abacavir Prodrugs.....	49
Specific Aim 2: <i>In Vitro</i> Characterization of Nanoformulated Prodrugs in MDM	50
Specific aim 3: PK and PD Characterization of Nanoformulated ABC Prodrugs in Wild Type Mice and in Murine Models of HIV-1.	50
CHAPTER 3. CREATION OF AN ABACAVIR NANOFORMULATED PHOSPHORAMIDATE PRO-DRUG	51
3.1. INTRODUCTION.....	52
3.2. METHODS AND MATERIALS	54
3.2.1. Chemicals.....	54
3.2.2. Synthesis of PABC	55
3.2.3. Human Peripheral Blood Cell Isolation and Culture.....	56
3.2.4. Antiretroviral Activity of PABC	57
3.2.5. Synthesis of Lipid-PLGA hybrid PABC Nanoparticles.....	57
3.2.6. Physicochemical Characterization of PABC Nanoparticles	58

3.2.7. MDM Uptake of PABC Nanoformulations	60
3.2.8. Antiretroviral Activity of Nanoformulated PABC	61
3.2.9. PABC Nanoparticle Subcellular Co-localization.....	61
3.2.10. Pharmacodynamics	62
3.3. RESULTS.....	63
3.3.1. PABC Synthesis and Characterization	63
3.3.2. Antiretroviral Activity of PABC	65
3.3.3. Preparation and Characterization of lipid-PLGA hybrid NPs.....	65
3.3.4. Macrophage Uptake	66
3.3.5. Antiretroviral Activity of PABC Nanoformulations	67
3.3.6. Subcellular NPs Localizations	68
3.3.7. Pharmacodynamics	68
3.4. DISCUSSION.....	70
3.5. CONCLUSIONS.....	74
3.6 SUMMARY.....	75
3.8. REFERENCES.....	88
CHAPTER 4. DEVELOPMENT AND CHARACTERIZATION OF A LONG- ACTING NANOFORMULATED ABACAVIR (ABC) PRODRUG	96
4.1. INTRODUCTION.....	97
4.2. MATERIALS AND METHODS	99
4.2.1. Chemicals.....	99
4.2.2. MABC Synthesis.....	99

4.2.3. Antiretroviral Activity of MABC	100
4.2.4. Nanoformulated MABC (NMABC).....	101
4.2.5. Physicochemical Characterizations of MABC and its Derivatives.....	102
4.2.6. Nanoparticle MDM Uptake and Retention	103
4.2.7. Antiretroviral Activity of MABC Nanoformulations.....	104
4.2.8. MABC Nanoparticle Subcellular Localization.....	105
4.2.9. PK Studies.....	106
4.2.10. Statistical Analyses.....	107
4.3. RESULTS.....	108
4.3.1. MABC Synthesis and Characterization.....	108
4.3.2. Antiretroviral Activity of MABC	109
4.3.3. Preparation and Physicochemical Characterization of the NMABC..	109
4.3.4. Nanoformulated Drug Uptake and Retention.....	110
4.3.5. Antiretroviral Activities of Nanoformulated MABC.....	111
4.3.6. Subcellular Nanoparticle Localizations	112
4.3.7. PK Studies.....	113
4.4. DISCUSSION.....	114
4.5. CONCLUSIONS.....	119
4.6. SUMMARY.....	120
4.6.1. MABC Synthesis.....	120
4.6.2. Synthesis of MABC Encased Nanoformulations.....	120
4.6.3. PK Evaluation of MABC Nanoformulations.....	120

4.7. REFERENCES..... 130

Chapter 5. Challenges and Future direction 138

LIST OF FIGURES

Figure 1.1. Life cycle of HIV Virus.....	33
Figure 1.2. Time course of HIV Disease progression without Therapy	34
Figure 1.3. Development of ART targeting different stage of HIV life cycle	35
Figure1.4. The HIV reservoir in HIV patient receiving cART	36
Figure 1.5. Macrophage uptake and biodistribution among the different organs including the lungs, liver, spleen and kidneys are dictated by size, shape and surface charge of nanoparticles.....	37
Figure 3.1. Synthesis of PABC	77
Figure 3.2. Characterization of PABC.....	78
Figure 3.3. Antiviral activity of ABC and PABC against HIV-1ADA in human monocyte derived macrophages (MDM).....	79
Figure 3.4. Synthesis and characterization of PABC loaded PLGA nanoparticles	80
Figure 3.4. Morphological analysis of drug PLGA nanoparticles.....	81
Figure 3.5. In vitro drug-release profile of PABC from PLGA matrix	82
Figure 3.6. MDM uptake and antiretroviral efficacy of ABC, PABC and L-NPABC	83
Figure 3.7. Subcellular localization of nanoformulated PABC in MDM.	85
Figure 3.8. Antiviral activity of PLGA-P-ABC NPs in hu-PBL-NSG mice.	86

Figure 4.1. Synthesis of MABC.....	121
Figure 4.2. Characterization of MABC	122
Figure 4.3. Antiviral activity of ABC and MABC in HIV-1ADA infected MDM ...	123
Figure 4.4. Morphology and stability of NMABC	124
Figure 4.5. Characterization of nanoformulated MABC using ¹ H-NMR spectroscopy	125
Figure 4.6. MDM uptake and retention of NMABC and FA-NMABC	126
Figure 4.7. Antiretroviral activity of NMABC and FA-NMABC measured in MDM	127
Figure 4.8. Subcellular localization of nanoformulated MABC in MDM.....	128
Figure 4.9. Plasma and tissue drug levels of nanoformulated MABC in mice..	129

LIST OF TABLES

Table 1.1. Classification of Antiretroviral Drugs.....	8
Table 3.1. Physicochemical Characterization of NPABC and L-NPABC.....	95

LIST OF ABBREVIATIONS

MP	Monocytes, dendritic cells and macrophages
NanoART	nanoformulated antiretroviral therapy
NRTI	Nucleoside reverse transcriptase inhibitor
NNRTI	Non-nucleoside reverse transcriptase inhibitor
3TC	Lamivudine
AZT	Azidothymidine
ABC	Abacavir
ABC-MP	Abacavir monophosphate
CBV-MP	Carbovir monophosphate
CBV-TP	Carbovir triphosphate
PABC	Phosphorochloridated Abavacir
MABC	Myrosityled Abacavir
L-NPABC	lipid-nanoPABC
NPABC	Long-Acting nanoformulated PABC
NMABC	Nanoformulated MABC
FA-NMABC	folate conjugated Nanoformulated MABC
FA	Folic acid
HIV	Human immunodeficiency virus

SIV	Simian immunodeficiency
NSG	Non-obese diabetic severe combined immunodeficiency-gcnull
AIDS	Acquired immunodeficiency syndrome
CCR5	Co-receptors of HIV
CXCR4	Co-receptors of HIV
ARVS	Acute retroviral syndrome
ELISA	Enzyme-linked immunosorbant assay
cART	Combination antiretroviral therapy
P407	Poloxamer 407, Pluronic F127
PLGA	poly (lactic-co-glycolic acid)
DSPG	Distearoylphosphatidylglycerol
DSPC	1,2-Distearoyl-sn-glycero-3-phosphocholine
DSPE-mPEG	1,2-distearoyl-sn-glycero-3-phosphoethanolamine-N methoxy(polyethylene glycol)
PEG	Polyethylene glycol
DMF	Dimethylformamide
THF	Tetrahydrofuran
DCM	Dichloromethane
DMSO	Dimethyl sulfoxide

PNP	Polymeric nanoparticles
PAMAM	Poly (amido amide)
DLS	Dynamic light scattering
PDI	Polydispersity index
PK/PD	Pharmacokinetic and Pharmacodynamic
SHIV	Simian-human immunodeficiency virus, a virus combining parts of HIV and
HSC	hematopoietic stem cell
MDM	Monocyte-derived macrophages
HU-PBL	Human-peripheral blood lymphocyte
HLA-DR	Human leukocyte antigen-
FOLR	Folate receptor
¹H-NMR	Proton-Nuclear magnetic resonance imaging
FTIR	Fourier transforms infrared spectroscopy
UPLC-MS/MS	Ultra-performance liquid chromatography
HPLC	High-performance liquid chromatography
TEM	Transmission electron microscopy
SEM	Scanning electron microscopy
MCSF	Macrophage-colony stimulating factor

MTT	3-(4,5-dimethylthiazol-2-yl)-2,5-diphenyltetrazolium bromide
DMEM	Dulbecco's modified eagle medium
PBS	Phosphate-buffered saline
RT	Reverse transcriptase
Rab5	Early endosomal compartments
RAB7	Late endosomal compartments
RAB11	Recycling endosomes
RAB14	Recycling endosomes
LAMP1	Lysosomal-associated membrane protein 1
PrEP	Pre-exposure prophylaxis
RME	Receptor mediated endocytosis
PCR	Polymerase chain reaction
EC₅₀	Effective concentration dose-50
MEC	Minimum effective concentration

CHAPTER 1
OVERVIEW AND STATEMENT OF THE
PROBLEMS

1.1 THE HUMAN IMMUNODEFICIENCY VIRUS (HIV): STRUCTURE AND LIFE CYCLE

HIV is a class of viruses belongs to a group called retroviruses, and a subclass of retroviruses called as lentiviruses. A long hiatus between initial infection and the onset of AIDS occurs following HIV infection. Like all viruses, HIV survives and reproduces inside living cells, hijacking the host cell's machinery to replicate. HIV mainly infects the CD4+ T lymphocytes and to a lesser extent mononuclear phagocytes (MP; monocytes, macrophages, and dendritic cells) as these cells are also express cell surface CD4, a prerequisite for HIV to enter. Once infected HIV commandeers the cell, where cells eventually loses its function [1-3].

The genomics of HIV composed of ribonucleic acid (RNA) molecules, whereas the genes of most other organisms including humans are composed of deoxyribonucleic acid (DNA). However, once inside the cell, HIV like other retroviruses convert their RNA into DNA by using enzyme reverse transcriptase (RT), followed by its incorporation into the human cell's genomes. To develop a delivery system for prevention of HIV, an understanding about the steps involved in HIV life cycle is crucial (Figure 1.1)[3-5]. There are multiple steps in the life cycle of HIV as explained below;

1. Binding and Fusion: The first step in the HIV entry process (Figure 1.1) is the attachment of a viral particle to the CD4 receptor and a co-receptor (either CCR5 or CXCR4) of the host cell. In particular, the gp120 of HIV bind to CD4 receptors, expressed on the surface of T lymphocytes, monocytes, macrophages and

dendritic cells. Binding to CD4 induce a conformational changes in the viral envelope that are necessary for membrane fusion and viral entry. The next step is the binding of gp120 to co-receptors CCR5 and CXCR4. After the first conformational change during the binding of gp120 to CD4 cell receptor, the viral gp120-gp41 glycoprotein complex undergoes further conformational changes, exposing the N-terminal domain of gp41 and allowing the fusion peptide sequence to insert into the cellular membrane of the host cell.

2. Reverse Transcription: The fusion stage is followed by the reverse transcription and integration stages. The reverse transcriptase (RT) enzyme converts single-stranded HIV RNA into double-stranded HIV DNA through a process called reverse transcription, so it can be integrated into the host DNA.

3. Integration: The new virus genetic material enters the nucleus of the CD4 cell and integrates itself into host genetic material with the help of integrase enzyme. Once the viral DNA has integrated into the host cell's DNA, the host cell is infected for the remainder of its life. The integrated viral DNA is now called as a provirus.

4. Transcription and Translation: The provirus DNA serves as a template for the creation of new viral RNA via a process known as transcription using the host cell enzymes. This results in the production of multiple copies of viral RNA. The newly formed viral RNA moves out of the infected cell's nucleus. The viral RNA carries code for the synthesis of viral proteins and enzymes through the translation process. The code is translated into long chains of amino-acids

(polypeptide chains), which fold to produce structural proteins such as the viral envelope and enzymes (reverse transcriptase, integrase, and proteases).

5. Assembly, Budding and Release: The protease enzymes cut the longer HIV proteins into individual proteins. When these come together with the virus genetic material, a new virus bud has been assembled. Budding is the final stage of the HIV virus life cycle. In this stage, the virus pushes itself out of the host cell, taking with it part of the membrane of the cell. This outer part covers the virus and contains all of the structures necessary to bind to a new CD4 cell and receptors and begin the process again. A single infected cell can release many new HIV particles which move on to infect other cells in various parts of the body, where the viral life cycle is repeated. The infected cells are eventually destroyed.

1.2 THE HIV PANDEMIC

In 1981, the CDC (USA) began investigation of rare opportunistic infections among a group of homosexual men. These patients were later confirmed to be severe immune deficient, and later their disease syndromes were coined as Acquired immune deficiency syndrome (AIDS) [6, 7]. In 1983, two independent groups in the United States and France simultaneously investigated the cause of these infections, and named Human T Lymphotropic Virus (HTLV-III) and Lymphadenopathy Associated Virus (LAV) respectively [8-11]. In addition to HTLV-III and LAV, a third virus name AIDS-associated Retrovirus (ARV) were isolated from AIDS patient, later found to be the same virus, and renamed as Human Immunodeficiency Virus, or HIV [12]. Since the epidemic began in the early 1980s, more than 75 million people have been infected and more than 30

million people have died of HIV-related infections. With 2.0 million new infections and 1.2 million deaths in 2014-2015, AIDS still remains the deadliest epidemic of our time. According to the recent report of the global AIDS epidemic, there are approximately 37 million people currently living with HIV/AIDS infections, corresponding to 0.8% of the total population of adults aged 15-49 years according to The Joint United Nations Programme on HIV and AIDS (UNAIDS) statistics[13, 14].

1.3 CLINICAL MANIFESTATIONS

HIV infection is distinguished into three phases; acute syndrome, clinical latency and clinical AIDS. Figure 1.2 shows a typical progression of the disease without antiretroviral treatment[15]. Note that CD4+ T cell counts drop rapidly during acute HIV disease, followed by a more gradual loss during clinical latency. During the early phase of infection, HIV can be detected followed by decline of plasma virus level to undetectable, and a phase of “latency” is ensured. The symptoms of early primary HIV illness, named as acute retroviral syndrome (ARS) can be seen within first 2-6 weeks. The symptoms are flu-like and non-specific, and include fatigue, fever, lymphadenopathy, pharyngitis, anorexia, candidiasis, splenomegaly, hepatomegaly, oral lesions, and macular erythematous rashes, ulcers of genitourinary system, photophobia, and weight loss among others. The usual neurological symptoms observed are aseptic meningitis and headache. Approximately 70% of HIV infected the patients experienced ARS [16, 17].

The phase of acute infection is characterized by the active reproduction of virus and rapid decline in CD4+ T cells count, followed by inversion of CD4 to CD8 cells ratios. The numbers of HIV in peripheral circulation are in a range of 10^5 to 10^6 HIV RNA copies/ ml. The acute HIV infection can be diagnosed by HIV-1 RNA testing, western blot assay, and by investigating HIV antigen and antibody using HIV enzyme-linked immunosorbent assay (ELISA).

Followed by initial high viremia peaks, the level of HIV in the blood falls off to very low to non-detectable, and a phase of "latency" ensues. During the latency phase, few HIV symptoms are observed in patients, oral, skin, constitutional complications and an obvious persistence of lymphadenopathy are typical. Though HIV load is very low, a high turnover of CD4+ T cells and HIV virion production persists during this phase. This stage of "latency" can be prolonged up to an average of 10 years without antiretroviral therapy (ART). Eventually, the viral load continues to increase and the next stage of HIV prognosis termed 'symptomatic HIV disease' begins.

In the late-stage of HIV infection, called Acquired immune deficiency syndrome (AIDS) viral load continues to increase. CD4+ T lymphocyte cell count declines to a level less than 200-349 cells/ μ L in children older than 5 years. At this stage patient immune system is severely impaired, and patient succumbs to many opportunistic infections or malignancies like rare cancers (Kaposi's sarcoma) and other HIV infection manifestations (such as neuropathy) that eventually lead to death. HIV Patients with AIDS without on antiretroviral therapy (ART) usually cannot survive more than three years [17-21].

1.4 ANTIRETROVIRAL THERAPY (ART)

Current regimen for ART includes combination of drugs that restrict HIV replication by targeting different stages of the viral life cycle. The use of a combination of antiretroviral drugs (ARVs) delay disease progression and diminish viral load for an extended period of time that led to profound decreases in morbidity and mortality rates in AIDS patient as well restricts HIV transmission from one person to another. A combination of protease inhibitor and nucleoside reverse transcriptase inhibitors (NRTIs) are the most used ART regimens. However, development of drug resistance, toxicity and complication associated with current regimen driving the development of novel antiviral agents that target HIV life cycle other than protease or reverse transcriptase. HIV entry inhibitors, viral integrase inhibitor that prevent integration of HIV DNA into the host DNA, virion maturation inhibitor etc. are currently potential emerging HIV targets for ART as shown in figure 1.3, The novel targets antiviral agents present new treatment options that are most likely to be fully effective against multi-drug resistance virus, and thus may act as synergistic to current other inhibitors[5].

ART is now prescribed for all adults with HIV infection, with an initial prescription includes combination of two NRTIs; tenofovir disoproxil fumarate/emtricitabine or abacavir/lamivudine and a third single or boosted drug, which should be a boosted protease inhibitor or integrase strand transfer inhibitor or a nonnucleoside reverse transcriptase inhibitor. Table 1.1 present the general classification of current ART used alone or in combinations.

Table 1.1. Classification of Antiretroviral Drugs

Classifications	Ref.
<u>Category:</u> Reverse Transcriptase (RT) Inhibitors	[22-
<u>MOA:</u> RT Inhibitors block a process a process called reverse transcription, by inhibiting the activity of RT enzyme; transcription of single-stranded HIV RNA to double-stranded HIV DNA.	24]
<u>Subcategory-1:</u> Nucleoside/nucleotide RT inhibitors (NRTIs)	
<u>MOA:</u> NRTIs act by blocking RT enzyme. These drugs competitively to natural nucleoside analogs get incorporated into HIV DNA, leading to termination of DNA synthesis.	
<u>Drugs:</u> Abacavir, Lamivudine, Tenofovir, Adefovir, Emtricitabine, Zidovudine, Entecavir, Zalcitabine, Didanosine, Festinavir, Stavudine, Tenofovir disoproxil fumarate, Apricitabine, Tenofovir alafenamide fumarate.	
<u>Subcategory-2:</u> Non-nucleoside RT inhibitors (NNRTIs)	
<u>MOA:</u> NNRTIs inhibit the reverse transcription by binding to a pocket near the active site that leads to conformational change of the enzyme.	
<u>Drugs:</u> Doravirine, Efavirenz, Etravirine, Nevirapine, Delavirdine, Rilpiverine.	
<u>Category:</u> Protease Inhibitors	[25,

MOA: Inhibit virus-specific processing of viral Gag and Gag-Pol polyproteins in HIV infected cells by inhibiting viral protease. ^{26]}

Drugs: Saquinavir, Lopinavir, Atazanavir, Darunavir, Ritonavir, Indinavir, Nelfinavir, Amprenavir, Fosamprenavir, Tipranavir

Category: Integrase Inhibitors [27]

MOA: Inhibit the activity of HIV integrase, and thus block the integration of viral DNA into the DNA of the host cell.

Drugs: Elvitegravir, Raltegravir, Dolutegravir.

Category: Fusion Inhibitors [28]

MOA: Inhibit the conformational changes required for viral membrane fusion with the cells, where it binds to the HIV-1 membrane glycoprotein. This inhibits HIV from entering a cell.

Drugs: Sifuvirtide , Enfuvirtide.

Category: Entry Inhibitors [28]

MOA: Bind to gp120 receptors on the outer surface of the cell, and thus interfere with the virus ability to enter into host cell.

Drugs: Maraviroc, Vicriviroc

Category: Maturation Inhibitors [29,

MOA: Maturation inhibitors block the last step in gag processing in which the viral capsid polyprotein is broken down, thereby inhibiting the ^{30]}

conversion of the polyprotein into the mature capsid protein. Consequentially, viral particles with a defective core is produced, and thus of non-infectious in nature.

Drugs: Alpha interferon, Bevirimat, Vivecon.

Category: Capsid Inhibitors [31]

MOA: Inhibitors of HIV-gag polypeptide assembly. Dismantles assembled HIV-1 capsid assembly tubes.

Drugs: under investigation

Newer categories under development: [32]

LEDGF-based inhibitors, Budding inhibitors, RNaseH inhibitors, Vpu/tetherin-based inhibitors, CA/TRIM5 α -based inhibitors, Vif/APOBEC3G-based inhibitors.

However, with the advent of current ART regimens, a profound decrease in morbidity and mortality rates in AIDS patient HIV is possible, but complete eradication is still a major challenge. The eradication of HIV is hampered by its ability to stay hidden in restricted anatomical sites and within infected blood cells to remain as a life-long infectious agent. It is much obvious that hidden virus into those anatomical reservoirs present a major challenge to combat HIV infection. Hence long-term use of ART regimens, which otherwise have adverse impacts, will continue at least in near future.

1.5 HIV RESERVOIR; A CHALLENGE IN HIV ERADICATION

Combination antiretroviral therapy (cART) has substantially reduced the morbidity and mortality rate in HIV patient, but patient must adhere to therapy for lifelong, and virus rapidly rebounds if therapy is discontinued [21, 33]. The major reason outlined the rebound of virus, and thus complete eradication is persistence of HIV reservoirs throughout the anatomical sites even patient is on ART [34, 35]. Therefore combat with latent virus in those reservoirs remains a formidable obstacle in complete eradication of HIV. This section focuses on recent advancement in understanding of where virus hides and established latency that would insight our efforts on designing formulation strategies that penetrate deep into these sites, and established a step toward the elimination of latent virus. The hide out of latent virus in a HIV patient is classified into two categories; 1) cellular reservoirs[36] and 2) anatomical reservoirs [37].

1.5.1. Cellular Reservoir

1.5.1.1. Memory T Cells

The HIV infected resting memory CD4+ T cells and lymphoid tissue of HIV patients on cART was reported to be the source of persistence latency in late 90's. More recently, both transitional memory CD4+ T cells (CD45RA-CCR7-CD27+) and central memory (CD45RA-CCR7+CD27+) have been reported as the major infected cells in HIV-infected patients receiving cART. Latency has also been identified in other T-cell subsets and other cell types are important to investigation, by which they may differ in mechanism of HIV persistence[36].

1.5.1.2 Naive T Cells

Persistence of latency in naive CD4+ T cells in HIV patients on cART has been reported, although the intensity of infection compared with memory CD4+ T cells is approximately 1–2 logs less. The concentration of HIV DNA in CD31+ naive CD4+ T cells (enriched for recent thymic emigrants), and CD31- naive CD4+ T cells (naïve cells that have undergone homeostatic proliferation) was found to be similar prior to and after cART. However, following cART the absolute number of infected naive CD4+ T cells was increased; suggesting that the reservoir of infected naive T cells may expand over time[36].

1.5.1.3 Hematopoietic Progenitor Cells

Recently, it has been evident that HIV can be persisting latently in CD34+ hematopoietic progenitor cells (HPCs). Integrated HIV DNA was detected in CD34+ HPCs from 40% of patients on suppressive cART. Although, *in vitro* replication of HIV in HPCs showed to be cytotoxic, persistence of latent HIV could be established in these cells. Further detailed investigation are requires to understand how latency persist in these cells, whether these cells harbor infectious virus, and whether these cells could be a source of rebound virus when patients discontinued cART[36].

1.5.1.4 Astrocytes

HIV infection of primary astrocytes and *In vitro* astrocyte cell lines results in integration but marginal virus replication that infers latent infection. Astrocytes isolated from the HIV infected patients exhibits the presence of integrated HIV

DNA, which linked to the HIV-associated dementia. However, such findings are from the viremic patients, further investigations on suppressive cART patient are require[36].

1.5.1.5 Monocyte-Macrophages

A number of factors lead to MP cell lineage of monocyte-macrophage as potential HIV-1 reservoirs. Monocytes circulate peripherally for up to three days before differentiate to macrophage. Viral replication in to these cells is more persistent in nature which contributes to the low-level virus production lasting life-span of cells. Limited expression of viral protein enables these cells to evade the immune system. However, the latency pool in monocytes-macrophages cells lineage is comparatively smaller than T-cells pools. Less than 1% of monocytes estimated to have HIV-1 proviral DNA, while about 50 in millions lymph nodes macrophages are found infected. The lesser extent of infection is results of low CD4 surface expression which impair virus binding efficacy, but also to restrictions in nuclear import and reverse transcription leading to limited infection. The monocyte-macrophage HIV-1 reservoir reportedly exhibits resistance to protease inhibitors (PIs). The overexpression of P-glycoprotein transporters in these cells lineages suggested being the mechanism of resistance that limits the bioavailability of PIs[36].

1.5.2 Anatomical Reservoir

1.5.2.1 Gastrointestinal Tract (GIT)

The GIT is prominent reservoir for latent HIV infected cells in suppressive cART patient. The concentration of integrated DNA in GIT is reported to be five to ten times higher than in peripheral blood mononuclear cells. Within GIT, the distribution of HIV-DNA and RNA differ, with rectum having highest concentration of HIV DNA, and ileum with highest concentration of HIV RNA. A nonsignificant decrease in HIV RNA, suggesting ongoing HIV replication was observed in patient on suppressive cART [34, 37].

1.5.2.2 Lymphoid Tissue

HIV infected CD⁺ T cells carrying integrated HIV DNA through the systemic and lymphatic circulation constitutes lymphoid tissue an important, although less studied reservoir in HIV patient receiving suppressive cART. Moreover, the follicular dendritic cells or other myeloid cells home to germinal center may provide a stable source of latent virus. The interaction of dendritic cells to T-cells may contribute to the ongoing latency in resting T-cells [34, 37].

1.5.2.3 Genitourinary Tract

The presence of HIV RNA is detected in genital secretion in 54% of women and in semen in 8 to 10% of men receiving cART, indicating a reservoir in genital tract, although the source remains unclear. In the CNS, the limited bioavailability of cART to genitourinary tract makes it susceptible for ongoing

latency in these site. Moreover, the blood-testis barrier in male genitourinary tract, specifically restrict the entry of immune cells. *In vitro* study revealed that human testicular tissue can support HIV reproduction, but whether HIV- infected cells persist in these sites remain unclear[34, 37].

1.5.2.4 Central Nervous System (CNS)

The CNS, with its long-lived unique cells, is identified as persistent reservoir for latent HIV in patient on cART. Since, the blood-brain barrier restrict the entry of cART and HIV-specific immune cells to the CNS, the CNS cells are more susceptible to HIV reservoir then peripheral cells and sites. Latently infected astrocytes and monocytes are potential source of HIV reservoir in brain. A low level of HIV RNA also has been detected in cerebrospinal fluid in about 10% of patients receiving cART. Further detailed investigation in HIV reservoir in CNS in patient on cART is desired [34, 37].

1.6 EFFORTS TOWARDS THE ERADICATION OF HIV-1 RESERVOIRS

Although the introduction of highly active antiretroviral therapy (HAART) has considerably improve the quality of life and life-expectancy of HIV patients, complete eradication of virus, is so far, not possible. Several strategies have been proposed, and under development to eradicate HIV completely. Considerably, structured treatment interruption (SIT) and immune activation that may boost the intensification of HAART are of particular interest[38].

SIT follows hypothesis that HIV specific immunity will be boosted by HAART interruption, through controlled exposure of virus over a predefined short

periods of time. It was expected that following several interruption, immune response will be adapted enough to control virus replication even in absence of HAART. However, despite intensive research and knowledge gained over SIT, the clinical outcome in terms of decreasing the intensity of lately infected cells population failed, in fact it has been associated with worsening the clinical outcome then of patients on HAART alone [39, 40].

Immune activation therapy was designed to eradicate resting CD4+ T cells out of latency, and may be in combination with HAART boost the protection of uninfected cells. Several CD4+ T cells activating agents have been investigated in clinical studies including OKT-3, IL-2, and valproic acid. Didanosine and enfuvirtide in combination with Hydroxyurea was reported to boost HAART. However, in all case, evidence existed for rebound of virus upon discontinuation of therapy. Additionally, toxicity associated with HAART intensification limits the implementing, and thus clinical outcome[36].

The advancement of technology such as RNA interference that would silence the viral promoters within cells pool in HIV-1 reservoir would overcome the necessity for viral gene expression as well circumvent the toxicity associated with HAART intensification and immune cells activation[41]. Although these strategies towards HIV eradication are worth pursuit, their clinical efficacy is severely compromised by the specificity and delivery. The lack of specificity, in particular, delivery of antiviral agent to the virus hideout would obviously emphasize the need for the new drug delivery approaches to achieve HIV-1 eradication. One of such interested drug delivery technology is utilizing body own

immunocytes. To this context, immunocytes, in particular mononuclear phagocytes (monocytes, macrophages, and dendritic cells) as drug delivery vehicle offer several advantages over conventional drug delivery [42].

1.6.1 Macrophage-Mediated Drug Delivery: A Promising Approach In Latent Virus Eradication

As discussed earlier (section 1.5.1.5), the long-lived macrophages make a perfect hideout for HIV for long period of time, thus constituting HIV reservoirs and posing a major challenge to complete virus eradication from HIV-infected patient. Mature HIV-1 can be stored within intracellular vesicles of macrophage for weeks (33). Evidences have suggested a key role of macrophages in the failure of the immune system to achieve HIV clearance within the acute and chronic phases of infection. Therefore, targeting drug delivery to monocytes/macrophages in particular, not only eliminates HIV but an opportunity to use the very mechanism(s) the virus uses to escape destruction[43]. Additionally, using macrophages as drug delivery vehicle offers several advantages over conventional drug administration regimens. These include predefined drug delivery to specific disease sites, in particular HIV anatomical hideouts; prolonged the biological half-life, thus PK of cART; controlled drug release; and minimize drug cytotoxicity and immunogenicity. In addition, macrophage-mediated delivery can act as “Trojan horses” carrying hidden therapeutic pay-loads while transporting across formidable barriers; such as, the blood brain barriers [42].

Despite such advantages, clinical outcome for such system is jeopardized for several reasons. First, a poor drug loading into macrophage cells makes it inefficient delivery vehicle. Second, entrapped therapeutic agents may degrade/disintegrate within cellular compartments, lysosomal compartment in particular. Third, the macrophage should ensure loaded drug to stay within cellular vesicles till the cell reach to the predefined site of action or disease site, thus loaded payloads should not be released prematurely. Fourth, the cell carriers should transport to the disease site in therapeutically efficient quantities. In particular, transmigrating capability of macrophages should not be compromised during drug entrapment. Finally, the drug formulations must be safe enough to ensure all biological function of cells [42].

Many of these hurdle can be overcome by pre-packing the drug load/s into polymeric matrix that ensure a safest way to load high drug content that not only preserve the drug loads within cellular organelles but also sustain the release for an extended period of time [44]. Incorporation of drugs into protective polymeric nanoparticulate system is of particular interest by overcoming specified challenges.

1.6.2 Design Consideration of Cell-Mediated Drug Delivery Construct

The concept of cell-mediated drug delivery is very promising and under development. Specific considerations must be addressed ahead of time while constructing cell-carriers, for example, adequate drug loading capacity, controlled drug release at site of action, preservation of drug inside polymeric matrix and

endosomal vesicles, efficient homing of these drug carrying cells to site of interest and safety are some of important issues[42].

1.6.2.1 Drug loading into the macrophages

Nanocarriers commonly have a polymeric matrix core that permits drug entrapment, while outer polymeric layer define the nanocarriers aqueous dispersion, systemic circulation time. The surface coating of these drug carriers have a notable impact on their interaction with macrophages that affects the cellular loading. In general, the macrophage uptake of charged nanoparticles are rapid and higher compared to neutral nanocarriers. Positively charged nanoparticles reported to accumulate in macrophages to a greater extent than negatively charged particles. The mechanism lies in the fact that positively-charged nanocarriers likely to adsorb more on negatively-charged cell membrane of macrophage, derived by electrostatic attraction[45]. Moreover, the cell entrapment of these nanocarriers can be facilitated through engineering the outer surface using specific receptor targeting moiety that recognize specific receptors expressed on the cell surface, in particular, Fc, complement, mannose and folic acid receptors are among some of notable targeted receptors[46].

The shape and size of nanocarriers have a significant impact upon cellular uptake. It has been reported that attachment of particles of different geometry to the macrophages surfaces are strongly dependent on shape and size. Particles that possess longest dimension, in the range of 2–3 μm exhibited superior attachment. The mechanism lie in the facts the macrophage evolved to engulf maximum number of bacteria, most of which exist in same size range.

Furthermore, the uptake of particles with the size about 1 μ m was significantly higher than particle with the size of about 500 nm[45]. Recently, the effects of shape on cellular uptake were investigated in alveolar rat macrophages using more than 20 shapes of polystyrene-based particles. It has been revealed that shape of particles at the point of contact; where it attaches to macrophage play an important role in phagocytosis. For example, the attachment of sharper end of ellipse with macrophage would facilitate particles internalization within minutes. In contrast, macrophage attached to the particle on dull end side would limit phagocytosis [47].

1.6.2.2 Drug preservation into the macrophages

The investigation of intracellular trafficking of the nanocarriers among other factors is of key important in defining the fate of drug encased nanocarriers once engulfed by macrophages. In particular, the drug loaded cargo need to bypass the lysosomes in order to avoid drug degradation within acidic cellular compartments [43]. In this context, the surface charge of nanocarriers is of key importance in defining the intracellular fate. For example, a diminished phagosomal acidification was observed with cationic polyamine coated nanoparticles compared with anionic protein coated nanoparticles. Therefore, the cationic nanoparticles sought to protect the drug from lysosomal degradation[48]. In a recent study, it revealed that encapsulation of catalase into the positively charged block copolymers (PEI-PEG and PL-PEG) leads to improve stability of enzyme in macrophage. In contrast, the loading of enzyme into negatively

charged polyion complex resulted in degradation of enzyme within macrophages[49].

The intracellular drug degradation can be circumvented by limiting the carriers being phagocytized, but attached to the cell surface. The “back-pack” attached to the monocytes/macrophages surface would be hitchhiked to the site of interest that also improve systemic circulation while preserved encased drug activity. The avidin coated nanoparticles reported to attach with biotinylated plasma membrane through the avidin-biotin complex to constitute stable “back pack”. However, further studies needed to investigate the drug carrying capacity and immunogenicity of such polymeric “back pack” [50].

1.6.2.3 Drug release from the macrophages

Mechanism underlying the unloading of these nanocarriers at the site of action remains an active area of investigation. However, a desired controlled release of cargo has modulated the dose and duration of exposure. To such end, cellular response to various physical or chemical stimuli can be utilized to trigger the release. Macrophages, along with mononuclear phagocytic cells, are known to produce and store the various compound within endosomal vesicle, followed by their released via exocytosis at disease site. A similar mechanism can be anticipated for the release of drug and /or drug -loaded carriers, when serve as drug delivery vehicles. However, further detail investigations are needed to understand the exact mechanism [42]. The release of drug can be modulated using external stimuli. For example, by modulating the intracellular concentration of Ca^{2+} the drug release can be triggered [51]. Furthermore, the use of mild

hypothermia was reported to control the release of drug-loaded liposomes from macrophages in tumor vicinity[52].

1.6.2.4 Drug depot

For cell-mediated drug delivery the numbers of drug carrying cells reach the site of action of key importance. For example, in case of CNS disorder the efficacy of cell-carriers is determined by the ability to cross the blood brain barrier (BBB) to elicit therapeutic end point. For most of cells-carriers the driving force to the disease site is chemotaxis; a process where most of MP migrate to the disease site following chemogradient. In many CNS disorder, such as Parkinson's and Alzheimer's disease, meningitis, encephalitis, prion disease and HIV-associated neurocognitive disorders (HAND) exhibited similar inflammatory components that recruit MP extensively to the disease periphery. Additionally, neural stem cells (NSCs) were also reported as drug delivery vehicle for gene delivery in brain. Indeed, these cells transmigrate more efficiently to the disease site including neoplastic brain lesions and ischemic lesions. However, the mechanism to which they transmigrate to the disease area is not clear yet, although NSCs reported to express a wide variety of receptors that may render them to respond to many chemotactic signals. In particular, activate microglia drive NSCs influx to the brain. Therefore, cell-mediated strategies can be employed to deliver wide range of neurotropic factors that otherwise restricted due to brain formidable barriers i.e. BBB [42].

In context of cell-mediated drug delivery of anticancer agent, MP are known to migrate in large number at tumor site, in particular, vascular and

hypoxic site, for example in prostate and breast carcinomas. Malignant tumors have lots more hypoxia due to their unorganized vasculature. The hypoxia driven cytokines from tumors cells and other physiological stress are the chemotactic markers that accumulate monocytes and macrophages in tumor vicinity that facilitate anticancer drug delivery to the cancerous region using these cells as delivery vehicle[53]. The advantages of cell-carriers in anticancer drug deliver are to avoid unwanted drug distribution and minimize off-target drug toxicity.

Cells-carriers can be deployed to the disease site by incorporating magnetic nanoparticles into the therapeutic cargo and fed to the cells carriers following accumulation at disease site with the aid of external applied magnetic field. Intravenous injections of RGD-coated magnetic liposomes in albino rats with brain inflammation exhibited 10-folds brain accumulation under the magnetic guidance compared to non-magnetic nanoparticles. RGD peptide facilitated selective binding of these nanoparticles to the surface of monocytes/macrophages that expressed integrin receptors on cellular surface [54].

1.6.2.5 Safety of cell-mediated drug delivery

One has to be cautious about safety concern while designing cell-carriers constructs. In particular, the MP migrates to the disease site is usually accomplished by release of reactive oxygen species (ROS) that cause cell damage. To this context, many of CNS therapeutic strategies are designed to limit the monocytes/macrophages infiltration the brain. Therefore, circumventing cytotoxicities for cell-based drug delivery construct is a prerequisite for

formulation development of cell-mediated drug delivery system. Nevertheless, in particular, brain delivery of macrophage-mediated nanoformulated catalase showed no cytotoxic effects [42]. Further detailed investigations are required to preclude any pitfall of cell-mediated drug delivery for acute and chronic applications.

1.7 DESIGN CONSIDERATION OF NANOMEDICINE FOR EFFICIENT CELL-CARRIERS

One has to be very cautious while choosing right drug packed particulate while constructing cells-based drug carriers in order to maximize the therapeutic outcome with least side effect, or that does not have any impact on the integrity of cellular carriers. The designs of nanocarriers need to be optimized in terms of particles size, shape, and surface chemistry to maximize the cellular uptake, and thus efficacy of loaded drug/s. All these characteristics are critical for clinical translation of these carrier system.

1.7.1 Shape, size and surface charge of nanocarriers

Nanoparticles shape and size are the critical parameter which affects the rate of macrophage uptake. Champion et al revealed that particles of size 2–3 μm in diameter exhibited maximal macrophage uptake via phagocytosis and attachment. However, the rate of internalizations is independent of by particle size. The particle size dependence of phagocytosis is governed primarily from the attachment of particles to the surface of macrophage. Furthermore, the macrophage membrane ruffles is hypothesized to be the reason of maximal

attachment of 2–3 μm microspheres, the elimination of which through osmotic swelling nearly diminished the peculiar size-dependence of phagocytosis. In particular, particles of size around $\sim 2 \mu\text{m}$ are phagocytosed more rapidly than smaller or larger particles. Alternately, particles with hydrophobic surface are uptake more rapidly via phagocytosis than particles with hydrophilic surfaces. Consequentially, particle surface are modified by neutral hydrophilic polymers such as polyethylene glycol (PEG) to modulate the phagocytosis. Nanoparticle synthesis methods and process should be choose and modulate based upon the targeted size. The aspects like drug/polymer ratio, polymer/surfactant concentration, solvent type and stirring/homogenization rate are some of few important considerations [47, 55, 56].

The impact of particles shape on phagocytosis is recently beginning to be investigated. Champion and Mitragotri [56] recently revealed from their finding that the shape of particles has crucial impact on phagocytosis by macrophages; the oblate ellipsoid particles are more rapidly phagocytosed than particles with spheres or prolate ellipsoid shapes. The shape of particles triggered phagocytosis via cell attachment and internalization. The shape-dependency of phagocytosis is potentially linked to the actin remodeling by the macrophage cytoskeleton, since phagocytosis is an actin–linked process. Since actin remodeling is energy deriving process, in theory, the shape that require more energy for actin remodeling, should be internalized slower. Therefore, the fact that oblate ellipsoids are phagocytosed more rapidly and efficiently than prolate ellipsoids is due to their lower aspect ratio and actin remodeling which require

less energy for internalization. Furthermore, it has been reported that cylindrical rods shape particles are advantageous in terms of macrophages uptake. The mechanism reflects the preference of macrophages for engulfment of most bacteria that have a rod shaped geometry in nature.

Surface charge of the nanoparticles has exhibited to be a major determinant of cellular uptake, which highly depends upon cell types. For macrophage uptake, the positively charged particles are more prone to sequestration by macrophages in the spleen, lungs and liver. In contrast, neutral and slightly negatively charged nanoparticles are of least preference for macrophage uptake [45].

1.7.2 Drug Loading and Encapsulation Efficiency

Drug loading or encapsulation efficiency of a formulation is a measure of intensity by which drug retain within polymeric matrix. In general a high drug loading or encapsulation is required that negate the need of higher dose of nanoparticles which otherwise administered a large volume of excipient/s. Drug loading measures the mass of the drug entrapped within a polymeric matrix during nanoparticle preparation compared to the mass of excipients. It is calculated from the following equation;

$$\text{Drug loading (\%)} = \frac{\text{(mass of drug in nanoformulation)}}{\text{(total mass of nanoformulation)}} \times 100$$

Whereas, encapsulation efficiency of a formulation measure the ratio of drug encapsulated in nanoformulations verses total drug added. It is important to

purify the nanoparticles to get rid of unencapsulated drug and surface adsorbed drug before calculating the drug encapsulation and loading parameters. Drug loading is dependent on the process of formulation, nature of excipients, and type of nanoparticle itself (polymeric nanoparticles, solid lipid nanoparticles, dendrimers, etc.). For drug loading analysis, freeze dried powder of formulation is disrupted in a solvent to release the encapsulated drug, whereas encapsulation efficiency is measure by analyzing remaining drug in purified supernatant. A higher drug loading indicates lesser amount of non-active excipients and small volume of injections needed to achieve a bioequivalent drug dose [57].

1.7.3 Drug Release

The rate and extent of drug release from polymeric matrix is very crucial to determine therapeutic efficacy of formulation. Drug release can be coined as the opposite of drug loading. In particular, drug release is a mass transfer process from the polymeric matrix to the surrounding release media. The release of encased drug in a media is governed by many factors including interaction of drug with excipients, chemical characteristics of drug and polymer and nature of release media itself.

The rate of drug release from a matrix can be calculated using Fick's law of diffusion. In facts, Ficks's law of diffusion is a mathematical simplification of a complex process driven by complex physicochemical parameters influencing the drug release[58].

1.8 ANIMAL MODELS OF HIV

Since HIV only infects human, it is a major hurdle in choosing a relevant animal model. HIV is specific to human immune cells, which are bound to specific genetic factors critical for their life cycle. These include binding of HIV to immune cells via CD4 receptor, and co-receptors CCR5 and CXCR4. Attempts were made to fabricate those receptors over murine cell, but yet not succeed, which in part, is due to absence of many human specific factors. Furthermore, attempts were made to generate a chimeric strain of HIV by modifying HIV itself; SHIV reported to replicate in monkey. Although, chimeric strain facilitates to immune responses to vaccine construct, but differ in response that was produced with HIV infection. Limited successes were seen with some other notable approach such as HIV encoded gene expression[59]. Therefore, to this end, there is a prime need to generate relevant animal model to study HIV-1 infection. Humanized mouse model, in this context studies as reasonable alternative.

Chronic humanized mouse model is accomplished by expression of human transgene or transplanting human tissue into immune deficient mice. Since these mice are immune deficient [severe combined immunodeficiency (SCID)] that involve mutation in *prkdc* gene that spontaneously deplete B and T cells population, the host-rejection of graft is lacking.

1.8.1 Human Peripheral Blood Lymphocytes (Hu-PBL) Reconstituted Mice

Humanized mouse model created by knock down of *Prkdc* gene successfully exhibited immunodeficiency but with leaky production of T and B cell, and high level of natural killer (NK) cells. Additionally, the mutation in IL-2

(gamma chain receptor) renders the lack of IL-2 signaling in B and T cells that leads to more efficient xenograft. Furthermore, the knock down of recombinase activating genes 1 or 2 (Rag1/Rag2) produce xenografts with no leaky B and T cells. Furthermore, the mutation of non-obese diabetic (NOD) gene leads to drop down of NK cells production. Therefore, combining all mutation produce a much stable engraftment generally referred to as NOD/scidIL- 2Rgc null (NSG) mice[60].

The Hu-PBL reconstituted mouse is prepared by injecting human PBL intraperitoneally into NSG mice that render them susceptible to HIV infection. The Hu-PBL reconstituted mouse showed upregulation of Human leukocyte antigen- DR (HLA-DR) and CCR5 that leads to production of xeno-reactive T cells. However, due to the graft-versus-host reactions, these mice are susceptible to die. Moreover, the mouse model is restricted by lack of hematopoiesis and graft-versus-host response, which limit their usefulness for chronic infection. However, the ease of preparation and availability make them alluring for acute infection studies [61].

1.9. SIGNIFICANCE OF THE PROJECT

ABC is an antiretroviral drug used for preventing and treating HIV/AIDS. It is a nucleoside analog acting as a chain terminator for the reverse transcriptase inhibitor and called a NRTI as a consequence. It is under the trade name Ziagen. Importantly viral strains that are resistance of zidovudine or lamivudine (3TC) can be sensitive to ABC. It has a variety of secondary toxicities that include nausea, headache, fatigue, vomiting, hypersensitivity reaction, diarrhea,

fever/chills, depression, rash, anxiety, URI, ALT, AST elevated, hypertriglyceridemia, and lipodystrophy. An important hypersensitivity syndrome is associated with its use. This reaction is strongly associated with a specific allele at the human leukocyte antigen B locus namely HLA-B*57:01. Nonetheless, it possesses the unique property of strong penetrance of the blood-brain barrier (BBB) and as such would be of significant use to restrict viral infection within the brain and spinal cord and used concurrently with agents designed to eradicate viral infection[62]. Thus, it is of significant interest to our group of investigators.

The study will be conducted in four phases. The first will explore the manufacturing capabilities of the novel nanoformulation. NMR tests will confirm the formation of the pro-drug. The second phase will be in preparing the pro-drug for polymer encasement with appropriate decoration with a targeting ligand or ligands. In the second phase size, charge, morphology and polydispersity will be measured. In the third stage, stability will be tested by taking the formulation from storage at 4 °C and 25 °C every 10 days for 60 days and measuring the same parameters developed in stage two. The fourth stage will test its antiretroviral responses by allowing monocyte derived macrophages to be infected following 1, 5, 10 and 15 day initial exposure to the variant nanoformulation manufactured at a spectrum of drug concentration. Toxicity measures for the monocyte-macrophages will be performed through viability and functional tests.

The studies will be focused on developing folic acid (FA) targeted, long-acting parenteral nanoformulations of Abacavir prodrugs. The overarching goals would be to extend the pharmacokinetic (PK) and pharmacodynamics (PD) profile of native hydrophilic counterpart i.e. ABC, specifically targeting them to macrophage receptors using folic acid ligand coating.

Long-acting parenteral nanoformulations circumvents several pitfalls of conventional oral drug delivery like treatment off-target toxicity, poor PK and biodistribution, drug-drug interactions and limited therapeutic end point. The long-acting nanoformulations results in targeted drug delivery to viral reservoir sites with uniformity in PK parameters. Several potent antiretroviral agents were discontinued due to their poor PK and undesirable physicochemical characteristics such as poor dissolution, instability in GIT fluids etc. Formulating such drugs as long-acting nanoformulation can circumvent such issues and probability of getting these drugs back to market is high. Because in nanoformulation encased drug is protected within polymeric matrix and inside stable intracellular compartments, the probability of drug-drug interaction with other drug and adverse effects will be considerably reduced[63].

The other important implication of long-acting nanoformulations is by reducing the dosing frequency and overall dose that lead to improved patient compliance by decreasing treatment associated anxiety in patients. Furthermore, long-action nanoformulations can ameliorate viral resistance and patient adherence against ART[64]. Specially, this will be very beneficial to the patients with concomitant substance abuse, which are usually non-adherent to treatment

regimens. Therefore, such patient's population is usually not treated with ART because of higher risk of transmission of resistant species of HIV-1 to uninfected individuals.

In future, with long-acting nanoformulations platforms using robust manufacturing procedures, once six months or even less frequent dosing regimen can be achieved. Such dosing regimen holds promising in HIV eradication as of their ability to reach deep penetrating in to HIV reservoir, which otherwise formidable to conventional dosing regimen. Even though complete eradication is not possible, the diminished of viral rebound can be feasible with such dosing regimen. Additionally, it is possible to administered long-action nanoformulations in to individual living in high-risk population as pre-exposure prophylaxis, or PrEP.

Long-acting nanoformulations by constructing macrophage-mediated delivery system even with frequent dosing could drastically improve the therapeutic outcome by penetrating deeper into anatomical HIV-1 reservoir. The ability of long-acting NanoART to penetrate deeper into these HIV reservoir tissue would considerably suppress viral production manes it provide a mean for immune system to better handle co-morbid conditions. This would turn very beneficial for patient with co-morbid conditions living in resources limited setting. Furthermore, the ability of long-acting NanoART to circumvent drug resistance and decrease drug associated toxicities present a means to reduce the cost associated with HIV management, especially in resource-limited settings[64].

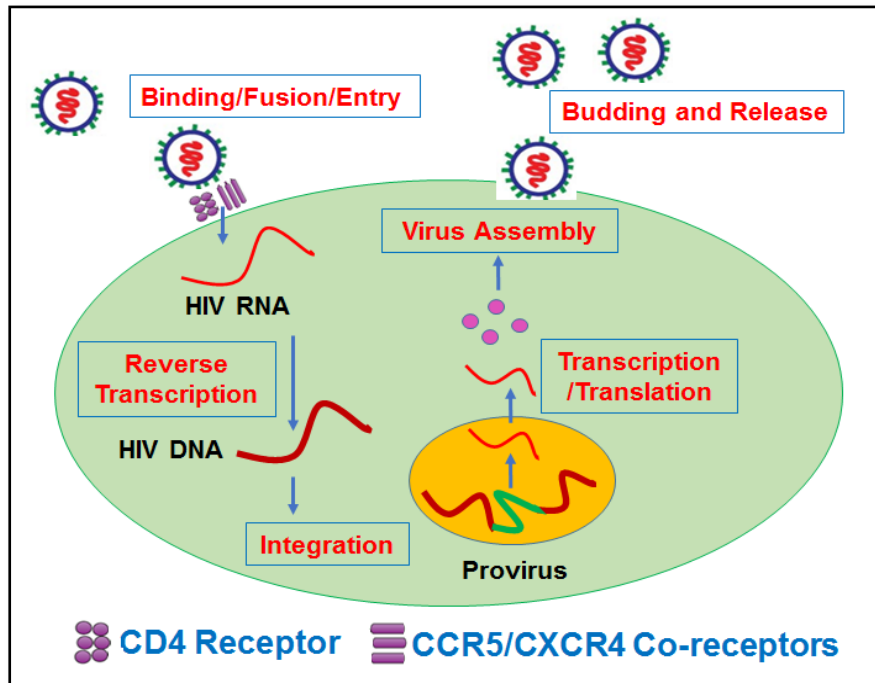


Figure 1.1. Life cycle of HIV Virus [2]

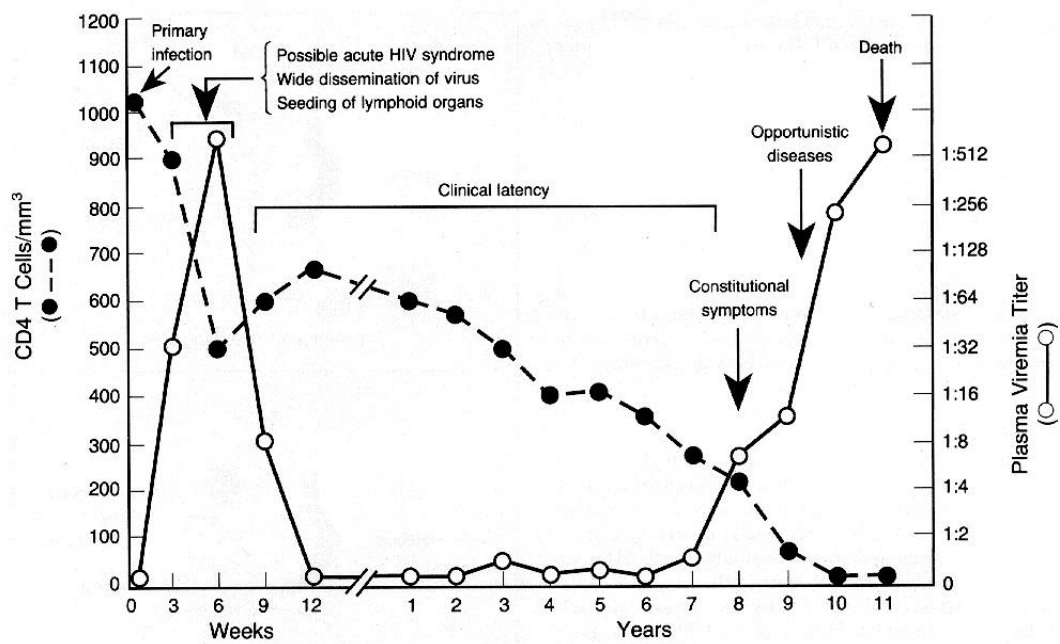
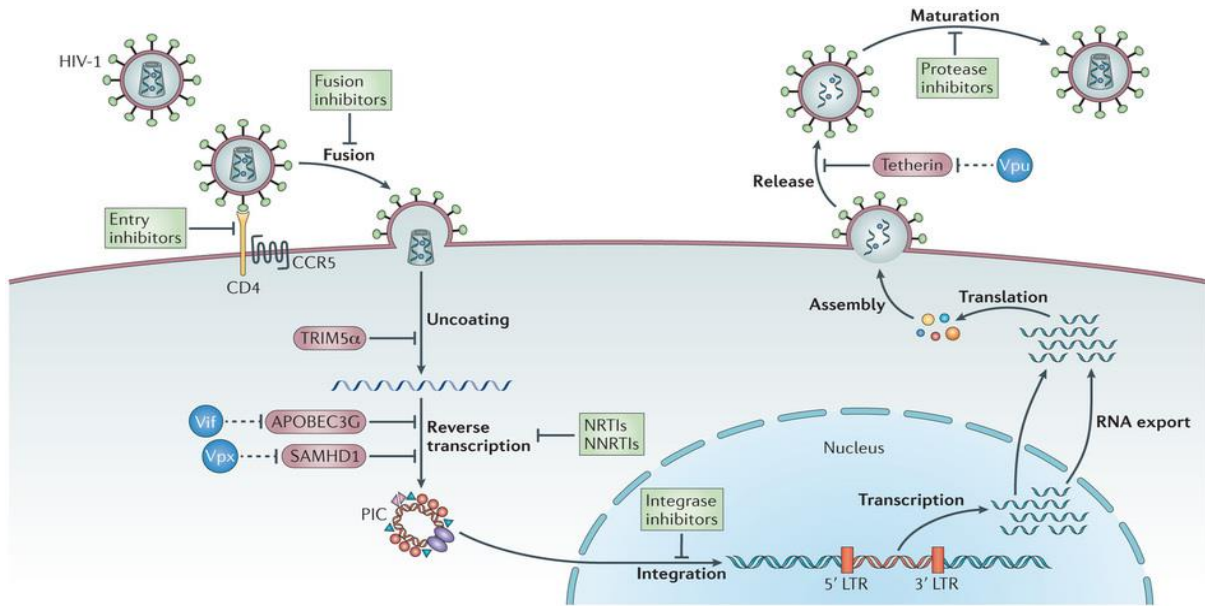


Figure 1.2. Time course of HIV Disease progression without Therapy [15]



Nature Reviews | Microbiology

Figure 1.3. Development of ART targeting different stages of HIV life cycle
[5]

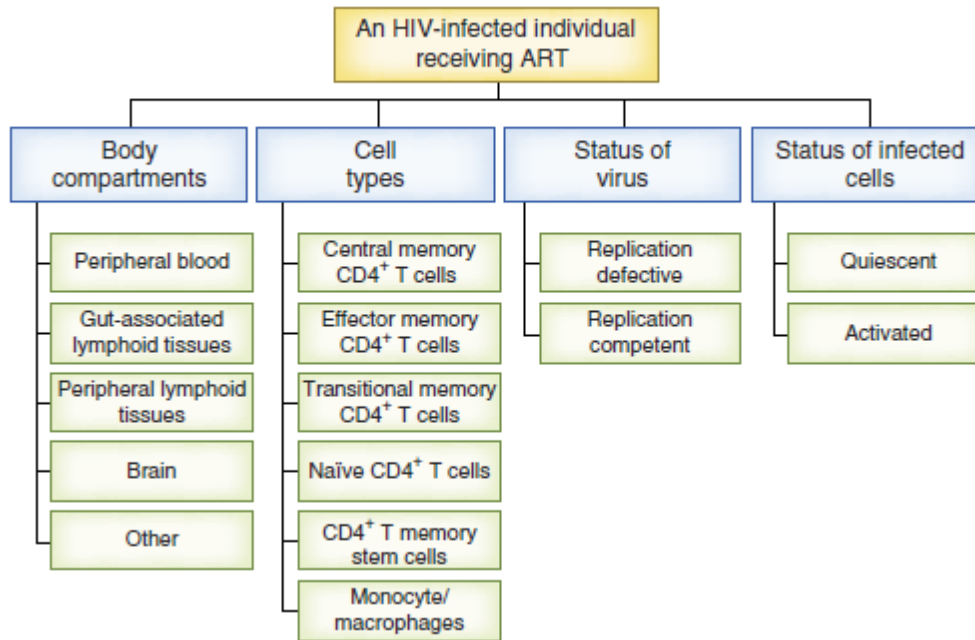


Figure 1.4. HIV reservoirs in HIV patients receiving cART [34]

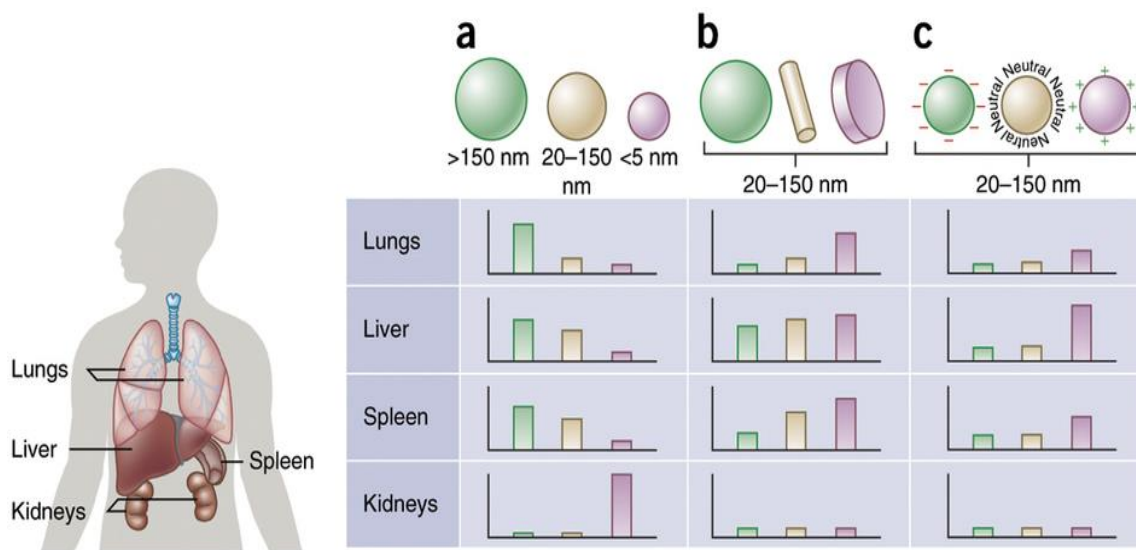


Figure 1.5. Macrophage particle uptake in different organs including the lungs, liver, spleen and kidneys are dictated by size, shape and surface charge of nanoparticles [45]

1.10 REFERENCES

1. J.R. Perilla and A.M. Gronenborn. Molecular Architecture of the Retroviral Capsid. *Trends in biochemical sciences*. 41:410-420 (2016).
2. B. Chen. HIV Capsid Assembly, Mechanism, and Structure. *Biochemistry*. 55:2539-2552 (2016).
3. A. Engelman and P. Cherepanov. The structural biology of HIV-1: mechanistic and therapeutic insights. *Nature reviews Microbiology*. 10:279-290 (2012).
4. F. Barre-Sinoussi, A.L. Ross, and J.F. Delfraissy. Past, present and future: 30 years of HIV research. *Nature reviews Microbiology*. 11:877-883 (2013).
5. S.B. Laskey and R.F. Siliciano. A mechanistic theory to explain the efficacy of antiretroviral therapy. *Nature reviews Microbiology*. 12:772-780 (2014).
6. H. Masur, M.A. Michelis, J.B. Greene, I. Onorato, R.A. Stouwe, R.S. Holzman, G. Wormser, L. Brettman, M. Lange, H.W. Murray, and S. Cunningham-Rundles. An outbreak of community-acquired *Pneumocystis carinii* pneumonia: initial manifestation of cellular immune dysfunction. *The New England journal of medicine*. 305:1431-1438 (1981).
7. M.S. Gottlieb, R. Schroff, H.M. Schanker, J.D. Weisman, P.T. Fan, R.A. Wolf, and A. Saxon. *Pneumocystis carinii* pneumonia and mucosal candidiasis in previously healthy homosexual men: evidence of a new acquired cellular immunodeficiency. *The New England journal of medicine*. 305:1425-1431 (1981).

8. R.C. Gallo. Historical essay. The early years of HIV/AIDS. *Science*. 298:1728-1730 (2002).
9. R.C. Gallo and L. Montagnier. The discovery of HIV as the cause of AIDS. *The New England journal of medicine*. 349:2283-2285 (2003).
10. F. Barre-Sinoussi, J.C. Chermann, F. Rey, M.T. Nugeyre, S. Chamaret, J. Gruest, C. Dauguet, C. Axler-Blin, F. Vezinet-Brun, C. Rouzioux, W. Rozenbaum, and L. Montagnier. Isolation of a T-lymphotropic retrovirus from a patient at risk for acquired immune deficiency syndrome (AIDS). *Science*. 220:868-871 (1983).
11. L. Montagnier. Historical essay. A history of HIV discovery. *Science*. 298:1727-1728 (2002).
12. J.A. Levy. Pathogenesis of human immunodeficiency virus infection. *Microbiological reviews*. 57:183-289 (1993).
13. D. Paraskevis, G.K. Nikolopoulos, G. Magiorkinis, I. Hodges-Mameletzis, and A. Hatzakis. The application of HIV molecular epidemiology to public health. *Infection, genetics and evolution : journal of molecular epidemiology and evolutionary genetics in infectious diseases*(2016).
14. N.R. Faria, A. Rambaut, M.A. Suchard, G. Baele, T. Bedford, M.J. Ward, A.J. Tatem, J.D. Sousa, N. Arinaminpathy, J. Pepin, D. Posada, M. Peeters, O.G. Pybus, and P. Lemey. HIV epidemiology. The early spread and epidemic ignition of HIV-1 in human populations. *Science*. 346:56-61 (2014).

15. G. Pantaleo, C. Graziosi, and A.S. Fauci. New concepts in the immunopathogenesis of human immunodeficiency virus infection. *The New England journal of medicine*. 328:327-335 (1993).
16. J.M. Costin. Cytopathic mechanisms of HIV-1. *Virology journal*. 4:100 (2007).
17. A.S. Fauci. Pathogenesis of HIV disease: opportunities for new prevention interventions. *Clinical infectious diseases : an official publication of the Infectious Diseases Society of America*. 45 Suppl 4:S206-212 (2007).
18. P. Piot and R. Colebunders. Clinical manifestations and the natural history of HIV infection in adults. *The Western journal of medicine*. 147:709-712 (1987).
19. S.L. Rowland-Jones. Timeline: AIDS pathogenesis: what have two decades of HIV research taught us? *Nature reviews Immunology*. 3:343-348 (2003).
20. V. Pirrone, N. Thakkar, J.M. Jacobson, B. Wigdahl, and F.C. Krebs. Combinatorial approaches to the prevention and treatment of HIV-1 infection. *Antimicrob Agents Chemother*. 55:1831-1842 (2011).
21. M. Chesney. Adherence to HAART regimens. *AIDS Patient Care STDS*. 17:169-177 (2003).
22. M.O. Akanbi, K.K. Scarsi, B. Taiwo, and R.L. Murphy. Combination nucleoside/nucleotide reverse transcriptase inhibitors for treatment of HIV infection. *Expert opinion on pharmacotherapy*. 13:65-79 (2012).

23. T. Cihlar and A.S. Ray. Nucleoside and nucleotide HIV reverse transcriptase inhibitors: 25 years after zidovudine. *Antiviral research*. 85:39-58 (2010).
24. E. De Clercq. Anti-HIV drugs: 25 compounds approved within 25 years after the discovery of HIV. *International journal of antimicrobial agents*. 33:307-320 (2009).
25. P. Messiaen, A.M. Wensing, A. Fun, M. Nijhuis, N. Brusselaers, and L. Vandekerckhove. Clinical use of HIV integrase inhibitors: a systematic review and meta-analysis. *PloS one*. 8:e52562 (2013).
26. Y. Pommier, A.A. Johnson, and C. Marchand. Integrase inhibitors to treat HIV/AIDS. *Nature reviews Drug discovery*. 4:236-248 (2005).
27. Z. Lv, Y. Chu, and Y. Wang. HIV protease inhibitors: a review of molecular selectivity and toxicity. *Hiv/Aids*. 7:95-104 (2015).
28. D.R. Kuritzkes. HIV-1 entry inhibitors: an overview. *Current opinion in HIV and AIDS*. 4:82-87 (2009).
29. A.A. Waheed and E.O. Freed. HIV type 1 Gag as a target for antiviral therapy. *AIDS research and human retroviruses*. 28:54-75 (2012).
30. P. Spearman. HIV-1 Gag as an Antiviral Target: Development of Assembly and Maturation Inhibitors. *Current topics in medicinal chemistry*(2015).
31. K. Braun, M. Frank, R. Pipkorn, J. Reed, H. Spring, J. Debus, B. Diding, C.W. von der Lieth, M. Wiessler, and W. Waldeck. HIV-1 capsid assembly inhibitor (CAI) peptide: structural preferences and delivery into human embryonic

lung cells and lymphocytes. *International journal of medical sciences*. 5:230-239 (2008).

32. C.S. Adamson and E.O. Freed. Anti-HIV-1 therapeutics: from FDA-approved drugs to hypothetical future targets. *Molecular interventions*. 9:70-74 (2009).

33. D. Looney, A. Ma, and S. Johns. HIV therapy-the state of art. *Curr Top Microbiol Immunol*. 389:1-29 (2015).

34. M.Z. Smith, F. Wightman, and S.R. Lewin. HIV reservoirs and strategies for eradication. *Current HIV/AIDS reports*. 9:5-15 (2012).

35. T.W. Chun, S. Moir, and A.S. Fauci. HIV reservoirs as obstacles and opportunities for an HIV cure. *Nature immunology*. 16:584-589 (2015).

36. A. Alexaki, Y. Liu, and B. Wigdahl. Cellular reservoirs of HIV-1 and their role in viral persistence. *Current HIV research*. 6:388-400 (2008).

37. R. Lorenzo-Redondo, H.R. Fryer, T. Bedford, E.Y. Kim, J. Archer, S.L. Kosakovsky Pond, Y.S. Chung, S. Penugonda, J.G. Chipman, C.V. Fletcher, T.W. Schacker, M.H. Malim, A. Rambaut, A.T. Haase, A.R. McLean, and S.M. Wolinsky. Persistent HIV-1 replication maintains the tissue reservoir during therapy. *Nature*. 530:51-56 (2016).

38. J. Lisziewicz and F. Lori. Structured treatment interruptions in HIV/AIDS therapy. *Microbes and infection / Institut Pasteur*. 4:207-214 (2002).

39. G.M. Ortiz, M. Wellons, J. Brancato, H.T. Vo, R.L. Zinn, D.E. Clarkson, K. Van Loon, S. Bonhoeffer, G.D. Miralles, D. Montefiori, J.A. Bartlett, and D.F.

Nixon. Structured antiretroviral treatment interruptions in chronically HIV-1-infected subjects. *Proceedings of the National Academy of Sciences of the United States of America*. 98:13288-13293 (2001).

40. J. Ghosn, M. Wirden, N. Ktorza, G. Peytavin, H. Ait-Mohand, L. Schneider, S. Dominguez, F. Bricaire, V. Calvez, D. Costagliola, and C. Katlama. No benefit of a structured treatment interruption based on genotypic resistance in heavily pretreated HIV-infected patients. *Aids*. 19:1643-1647 (2005).

41. N.S. Lee and J.J. Rossi. Control of HIV-1 replication by RNA interference. *Virus research*. 102:53-58 (2004).

42. E.V. Batrakova, H.E. Gendelman, and A.V. Kabanov. Cell-mediated drug delivery. *Expert opinion on drug delivery*. 8:415-433 (2011).

43. D. Guo, G. Zhang, T.A. Wysocki, B.J. Wysocki, H.A. Gelbard, X.M. Liu, J.M. McMillan, and H.E. Gendelman. Endosomal trafficking of nanoformulated antiretroviral therapy facilitates drug particle carriage and HIV clearance. *J Virol*. 88:9504-9513 (2014).

44. T.K. Vyas, L. Shah, and M.M. Amiji. Nanoparticulate drug carriers for delivery of HIV/AIDS therapy to viral reservoir sites. *Expert opinion on drug delivery*. 3:613-628 (2006).

45. E. Blanco, H. Shen, and M. Ferrari. Principles of nanoparticle design for overcoming biological barriers to drug delivery. *Nature biotechnology*. 33:941-951 (2015).

46. S. Gunaseelan, K. Gunaseelan, M. Deshmukh, X. Zhang, and P.J. Sinko. Surface modifications of nanocarriers for effective intracellular delivery of anti-HIV drugs. *Advanced drug delivery reviews*. 62:518-531 (2010).
47. J.A. Champion and S. Mitragotri. Shape induced inhibition of phagocytosis of polymer particles. *Pharmaceutical research*. 26:244-249 (2009).
48. L. Thiele, H.P. Merkle, and E. Walter. Phagocytosis and phagosomal fate of surface-modified microparticles in dendritic cells and macrophages. *Pharmaceutical research*. 20:221-228 (2003).
49. R.V. Benjaminsen, M.A. Matthebjerg, J.R. Henriksen, S.M. Moghimi, and T.L. Andresen. The possible "proton sponge" effect of polyethylenimine (PEI) does not include change in lysosomal pH. *Molecular therapy : the journal of the American Society of Gene Therapy*. 21:149-157 (2013).
50. A.C. Anselmo, J.B. Gilbert, S. Kumar, V. Gupta, R.E. Cohen, M.F. Rubner, and S. Mitragotri. Monocyte-mediated delivery of polymeric backpacks to inflamed tissues: a generalized strategy to deliver drugs to treat inflammation. *Journal of controlled release : official journal of the Controlled Release Society*. 199:29-36 (2015).
51. T. Sollner, M.K. Bennett, S.W. Whiteheart, R.H. Scheller, and J.E. Rothman. A protein assembly-disassembly pathway in vitro that may correspond to sequential steps of synaptic vesicle docking, activation, and fusion. *Cell*. 75:409-418 (1993).

52. V.M. Kulkarni, D. Bodas, D. Dhoble, V. Ghormade, and K. Paknikar. Radio-frequency triggered heating and drug release using doxorubicin-loaded LSMO nanoparticles for bimodal treatment of breast cancer. *Colloids and surfaces B, Biointerfaces*. 145:878-890 (2016).
53. R.D. Leek, C.E. Lewis, R. Whitehouse, M. Greenall, J. Clarke, and A.L. Harris. Association of macrophage infiltration with angiogenesis and prognosis in invasive breast carcinoma. *Cancer research*. 56:4625-4629 (1996).
54. S. Jain, V. Mishra, P. Singh, P.K. Dubey, D.K. Saraf, and S.P. Vyas. RGD-anchored magnetic liposomes for monocytes/neutrophils-mediated brain targeting. *International journal of pharmaceutics*. 261:43-55 (2003).
55. G. Sharma, D.T. Valenta, Y. Altman, S. Harvey, H. Xie, S. Mitragotri, and J.W. Smith. Polymer particle shape independently influences binding and internalization by macrophages. *Journal of controlled release : official journal of the Controlled Release Society*. 147:408-412 (2010).
56. K. Park. Effect of shape and size of polymer particles on cellular internalization. *Journal of controlled release : official journal of the Controlled Release Society*. 147:313 (2010).
57. K.S. Chu, A.N. Schorzman, M.C. Finniss, C.J. Bowerman, L. Peng, J.C. Luft, A.J. Madden, A.Z. Wang, W.C. Zamboni, and J.M. DeSimone. Nanoparticle drug loading as a design parameter to improve docetaxel pharmacokinetics and efficacy. *Biomaterials*. 34:8424-8429 (2013).

58. Y. Fu and W.J. Kao. Drug release kinetics and transport mechanisms of non-degradable and degradable polymeric delivery systems. *Expert opinion on drug delivery*. 7:429-444 (2010).
59. M. Nischang, G. Gers-Huber, A. Audige, R. Akkina, and R.F. Speck. Modeling HIV infection and therapies in humanized mice. *Swiss medical weekly*. 142:w13618 (2012).
60. D.E. Mosier, R.J. Gulizia, P.D. Maclsaac, B.E. Torbett, and J.A. Levy. Rapid loss of CD4+ T cells in human-PBL-SCID mice by noncytopathic HIV isolates. *Science*. 260:689-692 (1993).
61. G. Hoffmann-Fezer, C. Gall, U. Zengerle, B. Kranz, and S. Thierfelder. Immunohistology and immunocytology of human T-cell chimerism and graft-versus-host disease in SCID mice. *Blood*. 81:3440-3448 (1993).
62. C.A. Hughes, M.M. Foisy, N. Dewhurst, N. Higgins, L. Robinson, D.V. Kelly, and K.E. Lechelt. Abacavir hypersensitivity reaction: an update. *Ann Pharmacother*. 42:387-396 (2008).
63. E. Dolgin. Long-acting HIV drugs advanced to overcome adherence challenge. *Nat Med*. 20:323-324 (2014).
64. W.R. Spreen, D.A. Margolis, and J.C. Pottage, Jr. Long-acting injectable antiretrovirals for HIV treatment and prevention. *Curr Opin HIV AIDS*. 8:565-571 (2013).

CHAPTER 2

HYPOTHESIS AND SPECIFICS AIMS

2.1. HYPOTHESES

We proposed that macrophage-targeted nanoformulations of Abacavir prodrugs will facilitate uptake, retention and antiretroviral efficacy in cultured monocyte-derived macrophages (MDM), and will improve pharmacokinetics, biodistribution, and pharmacodynamics efficacy in murine models of HIV-1.

Our lab has pioneered in developing long-acting NanoART that may facilitate patient compliance by permitting once weekly or bi-weekly dosing regimen. It has been reported that macrophage are the first cells pools that encounter HIV first, and play a critical role through the HIV prognosis. Also, the natural ability of macrophage to reside at the site of virus hideout i.e. lymph-nodes, spleen, liver etc. further aid the beneficial of homing the drug depot at the site of action. Thus we posit that macrophage-targeted drug delivery can improve the PK profile and render the biodistribution at right place, thus improve therapeutic efficacy while reducing off-target toxicity of drug. We tested this hypothesis in following two parts of the projects;

Project 1: A phosphoramidate prodrug of abacavir (P-ABC), was synthesized to improve the biological activities of the parent nucleoside. The idea is to increase intracellular nucleoside 5'-O-triphosphate levels by bypassing rate-limiting monophosphorylation. This would lead to decreased activity of the virus encoded reverse transcriptase. A prodrug could readily incorporate into poly(lactic-co-glycolic acid) (PLGA) nanoparticles and as a consequence affect the efficacy of long-acting P-ABC nanoformulations as measured by pharmacokinetics and pharmacodynamics (PK and PD) tests

Project 2: A myristic acid derived hydrophobic prodrug of ABC (M-ABC) was synthesized. M-ABC would then be loaded at high concentrations into a decorated polymer coating with targeting ligands aimed to improve biodistribution, drug half-life and antiretroviral efficacy in viral target CD4+ T cells and monocyte-macrophages. To this end we incorporated M-ABC into poloxamer (P407) then decorated the particle with folic acid. These modifications positively affect macrophage uptake and antiretroviral efficacy

For both projects, hypothesis will be tested under following specific aims;

Specific Aim 1: Synthesis, Characterization and Nanoformulation of Abacavir Prodrugs

The objective was to synthesize phosphoramidate prodrug (PABC) (project 1), and myristoylated prodrugs (MABC) (project 2) of Abacavir. The prodrugs were characterized using ¹H-NMR, FTIR and mass spectroscopy. Antiretroviral activity as measured by the EC₅₀ was compared amongst the PABC, M-ABC and free ABC in MDM. The prodrugs were nanoformulated using PLGA (project 1) and poloxamers (P407) or folate conjugate poloxamers (FA-P407) (project 2) as excipients. Nanoformulated prodrugs were characterized for physicochemical parameters such as; size, size distribution (PDI), surface charge, drug loading and stability.

These parameters are of key importance in determining their cell cytotoxicity and cell interactions. The folate coating integrity determines the macrophage target ability, and thus antiretroviral efficacy and *in vivo* PK/PD fate of nanoformulated prodrugs.

Specific Aim 2: *In Vitro* Characterization of Nanoformulated Prodrugs in MDM

The objectives of this aim were to (a) determine the uptake, retention and antiretroviral efficacy of nanoformulated prodrugs in MDM; (b) study the intercellular trafficking of nanoformulated prodrugs in MDM; and (c) to assess the cytotoxicity of nanoformulated prodrugs in MDM. The overarching goal of this aim was to develop superior nanoformulation for animal testing that can be extrapolated for human testing in near future.

Specific aim 3: PK and PD Characterization of Nanoformulated ABC Prodrugs in Wild Type Mice and in Murine Models of HIV-1.

Optimized nanoformulations for both prodrugs from aims 1 and 2 were evaluated in murine models of HIV/AIDS. With optimized formulations (a) the PK testing in Balb/cJ mice were assessed to determine drug levels in plasma and tissue, and (b) correlated to antiretroviral efficacy in HIV infected NOD/scid-gcnull (hu-PBL-NSG) mice. The formulations were administered parenterally to Balb/cJ and hu-PBL-NSG mice. The drug bioavailability and therapeutic end points were determined.

CHAPTER 3
CREATION OF AN ABACAVIR
NANOFORMULATED PHOSPHORAMIDATE PRO-
DRUG

3.1. INTRODUCTION

Abacavir (ABC) is a nucleoside reverse transcriptase inhibitor (NRTI) that is used in combination with non-nucleoside reverse transcriptase inhibitors (NNRTIs), protease inhibitors (PIs) and integrase strand transfer inhibitors (InSTIs), as components of a first line treatment regimen for human immunodeficiency virus (HIV) infection by the National AIDS Control Organization [1, 2]. Notably, the viral strains that are resistant to zidovudine or lamivudine are sensitive to ABC [3]. However, ABC is associated with a dose dependent hypersensitivity response linked to the HLA-B*5701 allele that can be fatal if therapy is not discontinued [4]. Inefficient phosphorylation of ABC into its active metabolite carbovir-5'-triphosphate (CBV-TP) compromises the overall efficacy resulting in required high therapeutic doses of ABC [5]. Metabolic studies of ABC revealed that adenosine phosphotransferase predominantly metabolizes ABC to ABC-monophosphate (ABC-MP), which is subsequently converted to carbovir-5-monophosphate (CBV-MP) by cytosolic deaminase. CBV-MP is then anabolized to CBV-TP by cellular kinases. CBV-TP is the biologically active metabolite that terminates DNA synthesis by inhibiting the virus-encoded reverse transcriptase (RT) [5]. However, ABC has been shown to be a poor substrate for adenosine phosphotransferase, resulting in inefficient conversion to the monophosphate derivative (ABC-MP) [6]. Monophosphorylation is, thus, the rate-limiting step in determining the efficacy of ABC. In fact, the efficacy of the majority of nucleoside analogs, not only ABC, is compromised by the inefficient first-step monophosphorylation. Stavudine (d4T), zalcitabine, didanosine and

gemcitabine are examples where relatively poor monophosphorylation severely compromises the efficacy of the drug [7-9].

To overcome such challenges, several attempts have been made to deliver phosphorylated nucleoside analogs directly into the infected target cells [10]. ProTide technology that generates phosphorylated nucleoside analogs (pronucleotides) is widely utilized to bypass the poor phosphorylation step of nucleosides. Pronucleotides are phosphorylated prodrugs in which a masked phosphate moiety is covalently linked to the hydroxyl group of the nucleosides. Masking of the phosphate moiety through a benzyl ring at one end, and a L-alanine methyl ester at the other end improves the hydrophobic nature of these compounds, and thus facilitate cellular entry of the phosphorylated prodrug [11]. The concept of ProTide technology was first introduced for cancer treatment in 1982 with the synthesis of the pronucleotide prodrug, cytosine arabinoside 5'-monophosphate [12]. The clinical efficacy of the antiviral pronucleotides of adefovir dipivoxil and tenofovir disoproxil was confirmed and the drugs approved by the FDA [13-15]. Several other antiviral and anticancer pronucleotide prodrugs are under clinical development [10]. It is important to know whether a pronucleotide prodrug of ABC can result in improvement of antiretroviral activity. McGuigan et al. [16] reported the first application of ProTide technology to ABC and observed that the anti-viral potency of the ABC pronucleotide was improved significantly (70-fold) in human T4 lymphocyte CEM cells.

Lack of sustained and effective viral suppression rests in the inability of drugs to specifically target HIV viral reservoirs [17] which include lymph nodes,

gut-associated lymphoid tissue (GALT), spleen, central nervous system (CNS) and central memory lymphocytes and myeloid cells contained within the lymphoreticular tissues [18-20]. Lack of achievement of optimal drug levels in these reservoir sites can lead to the establishment and perpetuation of viral sanctuaries, and thus treatment failure [21, 22]. We posit that development of an effective delivery scheme for nucleoside prodrugs to extend plasma drug half-life and facilitate drug delivery into HIV anatomical reservoirs would increase their therapeutic utility.

In this study, a pronucleotide prodrug of ABC (PABC) was synthesized and encapsulated into a lipid-PLGA based nanocarrier. The mixed lipid outer covering of the PLGA core enabled the sustained release of drug cargo over an extended period of time. Antiretroviral efficacy of PABC and nanoformulated PABC were evaluated in human macrophages and a humanized mouse model of HIV infection.

3.2. MATERIALS AND METHODS

3.2.1. Chemicals

Abacavir (ABC) sulfate, phenyl dichlorophosphate, L-alanine methyl ester hydrochloride salt and poly (D, L-lactide-co-glycolide; lactide:glycolide (75:25), mol wt 66,000-107,000) (PLGA) were purchased from Sigma-Aldrich (St. Louis, MO). ABC sulfate was titrated with sodium bicarbonate to convert it into free-base. DSPE-mPEG_{2k} (distearoyl-phosphatidylethanolamine-methyl-polyethylene glycol conjugate-2000), DSPC (1, 2-distearoyl-sn-glycero-3-phosphocholine) and DSPG (1, 2-distearoyl-sn-glycero-3-phosphoglycerol) were purchased from

CordenPharama (Cambridge, MA). Phosphate-buffered saline (PBS), Optima grade water and high performance liquid chromatography (HPLC) grade acetonitrile, methanol, dichloromethane (DCM) and tetrahydrofuran (THF) were purchased from Fisher Scientific (Fair Lawn, NJ). Rabbit anti-human antibodies to Rab5, Rab7, Rab11, and Rab14, and AlexaFluor 488 conjugated goat anti-rabbit IgG were purchased from Santa Cruz Biotechnology (Dallas, TX). A dry argon atmosphere was practiced to perform the chemical reactions. Flash silica gels (32-63 μm) from Dynamic Adsorbents Inc. (Norcross, GA) were used to perform flash chromatography. Reactions were monitored by thin-layer chromatography using precoated silica plates (F-254 (250 μm) from SiliCycle Inc; Quebec City, Quebec, Canada) and visualized using ninhydrin or KMnO_4 staining or UV fluorescence. Fluorescein-modified PLGA was synthesized as described [23]

3.2.2. Synthesis of PABC

Step 1. Synthesis of phenyl (methoxy-L-alaninyl) phosphorochloridate:

Phenyl (methoxy-L-alaninyl) phosphorochloridate was synthesized as previously described [16]. Briefly, phenyl dichlorophosphate (1 mol, 3.02 g) and L-alanine methyl ester hydrochloride salt (1 mol, 2.00 g) was suspended in anhydrous DCM, and cooled to $-80\text{ }^\circ\text{C}$. To this mixture, a pre-cooled ($-80\text{ }^\circ\text{C}$) solution of anhydrous trimethylamine (2 mol, 2.90 g) in DCM was added drop-wise, and the reaction was stirred and gradually warm to room temperature over 16 h under an inert argon atmosphere. The solvent was removed using a rotavap to yield a white solid that was resuspended into diethyl ether and filtered. The filtrate was

concentrated by rotavap to give colorless oil that was resuspended in anhydrous THF, and used without further purification for the subsequent coupling step.

Step 2. Coupling of phenyl (methoxy-L-alaninyl) phosphorochloridate with ABC. ABC (1 mol) was dried by azeotroping from anhydrous pyridine, then suspended in anhydrous THF and cooled to 0°C under argon. Tert-butylmagnesium chloride (2 mol, 1.0 M solution in THF) was added to the mixture and stirring was continued for 10 min. Phosphorochloridate (3 mol, solution in THF) was added drop-wise to the deprotonated ABC and the reaction was stirred for 90 h at room temperature. The reaction was then cooled to 0°C and quenched with aqueous saturated ammonium chloride solution. The solvent was removed under vacuum, and the pure prodrug was isolated and purified using silica column chromatography. PABC was characterized using FTIR and ¹H-NMR spectroscopy. FTIR spectra of PABC was recorded and compared with that of ABC using a UATR-2 FTIR spectrometer (PerkinElmer Inc. Waltham, MA). ¹H-NMR spectra were recorded on a Varian INOVA 500 spectrometer. ¹H-NMR data was recorded in ppm downfield using trimethylsilyl as an internal reference standard.

3.2.3. Human Peripheral Blood Cell Isolation and Culture

Human peripheral blood lymphocytes (hu-PBL) and monocytes were isolated by leukapheresis from HIV-1 and -2 and hepatitis seronegative donors, and purified by countercurrent as described previously [24]. For cellular uptake and antiretroviral efficacy studies monocytes were plated in 12-well culture plates at 1.5×10^6 cells / well and differentiated into macrophages (MDM) [25] by

culturing in DMEM with 1% glutamine, 10% heat-inactivated pooled human serum, 1000 U/ml MCSF, 10 µg/ml ciprofloxacin and 50 µg/ml gentamicin for 7-10 days. Human peripheral blood lymphocytes were used for animal reconstitution as described below.

3.2.4. Antiretroviral Activity of PABC

The antiviral activity of PABC and native ABC against HIV-1 were determined in MDM [5]. MDM were incubated with various concentrations of ABC or PABC for 60 min followed by infection with HIV-1_{ADA} at a multiplicity of infection (MOI) of 0.01 infectious viral particles/ cell for 4 h. The MDM were washed extensively with PBS to remove excess virus particles. The cells were incubated an additional 10 days in the presence of the same concentration of drug used before infection. Cell culture medium was changed every other day with replacement of equivalent drug containing media. At day 10 post infection, supernatants were collected and analyzed for HIV-1 reverse transcriptase (RT) activity [26].

3.2.5. Synthesis of Lipid-PLGA hybrid PABC Nanoparticles

PBAC-loaded nanoparticles (NPs) of a mixed lipid outer shell and biodegradable PLGA inner core were prepared using the single - emulsion solvent evaporation method [27] and designated as lipid-nanoPABC (L-NPABC). PLGA and PABC (weight ratio 4:1) were dissolved in 2 ml of DCM to constitute the oil phase of the single emulsion. For the aqueous phase DSPG, DSPE-mPEG_{2k}, and DSPC (weight ratio of 1:5:10) were dissolved in chloroform, followed by slow solvent evaporation and overnight drying in a vacuum

desiccator. The formed lipid film was hydrated with 8 ml phosphate buffer (10 mM; pH 7.4) followed by vigorous mixing with vortex. The oil phase was then added dropwise to the aqueous phase with stirring. The mixture was then cooled on an ice bath and sonicated using a probe sonicator (Cole Parmer, Vernon Hills, IL, USA) at 20% amplitude until the desired particle size of ~250 nm was achieved. The DCM from the emulsion droplets was evaporated using a Buchi Rotavapor (New Castle, DE). Unencapsulated drug and polymers were removed by centrifugation at 20,000 × g for 20 min. After washing three times, purified NP pellets were resuspended in 10 mM phosphate buffer (pH 7.4) with 0.2% w/v P407 poloxamer as cryoprotectant, followed by freeze-drying to obtain a fine powder. The control formulation without lipid outer covering was fabricated using 5% polyvinyl alcohol (PVA) (w/v) as an emulsifier, and designated as NPABC. Fluorescently labeled L-NPABC were fabricated in the same manner using a mixture of fluorescein-labeled PLGA and unlabeled PLGA at a weight ratio of 3:1. The dye-labeled PLGA was synthesized as reported [23].

3.2.6. Physicochemical Characterization of PABC Nanoparticles

3.2.6.1. Nanoparticle size and charge

Size, size distribution (PDI) and surface charge of drug loaded NPs were measured by dynamic light scattering (DLS) using a Malvern Zetasizer, Nano Series Nano-ZS (Malvern Instruments Inc, Westborough, MA). Nanoparticle suspensions were diluted with water to optimize mass intensity then vortexed.

3.2.6.2. Nanoparticle morphology

The morphology of drug loaded NPs was determined by scanning electron microscopy (SEM) on a Hitachi S4700 field-emission scanning electron microscope (Hitachi High Technologies America Inc, Schaumburg, IL, USA). Particle surface morphology and the outer shell lipid coating over the PLGA inner core were characterized by transmission electron microscopy (TEM) using a Hitachi H7500 Transmission Electron Microscope (Hitachi High Technologies America Inc, Schaumburg, IL, USA). For TEM analysis, the NP suspensions were diluted in Milli-Q water and placed onto a copper grid, and air-dried at room temperature. For contrast enhancement, one drop of a 2% aqueous solution of sodium phosphotungstate was used as a negative stain. The images were recorded under bright-field conditions with exposure times of 2 s, and an accelerating voltage of 200 kV.

3.2.6.3. Drug loading and encapsulation efficiency (EE)

The amount of drug encapsulated in the polymeric matrix was determined by high performance liquid chromatography (Waters Breeze HPLC system, Waters Inc., Milford, MA, USA). Freeze-dried NPs (1 mg) were sonicated in 50 μ l THF, diluted with 1 ml methanol, vortexed for 10 s, then centrifuged at 10,000 \times g for 20 min. The supernatant was further diluted in mobile phase (35:65 v/v; acetonitrile/ 10 mM KH_2PO_4), followed by filtration using a 0.2 mm PVDF syringe filter. The sample components were separated on a Kinetex reversed phase C-18 column ((5 μ m, 150 \times 4.6 mm), Phenomenex, Torrance, CA) using a flow rate of 1.0 ml/min. The column effluent was monitored at 220 nm. The percentage

drug loading was calculated as the weight percentage of PABC encapsulated in a given mass of lyophilized NPs. The EE was calculated as (actual amount of drug encased in NPs) / (initial amount of drug used in NPs preparation) × 100%.

3.2.6.4. In vitro nanoparticle drug release

The *in vitro* release profile of PABC from L-NPABC or NPABC was determined using dialysis [28]. Specifically, in triplicate the drug-loaded NPs were dispersed in 1 ml PBS (0.1 M, pH 7.4) and placed in a dialysis pouch (cellulose membrane, mw cut-off 10kDa) in 30 ml of PBS with stirring at 37 °C. At 0.5, 1, 2, 4, 8, 12 and 48 h, 100 µl of the PBS was collected with replacement of an equal amount of fresh PBS. PABC in the aliquot was quantified by HPLC as described above.

3.2.7. MDM Uptake of PABC Nanoformulations

Uptake of PABC nanoformulations and free PABC were determined in human MDM [29, 30]. MDM were incubated with 100 µM free PABC or L-NPABC for various times from over 24 h. At each time point, MDM were washed 3 times with PBS to remove excess NPs or free drug. MDM were scraped into 1 ml of fresh PBS then pelleted by centrifugation at 950 × g for 8 min. The cell pellet was reconstituted in 200 µl of methanol, probe sonicated for 10 sec followed by centrifugation at 20,000 × g for 10 min. The supernatant was analyzed for drug content using HPLC. Cytotoxicity of PABC or nanoformulated PABC was determined using MTT (3-(4, 5-dimethylthiazol-2-yl)-2, 5-diphenyltetrazolium bromide) [30]. Briefly, MDM were treated with 50, 100 and 200 µM free PABC or nanoformulated PABC for 24 h. Following washing with PBS, the MDM were

incubated with 200 μ l of MTT working solution (0.5 mg/ml diluted in MCSF free media) for 30 min at 37°C. Dimethyl sulfoxide (DMSO; 200 μ l/well) was added to the cells and incubated for 5 min at 25°C. The absorbance at 490 nm was measured using a SpectraMax M3 Microplate reader (Molecular Devices, Sunnyvale, CA, USA).

3.2.8. Antiretroviral Activity of Nanoformulated PABC

To determine antiretroviral activity of nanoformulated PABC, MDM were treated with 100 μ M native ABC, free PABC or L-NPABC for 8 h. MDM were then washed 3 times with PBS to remove excess drug or NPs. On day 1, 5, 10 or 15 following treatment, MDM were infected with HIV-1_{ADA} at a MOI of 0.01 infectious viral particles /cell for 18 h. HIV-1 RT activity was measured in culture medium on day 10 post infection to determine viral replication [26]. As a secondary determinant of viral infection HIV-1 p24 protein expression in the MDM was determined by immunostaining [31].

3.2.9. PABC Nanoparticle Subcellular Co-localization

To evaluate the subcellular trafficking of nanoformulated PABC, human monocytes (5×10^5 cells/ well) were cultured in an 8 well Lab-Tek II CC2 chamber slide and differentiated into macrophages as described previously [31, 32]. MDM were treated with 100 μ M CF633-labeled L-NPABC for 8 h. The cells were washed 3 times with PBS to remove excess NPs. The cells were fixed with 4% PFA for 30 min, permeabilized with 5% Triton-X in PBS for 15 min, and blocked with 5% BSA and 0.1% Triton-X in PBS for 15 min. The cells were washed with 0.1% Triton and incubated overnight at 4°C followed by 1 h at room

temperature with primary antibody (1:50 dilution) against endocytic compartments; early endosomes (Rab5; sc-28570), late endosomes (Rab7; sc-10767) and recycling endosomes (RAB11 and Rab14; sc-9020 and sc98610). The cells were washed with 0.1% Triton-X in PBS and incubated with corresponding AlexaFluor 488-conjugated secondary antibody for 90 min at room temperature. ProLong Gold anti-fade reagent with DAPI (4, 6-diamidino-2-phenylindole) was added and the slide cover slipped. Cells were imaged with an LSM 510 microscope using a 63X oil lens (Carl Zeiss Microimaging, Inc., Dublin, CA, USA).

3.2.10. Pharmacodynamics

For pharmacodynamics studies, 8-10 week old NOD/SCID/IL2R γ c^{-/-} (NSG) mice ~~were mice~~ were obtained from a University of Nebraska Medical Center (UNMC) breeding colony. Breeding colony maintenance and animal pharmacodynamics studies were conducted according to protocols approved by the University of Nebraska Medical Center Institutional Animal Care and Use Committee. For pharmacodynamics studies, the mice were reconstituted with 25×10^6 hu-PBL per mouse by intraperitoneal injection one week prior to treatment [33]. Following hu-PBL reconstitution, mice were treated with 100 mg/kg of native ABC or an equivalent ABC dose of L-NPABC. Twenty-four hours after drug treatment, mice were injected intraperitoneally with HIV-1_{ADA} using a 10^4 tissue culture infectious dose 50(TCID₅₀)/mouse. Mice were sacrificed on day 10 post-infection, and blood and tissues were collected for fluorescence-activated cell sorting (FACS), HIV-1p24 staining and viral load analysis. Blood

samples were collected into Ca²⁺-EDTA-coated tubes. The spleen cells were isolated at the time of sacrifice and suspended in PBS. The expression of human CD45, CD3, CD4 and CD8 immune markers was determined in blood and spleen cells using flow cytometry as previously described[34]. Splenic RNA was extracted using TRIzol (Invitrogen). Quantitative RT-PCR was conducted to determine the human CD45, mouse GAPDH RNA and HIV-1gag RNA levels. For HIV-p24 antigen staining, spleens were fixed in 10% neutral buffered formalin and paraffin embedded. Serial 5 µm thick sections were cut, mounted on glass slides, and stained with human leukocyte antigen HLA-DR (dilution 1:100) and mouse monoclonal antibodies for HIV-1p24 (1:10 dilution), respectively. The antimouse, polymer based horseradish peroxidase-conjugated DAKO envision system was used as a secondary antibody for detection of HLA-DR and HIV-1 p24 using 3, 3-diaminobenzidine (DAB). Mayer's hematoxylin stain was used as a nuclear counterstain. The images were visualized with a Nikon Eclipse E800 microscope using NIS-Elements and a 40X objective. The number of HLA-DR + and HIV-1p24+ cells per section were counted and expressed as the percentage of HIV-1p24+ cells per HLA-DR+ cells in a section.

3.3. RESULTS

3.3.1. PABC Synthesis and Characterization

A phosphoramidate prodrug of abacavir (PABC) was synthesized to improve the biological activity of the parent nucleoside. The goal was to increase intracellular nucleoside 5'-O-triphosphate levels by circumventing the rate-limiting monophosphorylation of ABC by phosphotransferase as previously reported [5].

This would lead to decreased activity of the virus encoded RT [16]. PABC was synthesized by derivatization of the native compound with an enzyme cleavable phosphorochloridate moiety (figure 3) following a previously reported method, [16]. The covalent linkage of phosphorochloridate to the 5'-O-hydroxyl group of ABC was confirmed by nuclear magnetic resonance, Fourier transform infrared spectroscopy and tandem mass spectrometry ($^1\text{H-NMR}$, FTIR and MS/MS). As shown in Figure 3.2 A, the multiplet at 7.1-7.4 ppm in the $^1\text{H-NMR}$ spectrum corresponds to five protons from the benzene ring of the derivatizing phosphate moiety. The singlet at 3.70 ppm and the two doublets at 1.38 ppm represent the three methyl ester protons and gamma protons from alanine on the phosphate group. Successful synthesis was validated by comparison of the FTIR spectra of PABC to that of native ABC (Figure 3.2 B). Peaks at 1739 cm^{-1} and 1208 cm^{-1} in PABC FTIR spectrum, corresponding to carbonyl (C=O) and phosphate group (P=O) stretching of the phosphochloridate moiety, confirmed the conjugation of phosphochloridate with the ABC molecule. The peaks at 1588 cm^{-1} in the PABC and ABC FTIR spectra corresponded to CH_2 stretching of the native aromatic ring. Additionally, the peaks at 1035 cm^{-1} and 1021 cm^{-1} in the ABC and PABC spectra correspond to NH_2 broadening of the parent compound. Infusion into a Waters Xevo TQS micro triple quadrupole tandem mass spectrometer confirmed a molecular mass ion of 528.2, which corresponds to ABC with one phosphochloridate modification (data not shown). The details for the $^1\text{H-NMR}$ spectrum are; (CDCl_3): 7.49 (2s, 1H), 7.1-7.4 (m, 5H), 6.05-6.15 (m, 1H), 5.87-5.93 (m, 2H), 5.82 (br, 1H), 5.49-5.55 (m, 1H), 4.88 (br, 2H), 4.13-4.29 (m, 2H),

4.0-4.1 (m, 1H), 3.70 (s, 3H), 3.10-3.22(m, 1H), 3.01 (br, 1H), 2.73-2.85 (m, 1H), 2.06 (br, 2H), 1.60-1.80 (m, 1H), 1.38 (2d, 3H), 0.80-0.90 (m, 2H), 0.63 (app s, 2H).

3.3.2. Antiretroviral Activity of PABC

The antiretroviral activity of PABC compared to native ABC was determined in human MDM. MDM were treated with various concentrations of PABC or ABC bracketing EC_{50} for ABC (100 nM) prior to and continuous with HIV-1_{ADA} infection [5]. The HIV RT activity was assessed in infectious culture medium collected on day 10 day post-infection [26]. As shown in Figure 3.3 the EC_{50} for antiviral activity of PABC was improved 10-fold compared to native ABC. The EC_{50} for the PABC was ~15 nM compared to 150 nM for the native ABC.

3.3.3. Preparation and Characterization of lipid-PLGA hybrid NPs

Lipid-PLGA hybrid NPs loaded with PABC (L-NPABC) were synthesized using a modified single emulsion solvent evaporation technique as described previously [35]. A mixed lipid outer shell consisting of a 10:5:1 weight ratio of DSPC: DSPE-PEG2k: DSPG was incorporated over the drug loaded PLGA inner core to sustain the release of loaded cargo (Figure 3.5). A 2:1 weight ratio of PLGA core to lipid shell was used. In contrast to its hydrophilic native counterpart (ABC), PABC was readily incorporated into PLGA NPs. The percentage drug loading using hydrophilic native ABC was less than 1% (data not shown). A control formulation, without the outer lipid layer, was synthesized using 5% PVA (w/v) as the emulsifier in the same manner as L-NPABC and designated as NPABC. NP size, charge and surface morphology were characterized by DLS,

SEM and TEM. Table 1 summarizes the characteristics of NPABC and L-NPABC. The narrow PDI displayed by the nanoformulations indicates a relatively homogenous particle distribution. Furthermore, the morphology of L-NPABC, as determined by SEM and TEM, was observed to be spherical and around 200 nm in size, correlating with the size measured by DLS (Figure 3.4A, 3.4B). Examination of surface morphology by TEM confirmed an outer lipid covering over a PLGA core, potentially contributing to the sustained release of encased cargo [36] (Figure 3.5). As shown in Figure 3.5, in contrast to NPABC, the lipid layer of L-NPABC enabled sustained release of PABC from the PLGA matrix. A burst release was observed during the first 1 h for NPABC with more than 50% of drug released, and more than 95% of PABC released in the first 8 h. In contrast only 20% of PABC was released in the first 1 h for L-NPABC and less than 50% of PABC was released during the first 8 h., The cumulative PABC release reached 65% on day 1 and 73.5% on day 2 for L-NPABC compared to 95.2% on day 1 and 99.4% on day 2 for NPABC. Based upon the sustained drug release and improved drug encapsulation L-NPABC was selected for further *in vitro* and *in vivo* studies.

3.3.4. Macrophage Uptake

MDM uptake of L-NPABC and free PABC was determined over 24 h. MDM were exposed to 100 μM free PABC or L-NPABC for various times and drug uptake was quantified using HPLC. As shown in Figure 3.6A, MDM uptake of PABC was maximum at 8 h for both free PABC and L-NPABC. At 8 h, the cell PABC levels for L-NPABC was $7.6 \pm 0.8 \mu\text{g}/10^6$ cells, which was 6-fold greater

than that for free drug ($1.2 \mu\text{g}/10^6$ cells). After 8 h, cell drug levels declined, and drug levels for L-NPABC and free drug at 24 h were 2.5 ± 0.3 and $0.32 \mu\text{g}/10^6$ cells, respectively.

3.3.5. Antiretroviral Activity of PABC Nanoformulations

To determine whether improved encapsulation and sustained release of PABC encased into L-NPABC would translate to improved antiretroviral activity compared to free PABC or native ABC, MDM were treated with $100 \mu\text{M}$ native ABC, free PABC or L-NPABC for 8 h. At day 1, 5, 10 or 15 post-treatment MDM were infected with HIV -1_{ADA}. HIV RT activity and HIV p24 antigen expression were assessed in infectious supernatant and adherent MDM on day 10 post-infection. Decreased RT activity in MDM treated with nanoformulated PABC revealed that L-NPABC consistently decreased antiretroviral activity compared to that of free ABC or PABC. The RT activity was not decreased in the supernatant collected from MDM treated with native ABC, indicating either no uptake or rapid clearance of the native drug. However, HIV replication in MDM was suppressed by 95% using native ABC treated 24 h after HIV-1 exposure indicating drug penetration into the cells (data not shown). HIV replication using free PABC was reduced by 100% at day 1 $40 \pm 5.4\%$ at day 5, and minimal to no inhibition at days 10 and 15. In contrast L-NPABC suppressed viral replication by 100% at days 1 and 5 and $78 \pm 3.5\%$ and $52 \pm 4.5\%$ at days 10 and 15, respectively (Figure 3.6B). HIV p24 antigen expression in adherent MDM was assessed at 10 day post infection to cross validate the results for RT activity. P24 antigen staining showed increased viral infection from days 1 to 15 in MDM treated with

free ABC or PABC, whereas minimal to no p24 antigen was detected in MDM treated with L-NPABC at all time points (Figure 3.6C).

3.3.6. Subcellular NPs Localizations

Sub-cellular localization of fluorescein-labeled L-NPABC was determined using confocal microscopy. The physicochemical parameters of the fluorescein-labeled L-NPABC were similar to that of the unlabeled nanoformulations (data not shown). MDM were treated with 100 μ M fluorescein-labeled L-NPABC for 8h. The cells were washed, fixed, and stained with Rab5, -7, -11, and -14 endolysosomal protein antibodies as described previously [31, 32]. Rab5 and Rab7 antibodies identified the early and late endosomal compartments, whereas Rab11 and Rab14 antibodies identified recycling endosomal compartments. As shown in Figure 3.7A, the L-NPABC was co-localized predominantly in recycling endosomal compartments (Rab11 and Rab14), and observed as a yellow punctate pattern throughout the cytoplasm and perinuclear cell regions in the merged images of green compartments and red NPs. The percent overlap between endosomal compartments and L-NPABC were determined using ImageJ software and JACoP plug-in. L-NPABC showed significantly greater co-localization with recycling endosomal compartments ($38 \pm 2.5\%$ and $45 \pm 1.5\%$; Rab11 and Rab14) than with early and late endosomal compartments ($17 \pm 1.4\%$ and $20 \pm 2.3\%$; Rab5 and Rab7) (Figure 3.7B).

3.3.7. Pharmacodynamics

Antiretroviral efficacy of L-NPABC compared to native ABC was assessed in hu-PBL reconstituted NSG mice. Reconstituted mice were given a single

subcutaneous injection of 50 mg/kg of native ABC or an equivalent ABC dose of L-NPABC. Mice were infected with HIV-1_{ADA} 24 h following treatment and viral replication was determined at day 10 post infection (Figure 3.8A). As a measure of HIV infection, the numbers of HIV-1 p24⁺ cells among HLA-DR⁺ cells were evaluated in paraffin-embedded spleen sections. As shown in Figure 3.8B, compared to the untreated HIV infected controls, ABC treatment did not elicit protection from viral infection. In contrast, mice treated with L-NPABC showed a significantly lesser percentage of HIV-1p24⁺ cells per HLA-DR⁺ cells in spleen compared to untreated mice or mice treated with native ABC (Figure 3.8C). HIV-1 infection results in a gradual decline of CD4⁺ T cells in hu-PBL reconstituted NSG mice [37-39]. Thus, as a measure of viral infection, the CD4⁺ /CD8⁺ T-cell ratios were determined using FACS analysis of spleen cells and blood cells collected at study termination. Decreased numbers of CD4⁺ T cells and CD4⁺ /CD8⁺ T-cell ratios were observed in spleens from mice infected with HIV-1 with no treatment or ABC treatment. However, the CD4⁺ /CD8⁺ T-cell ratios in spleens from mice treated with L-NPABC prior to HIV infection were not decreased. The CD4⁺ /CD8⁺ T-cell ratios in spleen from L-NPABC treated mice were significantly higher than in mice infected with HIV-1 with no treatment or ABC treatment and were comparable to those from uninfected control mice (Figure 3.8D). However, there were no significant differences in CD4⁺ /CD8⁺ T-cell ratios among treatments groups and uninfected control mice in blood (data not shown). We also measured HIV-1gag RNA levels in spleen by reverse transcriptase polymerase chain reaction (RT-PCR) assay. L-NPABC treatment

suppressed HIV-1gag gene expression in spleen to 5 -folds. In contrast, treatment with native drug did not suppress HIV-1gag expression (Figure 3.8E).

3.4. DISCUSSION

Pronucleotides of ABC have been synthesized by others and provided two therapeutic advantages; (i) the direct administration of ABC-MP improved the antiviral efficacy in human macrophages and T-lymphocytes by circumventing the rate-limiting phosphorylation step and (ii) the deamination of ABC to CBV was bypassed, eliminating the CBV-associated renal and cardiac side effects [5]. Thus, direct administration of ABC-MP not only improved antiviral efficacy, but also improved the safety profile of ABC. With these results in mind, we synthesized PABC with 54% final yield and validated the synthesis using ¹H-NMR, FTIR and mass spectrometry. The EC₅₀ for HIV suppression was reduced 10-fold in human MDM for PABC compared to native ABC (15 nM vs 150 nM, respectively). The improved antiviral potency of PABC compared to ABC is likely a consequence of the increased intracellular nucleoside 5-O'-triphosphate level, which is limited by inefficient monophosphorylation of native ABC, as has been observed previously. In particular, metabolite studies have revealed that the phosphorylated ABC prodrug is metabolized predominantly to its active metabolite CBV-TP with no detectable CBV formation [5].

Further optimization of the phosphorylated prodrug into an effective delivery system for long-term and targeted treatment of HIV was required. One such strategy would be to encapsulate the phosphorylated ABC prodrug into a polymeric nanocarrier to prolong drug half-life, improve pharmacodynamics and

facilitate drug delivery to restricted anatomical reservoirs of HIV-1 persistence [34, 40]. Lipid–polymer hybrid nanoparticles comprised of a polymer core (e.g., PLGA) and lipid/lipid-PEG shell have emerged as versatile carriers due to their unique composition, possessing both polymeric nanoparticle and liposomal characteristics [27]. PLGA, a biodegradable and biocompatible FDA approved polymer, is used to form the biodegradable core matrix, which is then wrapped by a shell of mixed lipids [41]. The PLGA core matrix encases the therapeutic payload, whereas the mixed lipid monolayer ensures higher encapsulation and sustained release of the encased drug [42].

In the present work we prepared PABC loaded PLGA/lipid hybrid nanoparticles to prolong the pharmacological activity of PABC. To demonstrate that the mixed lipid monolayer provided higher drug encapsulation and sustained release of loaded cargo a control PLGA formulation without the lipids outer-layer (NAMC) was synthesized using PVA. L-NPABC were slightly larger in size than NPABC (240 ± 12.0 nm and 208 ± 15.3 nm, respectively) likely due to the presence of the lipid layer on the surface of the PLGA core [27]. The highly negative ζ -potential of both nanoformulations provides electrostatic repulsion between the particles to reduce aggregation, and promote a relatively narrow size distribution [23]. Drug loading of both nanoformulations was less than 10%, however drug loading of the L-NPABC particles was slightly higher than for NPABC particles demonstrating that the benefit of the lipid monolayer shell. The higher loading can be attributed to formation of lipid vesicles that entrap a small amount of drug through hydrophobic interaction or hydrogen bonding [27]. L-

NPABC also provided a more sustained drug release than PABC presumably due to the presence of a lipid bilayer acting to reduce PABC diffusion from the PLGA core. In addition to the lipid outer-layer, the PEG shield delays enzymatic degradation of PLGA matrix [43]. SEM showed that L-NPABC were spherical in shape with smooth surfaces, and TEM revealed the smooth covering of the outer lipid layer over the PLGA inner core. These morphologies were similar to those reported previously for PLGA/lipid hybrid NPs [36].

Mononuclear phagocytes (MP; monocytes, MDM and dendritic cells) have been shown by our and others studies to serve as drug reservoirs and carriers. These cells can facilitate drug carriage through their mobility, therapeutic cargo encasements and ability to home to viral target sites. To determine the effectiveness of this cell-based system for PABC nanoparticle storage and delivery human MDM were used to evaluate uptake, antiretroviral efficacy and subcellular trafficking L-NPABC. Our results demonstrated that L-NPABC showed a significantly increased macrophage drug uptake compared to free PABC that was attributed to higher uptake of the nanoformulation via phagocytosis [44]. As a consequence of enhanced uptake of PABC, the L-NPABC nanoformulations exhibited superior antiretroviral activity compared to free PABC or native ABC as measured by HIV RT activity and HIV-1 p24 antigen staining. The antiviral activity was maintained for 15 days after drug loading using L-NPABC, in contrast to 5 days for free prodrug and no protection for native drug. Previous work in our laboratory has shown that storage of nanoformulated antiretroviral drugs in late or recycling endosomal compartments of MDM

provides protection from drug metabolism in the same subcellular organelles that harbor HIV, and promotes sustained release of the encased therapeutic cargo. Co-localization of HIV and drug carrier in similar subcellular organelles boosts the antiretroviral activity of the drugs [31, 45]. Based upon these studies we determined whether L-NPABC would be trafficked similarly. Our results showed significantly higher co-localization of the L-NPABC in recycling endosomal compartments (Rab11 and Rab14) compared to early endosomes (Rab5) or late endosomes (Rab7). These results reflected the prolonged antiviral activity of L-NPABC nanoformulations compared to native ABC or free PABC. Of importance, no cytotoxicity was observed in MDM at the concentration of L-NPABC nanoformulations or PABC used for these studies.

These results suggested that sustained drug delivery and improved antiretroviral activity could be expected *in vivo* using L-NPABC. To determine whether L-NPABC could attenuate viral replication *in vivo* an acute HIV infection humanized mouse model was used. Hu-PBL-NSG mice were treated subcutaneously with L-NPABC or native ABC at equivalent doses, 24 h prior to HIV-1_{ADA} infection. Ten days later HIV infection was determined using immunohistochemistry and RT-PCR. Our data demonstrated that mice treated with nanoformulated PABC showed less HIV-1p24 antigen in spleen compared to HIV positive controls and animals treated with ABC. ABC treatment did not provide protection from viral infection. Since, HIV-1 infection results in a gradual decline of CD4⁺ T cells in hu-PBL-NSG mice [37-39], we determined CD4⁺ and CD8⁺ T cell populations in the spleen and blood. Mice that were treated with free

ABC or not treated (HIV+ control) showed a significant loss in CD4+ T cells in spleen. In contrast, in mice treated with L-NPABC depletion in CD4+ T cells was prevented. In addition the CD4+ /CD8+ T-cell ratios of L-NPABC treated mice were significantly higher than in mice treated with free ABC or not treated. However, there were no significant differences in CD4+ /CD8+ T-cell ratios in blood between HIV-infected and drug treated, HIV-infected and non-drug treated and non-infected control mice (data not shown). This could be related to the higher numbers of T-cells in the spleen, a viral reservoir compared to the blood in addition to the limitations in immune restoration within the hu-PBL-NSG HIV mice model [40]. Such limitations could be overcome by using CD34+ hematopoietic stem cell humanized mice, a chronic model of HIV infection [40]. As an additional measure of HIV replication, we determined HIV-1gag RNA levels in spleen by RT-PCR analysis. We observed that L-NPABC treatment suppressed HIV-1 replication to a greater extent compared to free drug or no treatment. These findings together suggest that the lipid coating over the PLGA core provides sustained release of PABC to prolong therapeutic activity.

3.5. CONCLUSIONS

We demonstrate that a phosphorylated prodrug of ABC (PABC) has improved antiretroviral activity over the native drug. The improved lipophilicity of PABC facilitated the encasement of the prodrug into PLGA nanoformulations with reasonable drug loading. Notably, coating the prodrug within a lipid-modified polymer matrix provided improved MDM uptake, retention and antiretroviral efficacy. Nanoformulations localized to recycling endosomal compartments in

macrophages as has been previously observed for nanoformulated atazanavir and ritonavir [31]. Of importance, in a humanized mouse model of HIV infection, antiretroviral activity of PABC was extended over 10 days when encased into lipid-PLGA following a single SC dose.

3.6 SUMMARY

The quest amongst academics and pharmaceutical scientists in HIV/AIDS research to transform short-acting antiretroviral drugs into long-acting reservoir targeted medicines is substantive as the field aims to improve compliance while reducing viral resistance and toxicity. A means to achieve this end rests in manufacture of nanoformulated phosphoramidate prodrugs for nucleoside reverse transcriptase inhibitors as it would do all that as well as improve antiretroviral responses. Thus, we encapsulated phosphorylated abacavir (PABC) into mixed polymeric and lipid excipients to facilitate available intracellular nucleoside 5-O'-triphosphates by bypassing rate-limiting parent drug monophosphorylation. We also reasoned that a long-acting nanoformulated PABC (NPABC) would improve ABC pharmacodynamics (PD) profiles. Herein, PABC was successfully synthesized then characterized by ¹H-NMR and FTIR spectroscopy. PABC antiretroviral activities were compared to native ABC by assessment of its half maximal effective concentration⁵⁰. A—PABC was incorporated into a PLGA-lipid nanoformulation then assessed for structural stability, morphologic integrity, cytotoxicity, and attenuation of HIV-1 replication. The latter two were determined by viral p24 staining and reverse transcriptase activity. Pharmacokinetic profiling was performed in Balb/C mice after a singular

intramuscular injection. Preliminary pharmacodynamic evaluation was determined in human peripheral blood lymphocyte (hu-PBL) reconstituted NOD/scid-IL-2Rgc mice-infected with HIV-1_{ADA}. Results demonstrated that antiretroviral responses were operative for ten days after single administration of in monocyte-derived macrophages and 10 days NPABC activity in virus-infected mice. These data, taken together, support the idea that antiretroviral responses could be achieved through intracellular delivery of NPABC. The PLGA-lipid matrix protected the drug from rapid elimination over 10 day's period.

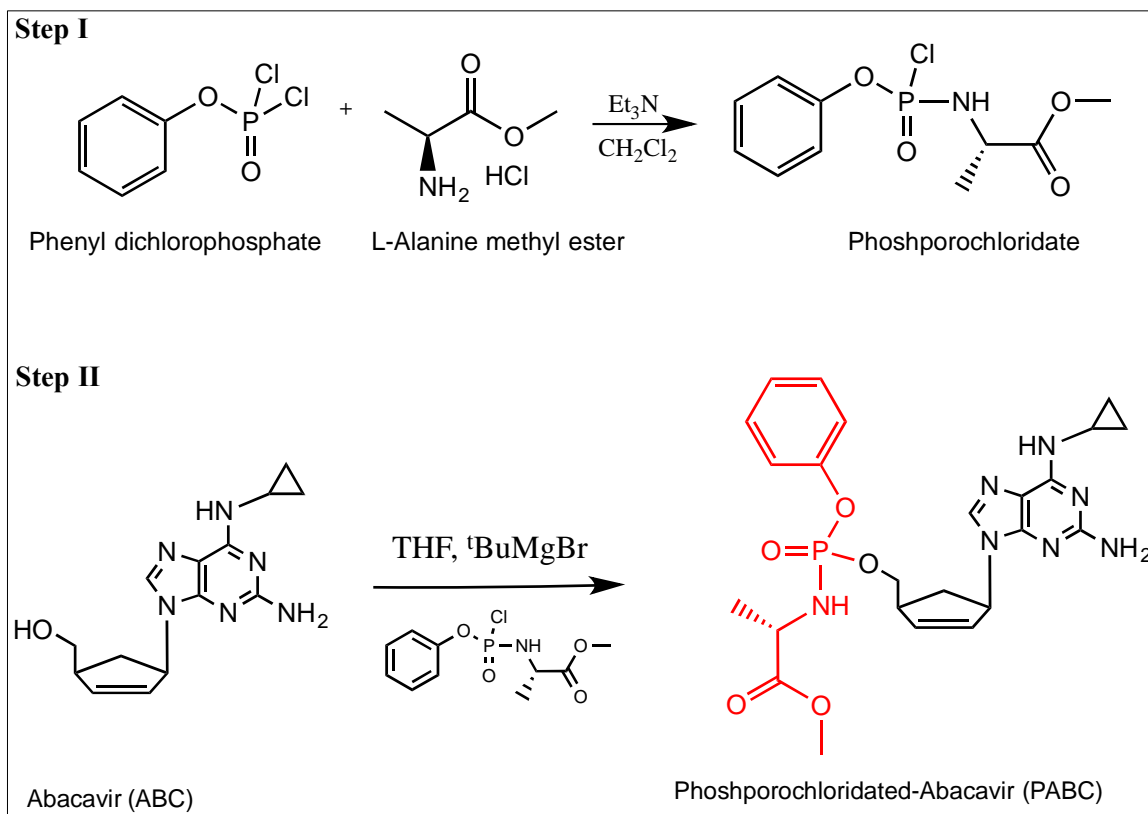


Figure 3.1. Synthesis of PABC. PABC was synthesized in two steps as illustrated at a final yield of 62%; Phosphorochloridate moiety was synthesized using phenyl dichlorophosphate and L-alanine methyl ester (step 1); followed by its coupling with ABC (step II) using tert-butylmagnesium chloride as base in THF.

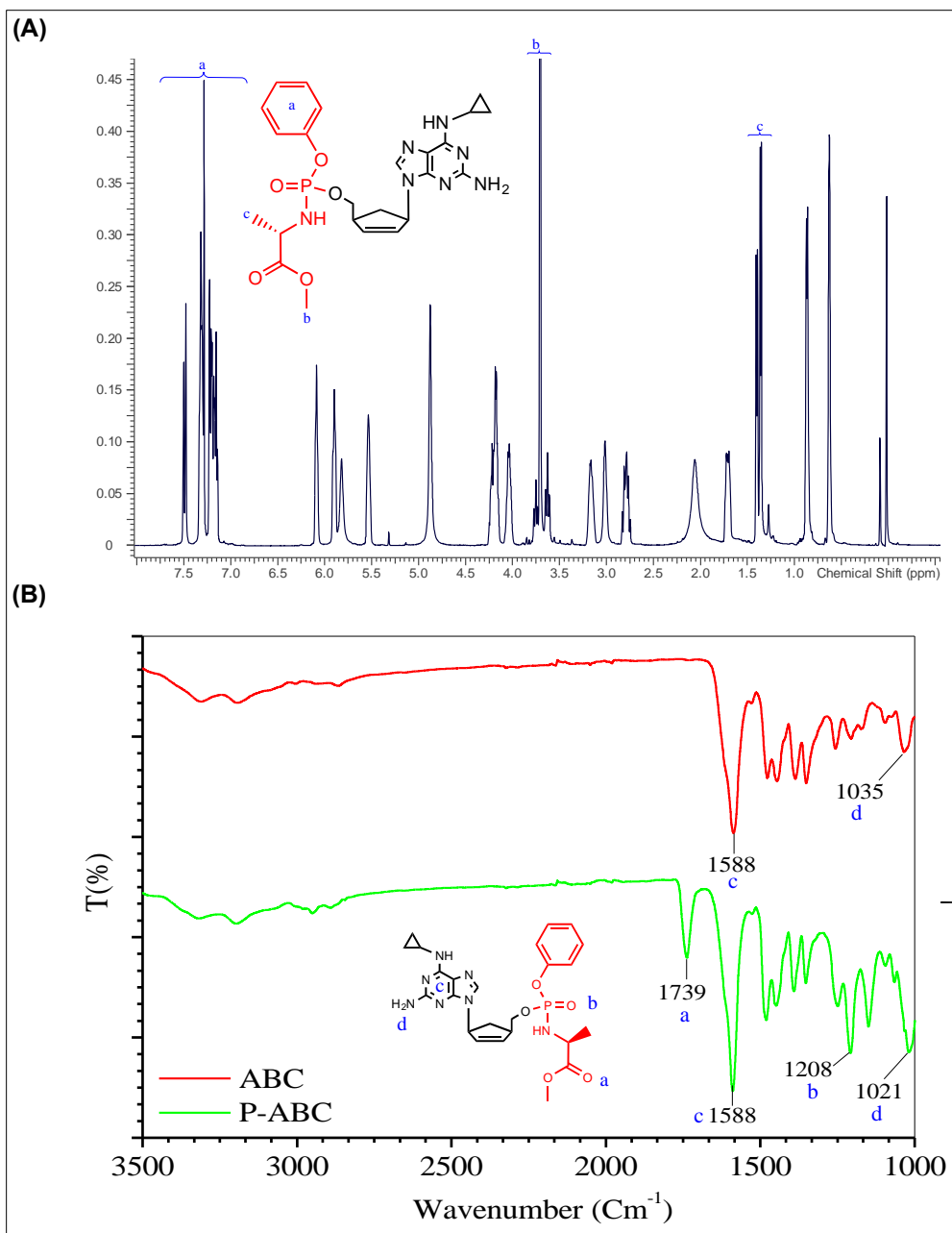


Figure 3.2. Characterization of PABC. The purified PABC was characterized using (A) the $^1\text{H-NMR}$ spectroscopy, which dictated the presence of a multiplet at 7.1-7.4 ppm corresponding to five protons from the benzene ring of the derivatizing phosphate moiety. The singlet at 3.70 ppm and two doublets at 1.38 ppm represent the three methyl ester protons and gamma protons from alanine on the phosphate group. (B) Peaks at 1739 cm^{-1} and 1208 cm^{-1} in the PABC FTIR spectrum correspond to carbonyl (C=O) and phosphate (P=O) stretching of the phosphochloridate moiety, whereas the peak at 1588 cm^{-1} in ABC and PABC spectra corresponds to CH_2 stretching of aromatic ring.

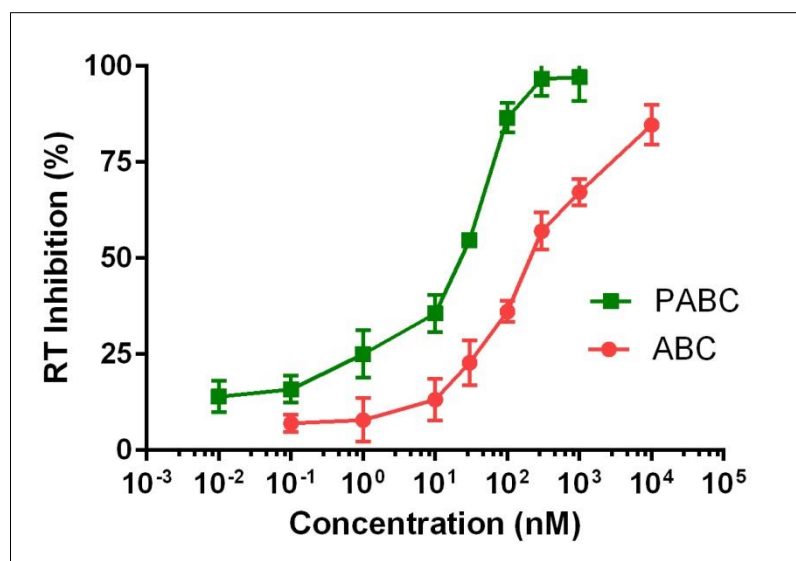


Figure 3.3. Antiviral activity of ABC and PABC against HIV-1_{ADA} in human monocyte derived macrophages (MDM). MDM were exposed to various concentrations of ABC or PABC for 60 min, followed by challenge with HIV-1_{ADA} at a multiplicity of infection of 0.01 infectious viral particles /cell for 4 h. HIV reverse transcriptase (RT) activity was measured on day 10 post infections. The EC₅₀ of PABC (~15 nM) was decreased about 10 -fold compared to native ABC (~150 nM)

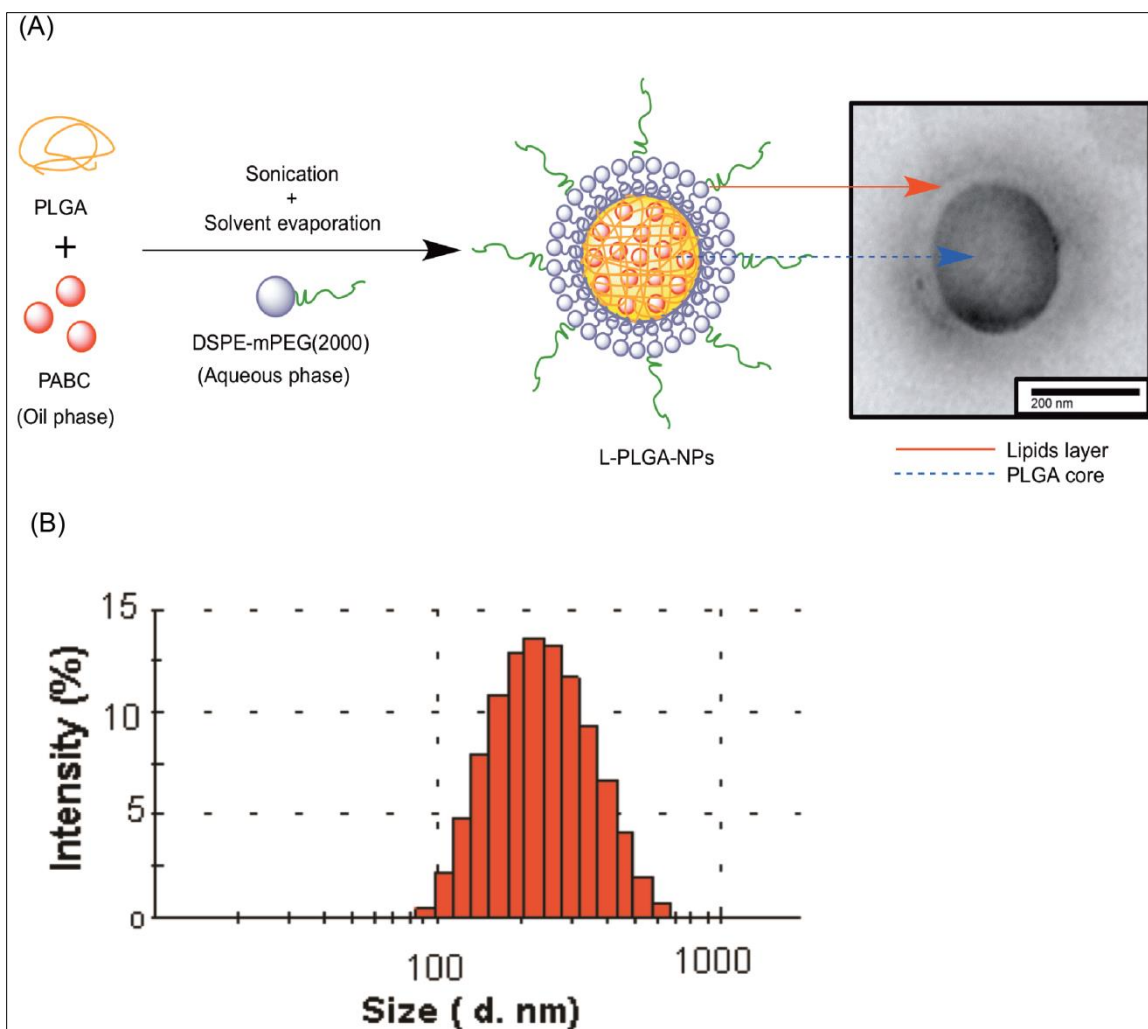


Figure 3.4. Synthesis and characterization of PABC loaded PLGA nanoparticles. (A) Drug encased nanoparticles of mixed lipid outer shell and biodegradable PLGA inner core were prepared using the single-emulsion solvent evaporation method. (B) PABC encased PLGA hybrid nanoparticles were of around 200nm in size as measured by dynamic light scattering.

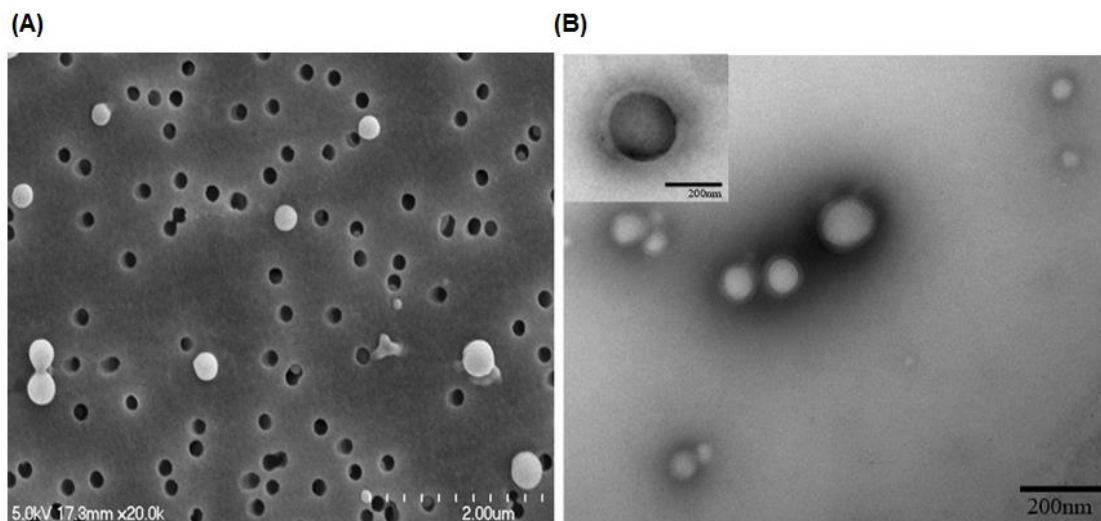


Figure 3.4. Morphological analysis of drug PLGA nanoparticles. Morphology of nanoparticles was measured using (A) SEM and (B) TEM analysis. Images of L-NPABC revealed morphology and surface coating of lipids respectively. The size of nanoparticles as measured by SEM and TEM are in accordance with DLS measurement.

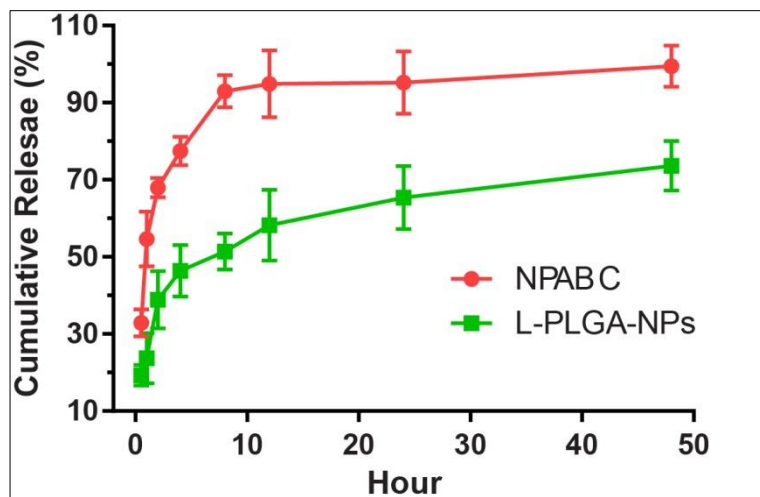


Figure 3.5. In vitro drug-release profile of PABC from PLGA matrix. The *in vitro* drug release of PABC was measured in Phosphate buffer (pH 7.4) at 37 °C. The cumulative drug PABC release from L-NPABC were measured and compared with NPABC (PLGA particles without lipid covering). At each time point 100 μ L of release media was collected with equal replacement of fresh media.

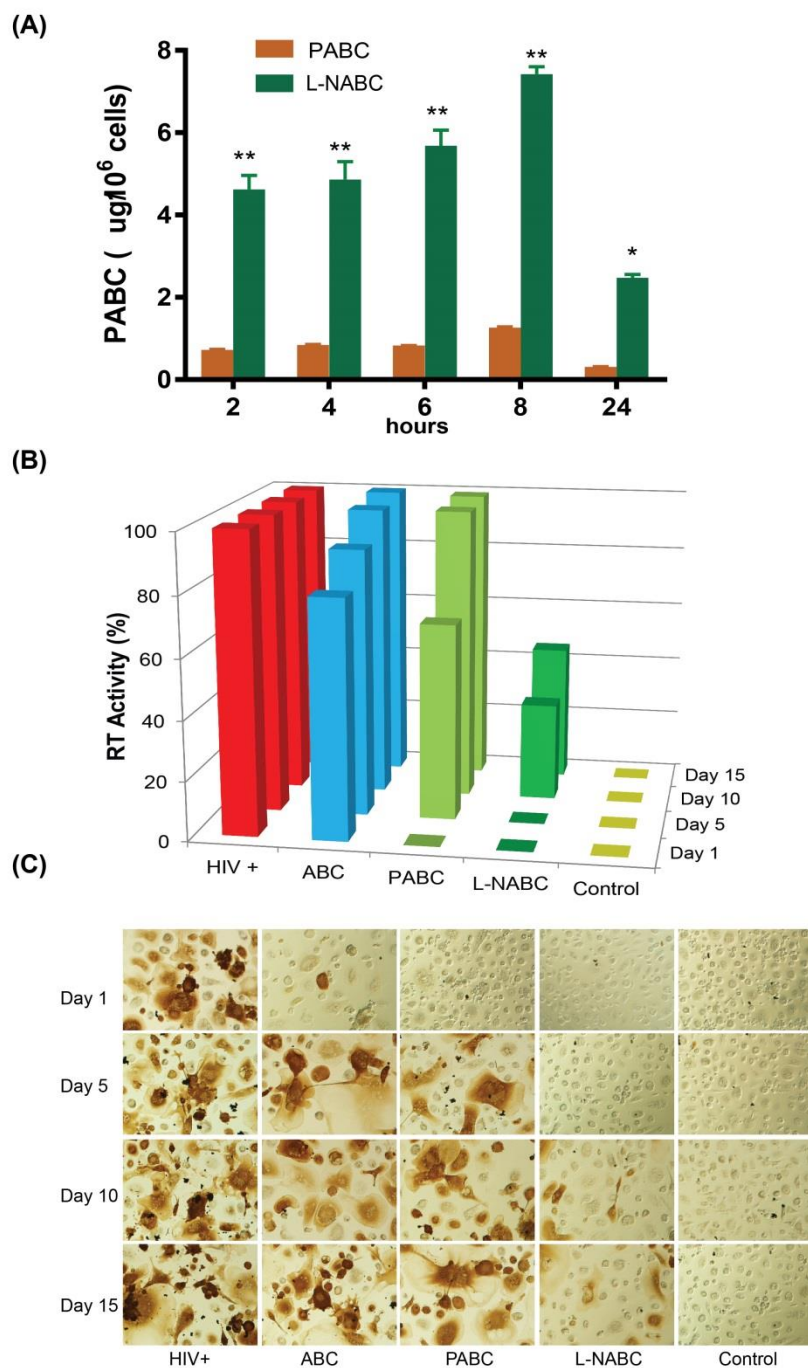


Figure 3.6. MDM uptake and antiretroviral efficacy of ABC, PABC and L-NPABC. (A) Drug and nanoformulation uptake was determined in MDM over 24 h following treatment with 100 μ M PABC or L-NPABC. Antiretroviral activity was determined in MDM treated with 100 μ M native ABC, free PABC or nanoformulated PABC for 8 h, then infected with HIV-1_{ADA} (MOI 0.1) at 1, 5, 10 or

15 days following drug loading. HIV replication was determined 10 days after infection by (B) HIV RT activity and (C) HIV p24 staining. For uptake studies, statistical differences were determined using Student's t-test (**P < 0.001 and *P < 0.05).

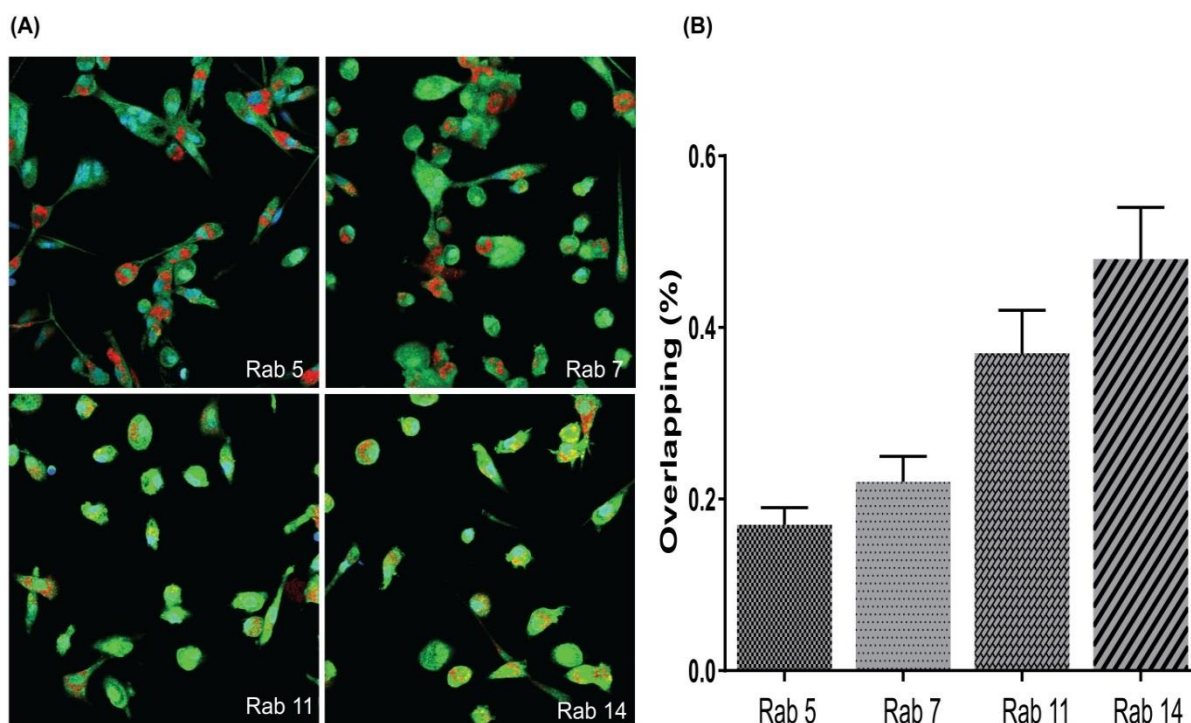


Figure 3.7. Subcellular localization of nanoformulated PABC in MDM. MDM cultured in 8 well Lab-Tek II CC² chamber slides were treated with 100 μ M fluorescein labeled L-NPABC for 8 h then fixed and stained with antibodies to Rab 5, 7, 11 and 14. (A) Co-localization is observed as a yellow punctate pattern throughout the cytoplasm and perinuclear cell regions in merged images of red NPs and green subcellular compartments. (B) Percent fluorescence overlap was quantitated using ImageJ software, and JACoP plug-in. Statistical differences were determined using Student's t-test (**P < 0.001 and *P < 0.05).

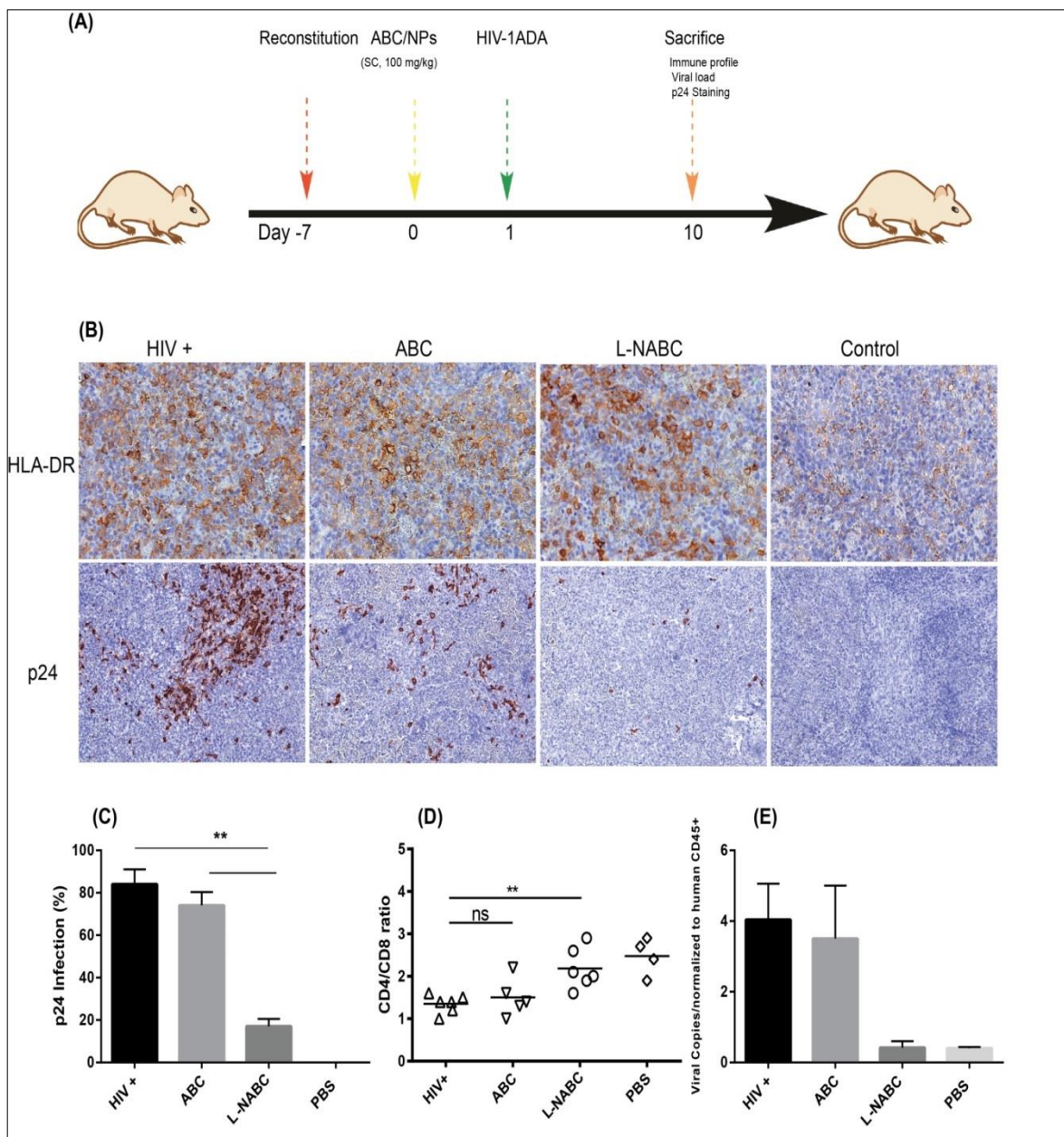


Figure 3.8. Antiviral activity of L-NPABC in hu-PBL-NSG mice. (A) Schematic illustration of *de/in vivo* study; antiretroviral response comparing nanoformulated PABC to free ABC was performed in HuPBL reconstituted NOD/scid-IL-2Rgc (NSG huPBL) mice-infected with HIV-1_{ADA}. Mice were subcutaneously injected with 100 mg/kg of ABC or equivalent dose using L-NPABC on day 1. Mice were infected with HIV-1_{ADA} one day later and scarified on day 10 post infection. (B) Spleens were collected on day 10 after infection, then sectioned and immunostained with antibodies specific for HLA-DR or HIV-1p24, and visualized

by DAB. (C) Number of HIV-1p24+ cells per section were counted and expressed as percent of HLA-DR+ cells. (D) Immune profiles (CD4+/CD8+ T cell ratios) were determined in spleen cells, and (E) HIV1gag RNA copies were measured in spleens cells and normalized to human CD45 expression as a human cell marker. Data are expressed as mean \pm SEM, and considered significant at $p < 0.001$ by student t-test.

3.8. REFERENCES

1. Adetokunboh OO, Schoonees A, Balogun TA, Wiysonge CS: Efficacy and safety of abacavir-containing combination antiretroviral therapy as first-line treatment of HIV infected children and adolescents: a systematic review and meta-analysis. *BMC infectious diseases* 15, 469 (2015).
2. Ibbotson T, Perry CM: Lamivudine/zidovudine/abacavir: triple combination tablet. *Drugs* 63(11), 1089-1098; discussion 1099-1100 (2003).
3. Wang LH, Chittick GE, Mcdowell JA: Single-dose pharmacokinetics and safety of abacavir (1592U89), zidovudine, and lamivudine administered alone and in combination in adults with human immunodeficiency virus infection. *Antimicrobial agents and chemotherapy* 43(7), 1708-1715 (1999).
4. Hughes CA, Foisy MM, Dewhurst N *et al.*: Abacavir hypersensitivity reaction: an update. *The Annals of pharmacotherapy* 42(3), 387-396 (2008).
5. Balzarini J, Aquaro S, Hassan-Abdallah A, Daluge SM, Perno CF, Mcguigan C: Improved antiviral activity of the aryloxymethoxyalaninyl phosphoramidate (APA) prodrug of abacavir (ABC) is due to the formation of markedly increased carbovir 5'-triphosphate metabolite levels. *FEBS letters* 573(1-3), 38-44 (2004).
6. Faletto MB, Miller WH, Garvey EP, St Clair MH, Daluge SM, Good SS: Unique intracellular activation of the potent anti-human immunodeficiency virus agent 1592U89. *Antimicrobial agents and chemotherapy* 41(5), 1099-1107 (1997).

7. Slusarczyk M, Lopez MH, Balzarini J *et al.*: Application of ProTide technology to gemcitabine: a successful approach to overcome the key cancer resistance mechanisms leads to a new agent (NUC-1031) in clinical development. *Journal of medicinal chemistry* 57(4), 1531-1542 (2014).
8. Balzarini J, Kang GJ, Dalal M *et al.*: The anti-HTLV-III (anti-HIV) and cytotoxic activity of 2',3'-didehydro-2',3'-dideoxyribonucleosides: a comparison with their parental 2',3'-dideoxyribonucleosides. *Mol Pharmacol* 32(1), 162-167 (1987).
9. Balzarini J, Herdewijn P, De Clercq E: Differential patterns of intracellular metabolism of 2',3'-didehydro-2',3'-dideoxythymidine and 3'-azido-2',3'-dideoxythymidine, two potent anti-human immunodeficiency virus compounds. *J Biol Chem* 264(11), 6127-6133 (1989).
10. Jordheim LP, Durantel D, Zoulim F, Dumontet C: Advances in the development of nucleoside and nucleotide analogues for cancer and viral diseases. *Nat Rev Drug Discov* 12(6), 447-464 (2013).
11. Serpi M, Madela K, Pertusati F, Slusarczyk M: Synthesis of phosphoramidate prodrugs: ProTide approach. *Curr Protoc Nucleic Acid Chem* Chapter 15, Unit15 15 (2013).
12. Rosowsky A, Kim SH, Ross J, Wick MM: Lipophilic 5'-(alkyl phosphate) esters of 1-beta-D-arabinofuranosylcytosine and its N4-acyl and 2,2'-anhydro-3'-O-acyl derivatives as potential prodrugs. *Journal of medicinal chemistry* 25(2), 171-178 (1982).

13. Agarwal K, Fung SK, Nguyen TT *et al.*: Twenty-eight day safety, antiviral activity, and pharmacokinetics of tenofovir alafenamide for treatment of chronic hepatitis B infection. *J Hepatol* 62(3), 533-540 (2015).
14. Sax PE, Wohl D, Yin MT *et al.*: Tenofovir alafenamide versus tenofovir disoproxil fumarate, coformulated with elvitegravir, cobicistat, and emtricitabine, for initial treatment of HIV-1 infection: two randomised, double-blind, phase 3, non-inferiority trials. *Lancet* 385(9987), 2606-2615 (2015).
15. Reddy KR, Matelich MC, Ugarkar BG *et al.*: Pradefovir: a prodrug that targets adefovir to the liver for the treatment of hepatitis B. *Journal of medicinal chemistry* 51(3), 666-676 (2008).
16. Mcguigan C, Harris SA, Daluge SM *et al.*: Application of phosphoramidate pronucleotide technology to abacavir leads to a significant enhancement of antiviral potency. *Journal of medicinal chemistry* 48(10), 3504-3515 (2005).
17. Chun TW, Moir S, Fauci AS: HIV reservoirs as obstacles and opportunities for an HIV cure. *Nature immunology* 16(6), 584-589 (2015).
18. Fois AF, Brew BJ: The Potential of the CNS as a Reservoir for HIV-1 Infection: Implications for HIV Eradication. *Current HIV/AIDS reports* 12(2), 299-303 (2015).
19. Massanella M, Fromentin R, Chomont N: Residual inflammation and viral reservoirs: alliance against an HIV cure. *Current opinion in HIV and AIDS* 11(2), 234-241 (2016).

20. Lorenzo-Redondo R, Fryer HR, Bedford T *et al.*: Persistent HIV-1 replication maintains the tissue reservoir during therapy. *Nature* 530(7588), 51-56 (2016).
21. Swenson LC, Min JE, Woods CK *et al.*: HIV drug resistance detected during low-level viraemia is associated with subsequent virologic failure. *Aids* 28(8), 1125-1134 (2014).
22. Li JZ, Paredes R, Ribaldo HJ *et al.*: Low-frequency HIV-1 drug resistance mutations and risk of NNRTI-based antiretroviral treatment failure: a systematic review and pooled analysis. *Jama* 305(13), 1327-1335 (2011).
23. Edagwa BJ, Guo D, Puligujja P *et al.*: Long-acting antituberculous therapeutic nanoparticles target macrophage endosomes. *FASEB J* 28(12), 5071-5082 (2014).
24. Meltzer MS, Gendelman HE: Effects of colony stimulating factors on the interaction of monocytes and the human immunodeficiency virus. *Immunology letters* 19(3), 193-198 (1988).
25. Dou H, Destache CJ, Morehead JR *et al.*: Development of a macrophage-based nanoparticle platform for antiretroviral drug delivery. *Blood* 108(8), 2827-2835 (2006).
26. Kalter SS, Heberling RL, Barry JD, Kuramoto IK, Holland PV, Sazama K: Detection of antibody to immunodeficiency viruses by dot immunobinding assay. *Journal of clinical microbiology* 30(4), 993-995 (1992).

27. Hu Y, Hoerle R, Ehrich M, Zhang C: Engineering the lipid layer of lipid-PLGA hybrid nanoparticles for enhanced in vitro cellular uptake and improved stability. *Acta Biomater* 28, 149-159 (2015).
28. Avgoustakis K, Beletsi A, Panagi Z, Klepetsanis P, Karydas AG, Ithakissios DS: PLGA-mPEG nanoparticles of cisplatin: in vitro nanoparticle degradation, in vitro drug release and in vivo drug residence in blood properties. *Journal of controlled release : official journal of the Controlled Release Society* 79(1-3), 123-135 (2002).
29. Balkundi S, Nowacek AS, Veerubhotla RS *et al.*: Comparative manufacture and cell-based delivery of antiretroviral nanoformulations. *International journal of nanomedicine* 6, 3393-3404 (2011).
30. Nowacek AS, Miller RL, Mcmillan J *et al.*: NanoART synthesis, characterization, uptake, release and toxicology for human monocyte-macrophage drug delivery. *Nanomedicine* 4(8), 903-917 (2009).
31. Guo D, Zhang G, Wysocki TA *et al.*: Endosomal trafficking of nanoformulated antiretroviral therapy facilitates drug particle carriage and HIV clearance. *Journal of virology* 88(17), 9504-9513 (2014).
32. Puligujja P, Mcmillan J, Kendrick L *et al.*: Macrophage folate receptor-targeted antiretroviral therapy facilitates drug entry, retention, antiretroviral activities and biodistribution for reduction of human immunodeficiency virus infections. *Nanomedicine* 9(8), 1263-1273 (2013).

33. Roy U, Mcmillan J, Alnouti Y *et al.*: Pharmacodynamic and antiretroviral activities of combination nanoformulated antiretrovirals in HIV-1-infected human peripheral blood lymphocyte-reconstituted mice. *The Journal of infectious diseases* 206(10), 1577-1588 (2012).
34. Puligujja P, Balkundi SS, Kendrick LM *et al.*: Pharmacodynamics of long-acting folic acid-receptor targeted ritonavir-boosted atazanavir nanoformulations. *Biomaterials* 41, 141-150 (2015).
35. Liu Y, Li K, Pan J, Liu B, Feng SS: Folic acid conjugated nanoparticles of mixed lipid monolayer shell and biodegradable polymer core for targeted delivery of Docetaxel. *Biomaterials* 31(2), 330-338 (2010).
36. Hu Y, Ehrich M, Fuhrman K, Zhang C: In vitro performance of lipid-PLGA hybrid nanoparticles as an antigen delivery system: lipid composition matters. *Nanoscale research letters* 9(1), 434 (2014).
37. Mosier DE, Gulizia RJ, Macisaac PD, Torbett BE, Levy JA: Rapid loss of CD4+ T cells in human-PBL-SCID mice by noncytopathic HIV isolates. *Science* 260(5108), 689-692 (1993).
38. Mosier DE: Distinct rate and patterns of human CD4+ T-cell depletion in hu-PBL-SCID mice infected with different isolates of the human immunodeficiency virus. *J Clin Immunol* 15(6 Suppl), 130S-133S (1995).
39. Poluektova LY, Munn DH, Persidsky Y, Gendelman HE: Generation of cytotoxic T cells against virus-infected human brain macrophages in a murine model of HIV-1 encephalitis. *J Immunol* 168(8), 3941-3949 (2002).

40. Dash PK, Gendelman HE, Roy U *et al.*: Long-acting nanoformulated antiretroviral therapy elicits potent antiretroviral and neuroprotective responses in HIV-1-infected humanized mice. *Aids* 26(17), 2135-2144 (2012).
41. Danhier F, Ansorena E, Silva JM, Coco R, Le Breton A, Preat V: PLGA-based nanoparticles: an overview of biomedical applications. *Journal of controlled release : official journal of the Controlled Release Society* 161(2), 505-522 (2012).
42. Colombo S, Cun D, Remaut K *et al.*: Mechanistic profiling of the siRNA delivery dynamics of lipid-polymer hybrid nanoparticles. *Journal of controlled release : official journal of the Controlled Release Society* 201, 22-31 (2015).
43. Cai Q, Shi G, Bei J, Wang S: Enzymatic degradation behavior and mechanism of poly(lactide-co-glycolide) foams by trypsin. *Biomaterials* 24(4), 629-638 (2003).
44. Nicolete R, Dos Santos DF, Faccioli LH: The uptake of PLGA micro or nanoparticles by macrophages provokes distinct in vitro inflammatory response. *Int Immunopharmacol* 11(10), 1557-1563 (2011).
45. Arainga M, Guo D, Wiederin J, Ciborowski P, Mcmillan J, Gendelman HE: Opposing regulation of endolysosomal pathways by long-acting nanoformulated antiretroviral therapy and HIV-1 in human macrophages. *Retrovirology* 12, 5 (2015).

Table 3.1. Physicochemical characteristics of NPABC and L-NPABC. Data represent mean \pm SD, n= 3.

Formulations	Particle	PDI	Zeta	Drug
NPABC ^b	208 \pm 17	0.18 \pm 0.05	-17.6 \pm 1.7	4.5 \pm 0.7
L-NPABC ^c	240 \pm 10	0.22 \pm 0.03	-21.6 \pm 2.7	7.5 \pm 0.4

^a Drug loading efficiency = (mg of PABC encapsulated in NP/ mg of lyophilized NP) \times 100.

^b NPABC = PABC-loaded within PLGA matrix

^c L-NPABC= PABC-loaded within PLGA matrix and coated with DSPC, DSPG and DSPE-PEG_{2k}

**CHAPTER 4. DEVELOPMENT AND
CHARACTERIZATION OF A LONG-ACTING
NANOFORMULATED ABACAVIR (ABC) PRODRUG**

4.1. INTRODUCTION

Treatment of human immunodeficiency virus (HIV) infection mandates early and lifelong treatment with combination antiretroviral therapy (cART) [1]. One impediment in reaching successful clinical outcomes is lack of adherence to cART drug regimens that serve to sustain reductions in viral load and maintain CD4+ T lymphocyte numbers [2, 3]. Maintaining cART drug levels is essential to protect susceptible cell populations and enable sustained antiviral responses to preclude the development of viral resistance [1]. Lack of achievement of LC/MS-I treatment outcomes rests in the inability of drugs to specifically target viral reservoirs [4]. These include gut-associated lymphoid tissue (GALT), lymph nodes, spleen, the central nervous system (CNS), and specifically central memory lymphocytes and myeloid cells contained within the lymphoreticular tissues [5-7]. Limitations in drug bioavailability have affected therapeutic outcomes [8]. All can lead to the perpetuation of viral sanctuaries and accelerate cART failures [9, 10]. We posit that the development of long-acting viral reservoir targeted nanoformulated ART (nanoART) can overcome such limitations while reducing drug toxicity and metabolism, improving drug targeting, and facilitating slow release of drug cell-carried cargos. These ultimately serve to improve antiretroviral drug pharmacokinetics (PK) and pharmacodynamics (PD) [11-15]. To such ends, our laboratory has pioneered the development of nanoART [16-19]. Our nanoformulations show further improvements in design through ligand surface engineering [13, 19] serving to facilitate uptake into virus target cells. Mononuclear phagocytes (MP; monocytes, macrophages and dendritic cells)

serve as drug carriers. These cells facilitate drug carriage through their mobility, rapid delivery, cargo encasements, and abilities to deploy drug to viral target tissues [20]. To such ends, the ability of nanoART to home drug depots to viral reservoirs represents notable advantages over conventional therapy [21]. This explains the need for an interdisciplinary program serving to encapsulate antiretroviral drugs into polymeric nanoparticles for MP drug delivery and enabling PK and PD testing [16, 17, 19, 22].

An obstacle toward success has been the difficulty in formulating the many available hydrophilic antiretroviral drugs into nanoparticles for parenteral administration. Thus, a platform was constructed to convert the drug abacavir (ABC) into a hydrophobic compound through esterification using myristic acid. Of interest, fatty acid analogues of myristic acid can inhibit N-myristoyltransferase, an enzyme that catalyzes myristoylation which is needed for activity of several proteins involved in the life cycle of HIV [23-27]. With this in mind, myristoylated ABC (called, MABC) was synthesized then formulated into nanosuspensions. This enabled the formation of hydrophobic drug crystals that were then placed into poloxamer-coated nanoparticles. Improved antiretroviral activity was observed for the modified ABC. Pro-longed antiretroviral activity was realized with the establishment of drug depots in Rab endosomes. Prolonged drug MP carriage and PK supports the opinion that MABC holds promise to extend the drug armamentarium for HIV/acquired immune deficiency syndrome (AIDS) therapy.

4.2. MATERIALS AND METHODS

4.2.1. Chemicals

ABC sulfate, myristic acid, poloxamer 407 (P407), folic acid (FA), and CF633-succinimidyl ester were purchased from Sigma-Aldrich (St. Louis, MO, USA). ABC sulfate was converted into free-base using sodium bicarbonate. The chemical reactions were performed under a dry argon atmosphere. Flash chromatography was performed using 32-63 μm flash silica gels from Dynamic Adsorbents, Inc. (Norcross, GA, USA). Reactions were followed by thin-layer chromatography on precoated silica plates (250 μm) F-254 from SiliCycle Inc (Quebec City, QC, Canada). The compounds were visualized by UV fluorescence or by staining with ninhydrin or KMnO_4 stains. High performance liquid chromatography (HPLC) grade methylene chloride, acetonitrile, methanol, dimethylformamide (DMF), LC/MS-grade water, and phosphate-buffered saline (PBS) were purchased from Fisher Scientific (Fair Lawn, NJ, USA). Rabbit anti-human antibodies to LAMP1, Rab7, Rab11, Rab14, and AlexaFluor 488 conjugated goat anti-rabbit IgG were purchased from Santa Cruz Biotechnology (Dallas, TX, USA). Folate-modified P407 (FA-P407) and CF633-modified P407 were synthesized as described [20].

4.2.2. MABC Synthesis

ABC (3.49 mmol, 1 equivalent) was dried by azeotroping from anhydrous pyridine, then suspended in anhydrous DMF and cooled to 0 °C under argon. Selective silylation of the 5-hydroxyl group of ABC was conducted by adding *tert*-butyldimethylsilyl chloride (TBSCl) (4.18 mmol, 1.2 equivalents) and imidazole

(5.23 mmol, 1.5 equivalents) to the suspension with continuous stirring for 16 h after which the desired silylated product was isolated by flash chromatography purification and characterized by proton nuclear magnetic resonance ($^1\text{H-NMR}$) spectroscopy. The amino group in the silylated ABC was then protected by reacting with methoxytriphenyl chloride (DMTr-Cl) (5.05 mmol, 2.2 equivalents) in anhydrous pyridine solvent to yield orthogonally protected ABC. Selective cleavage of the silyl group was achieved using tetra-*n*-butylammonium fluoride (4.87 mmol, 2.5 equivalents) to afford the free primary alcohol that was coupled with myristic acid (3.36 mmol, 2 equivalents) using 1-[Bis(dimethylamino)methylene]-1H-1,2,3-triazolo[4, 5-b]pyridinium 3-oxid hexafluorophosphate (HATU) (3.63 mmol, 2.2 equivalents) and *N,N*-diisopropylethylamine (DIEA) (8.26 mmol, 5 equivalents) in DMF. Finally, cleavage of DMTr using trifluoroacetic acid produced MABC after purification; $^1\text{H-NMR}$ spectrum specifics: R_f 0.38 (9:1 $\text{CH}_2\text{Cl}_2/\text{MeOH}$); $^1\text{H-NMR}$ (500 MHz, CD_3OD) δ 0.60-0.67 (br, 2H), 0.82-0.94 (m, 5H), 1.21-1.50 (br, 23H), 1.69-1.80 (m, 3H), 2.60-2.74 (br, 1H), 2.82 (t, $J = 8.6$ Hz, 1H), 2.85 (t, $J = 8.6$ Hz, 1H), 2.96-3.12 (br, 2H), 3.61 (dd, $J = 5.3, 10.8$ Hz, 1H), 3.68 (dd, $J = 5.3, 10.8$ Hz, 1H), 5.77-5.80 (br, 1H), 5.92-5.98 (m, 1H), 6.16-6.33 (m, 1H), 8.01 (s, 1H).

4.2.3. Antiretroviral Activity of MABC

Human peripheral blood monocytes were obtained from HIV-1 and -2 and hepatitis seronegative donors and purified using counter-current centrifugal elutriation [28]. The monocytes were cultured and differentiated into macrophages (MDM) using DMEM with 10% heat-inactivated pooled human

serum, 1% glutamine, 50 µg/ml gentamicin, 10 µg/ml ciprofloxacin and 1000 U/ml MCSF for 7-10 days [29]. The antiviral activity of native drug and prodrug against HIV-1 was determined in human MDM at day 10 post-infection as described [30]. Briefly, MDM were exposed to various concentrations of ABC or MABC for 60 min followed by challenge with HIV-1_{ADA} at a multiplicity of infection (MOI) of 0.01 infectious viral particles/cell. After 4 h of incubation, cells were washed three times with PBS to remove excess virus followed by incubation with the same concentration of drug used before infection. Cells were cultured for an additional 10 days with half media changes every other day with equivalent replacement of drug containing media. Supernatants were collected at day 10 after viral infection, and the level of viral replication was determined by HIV reverse transcriptase (RT) activity [31].

4.2.4. Nanoformulated MABC (NMABC)

Crystalline MABC was encased in poloxamer P407 (NMABC) using high-pressure homogenization (Avestin EmulsiFlexC3; Avestin, Inc., Ottawa, ON, Canada) [16, 19]. Briefly, a suspension of 1% (w/v) MABC and 0.5% (w/v) P407 in 10 mM HEPES buffer (pH 5.5) was premixed overnight at room temperature to generate drug containing polymeric micelles. Suspensions were then homogenized by high-pressure homogenization (20,000 PSI) until the desired particle size of ~250 nm was achieved. Folate-targeted nanoformulation (FA-NMABC) was prepared in an analogous manner from a premix of 0.5% polymer as FA-P407 and P407 (60:40% w/w) [20]. Crude nanoformulations were purified by differential centrifugation at 5000 × g for 5 min to remove aggregated

particles. Further centrifugation at 20,000 × g for 20 min was used to remove the free MABC and polymeric micelles. Purified nanoparticle pellets were resuspended in 10 mM HEPES buffer (pH 5.5) for physicochemical characterization and for *in vitro* and *in vivo* studies. To prepare CF633-P407 labeled nanoformulations, CF633-P407 and P407 were dissolved in methanol at a weight ratio of 1:5 [20, 32]. Methanol was then evaporated to generate a thin polymer film that was rehydrated using 10 mM HEPES buffer (pH 5.5) to yield a final excipient concentration of 0.5% (w/v). To this polymer solution, free MABC was added at a 1% (w/v) ratio. The suspension was protected from light and premixed at room temperature for 16 h. The suspension was homogenized and purified as described earlier for unlabeled formulations. CF633-labeled folate-targeted nanoformulations were prepared similarly where CF633-P407, P407, and FA-P407 were dissolved in methanol at a weight ratio of 1:2:2.

4.2.5. Physicochemical Characterizations of MABC and its Derivatives

MABC was characterized using ¹H-NMR and Fourier transform infrared (FTIR) spectroscopy. ¹H-NMR spectra were recorded on a Varian INOVA 500 MHz spectrometer (Varian, Inc., Palo Alto, CA, USA). ¹H-NMR data is reported in ppm downfield from trimethylsilyl as an internal standard. FTIR spectra were recorded using a Spectrum Two UATR-Two FTIR spectrometer (PerkinElmer, Inc. Waltham, MA, USA). Nanoformulations were characterized for their particle size, polydispersity index (PDI), and zeta potential by dynamic light scattering (DLS) using a Malvern Zetasizer, Nano Series Nano-ZS (Malvern Instruments, Inc., Westborough, MA, USA). The morphology of the nanoformulations was

examined by scanning electron microscopy (SEM) using a Hitachi S4700 field-emission scanning electron microscope (Hitachi High Technologies America, Inc., Schaumburg, IL, USA) [16]. Stability of the nanoformulation suspensions was assessed at room temperature (25 °C) and at 4 °C for a period of 8 weeks by measuring particle size and PDI by DLS. Drug loading, i.e. the weight percentage of MABC encapsulated in a given mass of lyophilized nanoformulation, was determined by UPLC-MS/MS (tandem mass spectrometry). To determine drug concentration in purified nanosuspensions, an aliquot of the nanosuspension was extracted using methanol and analyzed by UPLC-MS/MS [20].

4.2.6. Nanoparticle MDM Uptake and Retention

Uptake and retention of nanoformulations were determined in human MDM [16, 33]. Briefly, MDM were treated with nanoformulations at a concentration of 100 µM MABC. Cell uptake was assessed at different time points without any media changes. At each time point, adherent MDM were washed three times with 1 ml of PBS, scraped into 1 ml of fresh PBS and pelleted by centrifugation at 950 x g for 8 min. The cell pellet was reconstituted in 200 µl methanol and probe sonicated followed by centrifugation at 20,000 x g for 20 min. The supernatant was analyzed for drug content using UPLC/MS-MS.

To determine involvement of folate receptors (FOLR) in MDM uptake of the folate-targeted nanoformulation, cells were pre-incubated with 50 µM free folic acid for 60 min prior to treatment with 100 µM FA-NMABC. For cell retention studies, MDM were treated with 100 µM of nanoformulated MABC for 8 h; cells

were then washed with PBS to remove free drug or unincorporated nanoparticles, followed by further incubation in MCSF-free medium without nanoformulation. At days 1, 5, 10, and 15, cells were washed, collected, and analyzed for drug content as described for uptake studies. Cell viability was determined using 3-(4, 5-dimethylthiazol-2-yl)-2, 5-diphenyltetrazolium bromide (MTT) [16]. Briefly, MDM were treated with 10, 50, 100, and 200 μ M NMABC or FA-NMABC for 24 h. The adherent cells were washed with PBS, and 200 μ l of MTT working solution (0.5 mg/ml diluted in MCSF free media) was added to the cells followed by incubation at 37 °C for 30 min and washing with PBS. DMSO (200 μ l/well) was added to the cells and incubated for 5 min at 25 °C. The absorbance at 490 nm was measured using a SpectraMax M3 Microplate reader (Molecular Devices, Sunnyvale, CA, USA).

4.2.7. Antiretroviral Activity of MABC Nanoformulations

MDM were treated with 100 μ M MABC using free MABC or nanoformulations for 8 h. The cells were washed with PBS to remove excess free drug and nanoparticles. The MDM were challenged with HIV-1_{ADA} at a MOI of 0.01 infectious viral particles /cell for 18 h on day 1, 5, 10, and 15. Progeny virion production was measured by RT activity in culture medium [31]. HIV-1 p24 protein expression was assessed in adherent cells [32]. The cells were washed with PBS and fixed with 4% paraformaldehyde (PFA) for 15 min at room temperature. The cells were blocked using 10% bovine serum albumin (BSA) containing 1% Triton X-100 in PBS for 30 min at room temperature. Following blocking, cells were incubated with HIV-1 p24 mouse monoclonal antibodies

(1:50; Dako, Carpinteria, CA, USA) for overnight at 4 °C, followed by 1 h incubation at room temperature. HRP-labeled polymer anti-mouse secondary antibody (Dako EnVision® System; Dako, Carpinteria, CA, USA) was added (one drop/well). Hematoxylin (500 µl per well) was added to counterstain the nuclei, and images were captured using a Nikon TE300 microscope with a 20X objective.

4.2.8. MABC Nanoparticle Subcellular Localization

To determine subcellular localization of nanoformulated MABC, human monocytes were cultured in an 8 well Lab-Tek II CC2 chamber slide at a density of 5×10^5 cells/well and differentiated into macrophages as described previously [20]. MDM were treated with 100 µM of MABC using CF633-labeled NMABC or FA-NMABC for 8 h, washed with PBS, fixed, and stained using subcellular compartment antibodies [20, 32]. Briefly, cells were fixed with 4% PFA for 30 min at room temperature, permeabilized using 5% Triton-X in PBS for 15 min, and blocked with 5% BSA and 0.1% Triton-X in PBS. The cells were then incubated overnight at 4 °C for 1 h at room temperature with primary antibody (1:25 dilution in 5% BSA and 0.1% Triton-X in PBS) for respective endocytic compartments: late endosomes (Rab 7; sc-10767), recycling endosomes (RAB11 and Rab14; sc-9020 and sc98610), and lysosomes (LAMP1; sc-5570). The cells were washed extensively using 0.1% Triton-X in PBS and subsequently were incubated with secondary antibody conjugated with AlexaFluor 488 for 60 min at room temperature. The cells were covered with ProLong Gold anti-fade reagent with DAPI I (4,6-diamidino-2-phenylindole), cover slipped, and imaged with an

LSM 510 microscope using a 63X oil lens using an LSM 510 confocal microscope (Carl Zeiss Microimaging, Inc., Dublin, CA, USA).

4.2.9. PK Studies

Animal PK studies were conducted in accordance with the University of Nebraska Medical Center Institutional Animal Care and Use Committee (IACUC). Male Balb/cJ mice (Jackson Labs, Bar Harbor, ME, USA) were maintained on a folate deficient diet (Harlan Teklad TD.00434; Harlan Laboratories, Inc., Indianapolis, IN, USA) for two weeks prior to treatment and throughout the study. Mice were injected intramuscularly (IM) with 50 mg/kg ABC equivalents using native ABC, NMABC, or FA-NMABC in PBS. On days 1, 3, 5, 7, 9, 12, and 14 after drug treatment approximately 50 μ l blood was collected by cheek bleeding, and immediately 40 μ l was added into 1 ml of acetonitrile for drug analysis. Internal standard (IS; 10 μ l) was added to each sample and consisted of 0.665 μ g/ml d_4 -ABC, and 0.5 μ g/ml lopinavir. Samples were centrifuged at 17,000 x g for 10 min, and supernatants were dried using a ThermoScientific Savant Speed Vacuum (ThermoScientific, Waltham, MA, USA), reconstituted in 100 μ l of 80% v/v methanol in LC/MS- grade water, and 10 μ l was injected directly for MABC UPLC-MS/MS analysis. Thirty μ l of the reconstituted samples were diluted with 50 μ l water for ABC UPLC-MS/MS analysis. Final concentrations for both d_4 -ABC (IS for ABC) and lopinavir (IS for MABC) were 50 ng/ml. Standard curves of ABC or MABC were prepared similarly, in blood collected from control mice in the range of 0.35-3500 ng/ml and 0.125-1250 ng/ml, respectively. A Waters ACQUITY H-class UPLC system (Waters, Milford, MA, USA) connected to a

Waters Xevo TQS-micro mass spectrometer with electrospray ionization (ESI) source was used for drug quantitation. Chromatographic separation of 10 μ l ABC sample injections was achieved on an ACQUITY UPLC CSH C18 column (1.7 μ m, 100 mm x 2.1 mm) using a 13 min gradient of mobile phase A (7.5 mM ammonium bicarbonate in grade water, adjusted to pH 7 with glacial acetic acid) and mobile phase B (100% LC/MS- grade methanol) at a flow rate of 0.25 ml/min. The initial mobile phase composition was 10% B for the first 2.5 min and was gradually increased to 95% B in 6.5 min and held constant for 1.5 min. Mobile phase B was then reset to 10% in 0.45 min, and the column was equilibrated for 2.25 min before the next injection. MABC chromatographic separation was achieved using the same CSH C18 column and mobile phases but with a 16 min isocratic method using 81% mobile phase B and flow rate of 0.3 ml/min. ABC and MABC were detected at a cone voltage of 8V and 16 V, respectively, and a collision energy of 16 V and 30 V, respectively, in the positive ionization mode. Multiple reaction monitoring (MRM) transitions used for ABC, MABC, d₄-ABC, and lopinavir were 287.14 > 191.00, 497.18 > 191.07, 291.14 > 79.02, and 629.18 > 447.2 (m/z) respectively. Spectra were analyzed and quantified by MassLynx software version 4.1. All calculations were made using analyte peak area to internal standard peak area ratios.

4.2.10. Statistical Analyses

Drug uptake and retention data were analyzed by one-way analysis of variance (ANOVA) and Student's t-test using GraphPad Prism software (GraphPad Software, Inc., La Jolla, CA, USA). Confocal images were analyzed

as percent overlap using ImageJ software with JACoP plugin to quantify the amount of overlap between labeled nanoparticles and labeled endocytic compartments. Differences of mean percent overlap between nanoformulations were analyzed using Student's t-test. Experiments were performed three times unless otherwise specified. Animal studies were conducted with five animals per treatment group. Statistical analysis was performed by 2-way ANOVA and Bonferroni's Multiple Comparison test. Results are expressed as mean \pm standard error of mean. Results were considered significant at a p value < 0.05 .

4.3. RESULTS

4.3.1. MABC Synthesis and Characterization

In its native form, ABC has restricted intracellular and tissue penetrance [30, 34]. Its hydrophilic nature also poses challenges for nanoformulation preparations. To facilitate encapsulation of ABC into a poloxamer-stabilized nanosuspension, MABC, a hydrophobic prodrug of ABC, was synthesized. This was accomplished through derivatization of the native compound with a cleavable fatty acid ester (Figure 4.1). Covalent linkage of myristic acid to the 5'-O-hydroxyl group of ABC was confirmed by nuclear magnetic resonance, Fourier transform infrared spectroscopy and tandem mass spectrometry ($^1\text{H-NMR}$, FTIR and MS/MS). Specifically, the triplet at 2.36 ppm in the $^1\text{H-NMR}$ spectrum of MABC represents two fatty acid methylene protons adjacent to the carbonyl group linked to ABC, while the broad multiplet signal in the region of 1.21-1.50 ppm of the spectrum corresponds to 20 hydrogens of the repeating methylene units of the fatty acid chain (Figure 4.2A). This was confirmed by comparing FTIR

spectra of MABC to that of native ABC and myristic acid (Figure 4.2C). The presence of alkane stretching ($\text{CH}_2\text{-CH}_2$) peaks at 2915 cm^{-1} and 2850 cm^{-1} in the FTIR spectrum of MABC confirmed that the alkane chain of the derivatizing fatty acid (2913 and 2847 cm^{-1}) with the parent drug occurred. The peaks at 1595 cm^{-1} in MABC and 1588 cm^{-1} in the ABC FTIR spectra corresponded to CH_2 stretching of the native aromatic ring. Peaks at 1673 and 1696 cm^{-1} in MABC and myristic acid corresponded to C=O fatty acid attachments. The peak at 1033 cm^{-1} and 1030 cm^{-1} in ABC and MABC spectra corresponded to NH_2 broadening of the parent compound. Infusion into a Waters Xevo TQS micro mass spectrometer confirmed a molecular mass ion of 496.2 , which corresponds to ABC with one myristoyl group (data not shown).

4.3.2. Antiretroviral Activity of MABC

The antiretroviral activities of MABC and native drug were compared in MDM. Various concentrations of ABC or MABC bracketing the EC_{50} for ABC were added to MDM prior to and continued with $\text{HIV-1}_{\text{ADA}}$ infection [30]. Antiretroviral activity was determined by measuring RT activity in culture fluids collected 10 days after drug treatment and infection. The antiviral activity of MABC as determined by the EC_{50} for viral suppression was comparable to that of the parent drug ($\sim 100\text{ }\mu\text{M}$) (Figure 4.3).

4.3.3. Preparation and Physicochemical Characterization of the NMABC

Poloxamer nanoformulations of MABC were prepared by high-pressure homogenization as previously described [16, 18]. Nanoparticles in suspension were characterized by DLS and SEM. The physicochemical parameters of

NMABC and FA-NMABC nanoparticles were similar. The size, PDI, and zeta potential of NMABC nanoparticles were 160 ± 10 nm, 0.2 ± 0.1 , and -27.5 ± 2.5 mV, respectively. Similarly, the size, PDI and zeta potential of FA-NMABC nanoparticles were 170 ± 12 nm, 0.15 ± 0.04 , and -33.7 ± 3.7 mV, respectively. Relatively low PDI values displayed by the two nanoformulations indicated a narrow particle size distribution within the suspensions. Morphologically both NMABC and FA-NMABC were observed to be cylindrical rods of 200 nm in size as determined by SEM, correlating with particle size determined by DLS (Figure 4.4A & B). The stability of nanoformulations over time and temperature was assessed by measuring the NMABC particle sizes over a period of 8 weeks at 4 °C and 25 °C. During this time, the size and PDI did not change significantly at either of the two temperatures (Figure 4.4C & D), an indication that the nanoformulations remained stable for at least two months. Drug loading for NMABC and FA-NMABC nanoformulations was found to be 62 ± 1.5 and $65 \pm 2.4\%$ respectively. Lyophilized formulation powders were also characterized by magnetic resonance spectroscopy in DMSO. The presence of a singlet at 3.7 ppm in the $^1\text{H-NMR}$ spectrum of the formulation corresponds to the repeating methylene- units (next to oxygen) of the polymer. Peaks corresponding to the myristoylated prodrug protons were also evident in the formulation spectrum.

4.3.4. Nanoformulated Drug Uptake and Retention

To determine whether FOLR targeting would enhance MDM uptake and consequently retention of MABC, MDM were treated with 100 μM MABC using NMABC or FA-NMABC for up to 8 h. MDM uptake of nanoformulated MABC

increased over time and reached a maximum at 8 h. As shown in Figure 4.6A, an up to 2.5-fold increase in uptake was observed for FA-NMABC compared to NMABC. Cell MABC concentrations for FA-NMABC nanoformulations were 5.12 ± 0.2 , 11.3 ± 0.3 , 19.07 ± 1.2 , and $24.7 \pm 1.5 \mu\text{g}/10^6$ cells at 1, 2, 4, and 8 h, compared to 2.1 ± 0.1 , 3.5 ± 0.2 , 8.6 ± 1.2 , and $11.3 \pm 1.5 \mu\text{g}/10^6$ cells for NMABC formulations at the same time points. In order to deduce whether improved uptake of FA-NMABC was mediated by the FOLR, MDM were incubated with excess free folic acid ($50 \mu\text{M}$) prior to treatment. As shown in Figure 4.6A, blocking FOLR with excess folic acid decreased FA-NMABC uptake to levels similar to that of NMABC. Substantial (1.5 to 3 orders of magnitude) differences were observed in the extent of MABC retention in MDM over 15 days with FA-NMABC compared to NMABC, reflecting the initial enhanced uptake using the folate-targeted nanoformulation (Figure 4.6B). The uptake and retention of MABC using FA-NMABC was significantly greater than that observed for NMABC (Student's t-test, $**P < 0.001$). The concentration of nanoformulations used ($100 \mu\text{M}$) did not induce cell toxicity as determined by the MTT assay (data not shown).

4.3.5. Antiretroviral Activities of Nanoformulated MABC

To determine whether improved hydrophobicity of MABC and subsequent improved uptake and retention in MDM using MABC nanoformulations would translate into improved antiretroviral activity, MDM were treated with $100 \mu\text{M}$ native ABC, free MABC, NMABC or FA-NMABC for 8 h. Following treatment, MDM were challenged with HIV-1_{ADA} at an MOI of 0.1 on days 1, 5, 10, and 15

post-treatment. Decreased RT activity in infectious supernatants collected on day 10 post-infection revealed that FA-NMABC exhibited enhanced antiretroviral activity compared to NMABC or free MABC (Figure 4.7A). RT activity was not decreased in supernatants collected from MDM treated with native ABC, suggesting either no uptake or rapid metabolism of the native drug. However, native ABC suppressed HIV RT activity by 100 and 95% when cells were treated 12 and 24 h after HIV-1 exposure (data not shown). HIV replication using FA-NMABC was suppressed by $100 \pm 2.3\%$ at days 1 and 5 and by $88 \pm 3.4\%$ and $70 \pm 2.5\%$ at days 10 and 15; whereas, NMABC suppressed viral replication by $100 \pm 1.5\%$, $78 \pm 1.7\%$, $72 \pm 3.5\%$, and $52 \pm 4.5\%$ at days 1, 5, 10 and 15, respectively. Minimal or no inhibition was achieved using free MABC (Figure 4.7A). RT activity was cross-validated by evaluating HIV-1 p24 antigen expression in adherent MDM 10 days post-infection. MDM treated with free MABC or NMABC showed increased viral infection from days 1 to 15, as observed by the intensity of brown staining of p24 antigen; whereas, minimal to no p24 antigen was detected in MDM treated with FA-NMABC measured at all time points (Figure 4.7B).

4.3.6. Subcellular Nanoparticle Localizations

Sub-cellular localization of the nanoformulations taken up by MDM was assessed using confocal microscopy. MDM were treated with $100 \mu\text{M}$ CF633-labeled NMABC or FA-NMABC for 8h. Physicochemical parameters for CF633-labeled nanoformulations were similar to that of unlabeled nanoformulations (data not shown). After incubation, cells were washed, fixed, and stained with

antibodies to endosomal compartments as described [20, 32]. Rab7 antibody identified the late endosomal compartments, Rab11 and Rab14 antibodies identified compartments involved in recycling, and LAMP1 (lysosomal-associated membrane protein 1) antibody identified the lysosomal compartments. Co-localization was seen as a yellow punctate pattern throughout the cytoplasm and perinuclear cell regions in the merged images of red nanoparticles and green compartments. For both nanoformulations co-localization was found predominantly in recycling endosomes compared to late endosomal and lysosomal compartments (Figure 4.8A). Percent overlap between endosomal compartments and nanoformulations, as determined using ImageJ software and JACoP plug-in, showed greater co-localization of nanoparticles with recycling endosomal compartments ($46 \pm 2.4\%$ and $62 \pm 1.5\%$, Rab11 and Rab14 for NMABC; 70 ± 1.7 and 79 ± 4.3 , Rab11 and Rab14 for FA-NMABC) than with lysosomal and late endosomal compartments ($27 \pm 1.8 \%$ and $36 \pm 2.3 \%$, LAMP1 and Rab7 for NMABC; 34 ± 3.2 and 64 ± 2.8 , LAMP1 and Rab7 for FA-NMABC) (Figure 4.8B). FA-NMABC exhibited significantly greater co-localization with all compartments compared to NMABC (* $P < 0.05$).

4.3.7. PK Studies

To determine whether improved hydrophobicity and encapsulation of MABC into poloxamer nanoformulations would translate into sustained blood ABC drug levels *in vivo*, mice were injected IM with 50 mg/kg of native ABC or an equivalent ABC dose as NMABC or FA-NMABC. Mice have approximately 10-fold higher free folate levels than humans, and excess folate may block the

FOLR and interfere with rapid uptake of FA-targeted nanoformulation [35]. Thus, prior to treatment, mice were placed on folate-deficient diet for 2 weeks to reduce plasma folate levels [18]. For ABC and MABC analysis, whole blood was collected immediately into acetonitrile to inhibit the activity of esterases, which would cleave the myristoyl group from MABC, and adenosine deaminase, which could convert ABC to carbovir [30]. ABC blood levels measured at days 1, 3, 5, 7, 9, 12, and 14 post treatments were significantly higher in mice treated with FA-NMABC compared to those treated with NMABC or native ABC. MABC was lower than the limit of quantitation (< 0.125 ng/ml) in all samples, indicating rapid conversion of the MABC to ABC in blood. By day 14, ABC blood levels were 36 ± 4.7 ng/ml, 21 ± 3.8 ng/ml, and below the limit of quantitation (0.5 ng/ml) in mice treated with FA-NMABC, NMABC and native drug, respectively (Figure 4.9).

4.4. DISCUSSION

Currently, the nucleoside reverse transcriptase inhibitor ABC is recommended as a component of a first line treatment regimen by the National AIDS Control Organization [36]. In combination with two other NRTIs, for example, zidovudine and lamivudine (3TC) such as Trizivir, it is part of a three-drug antiretroviral regimen [36, 37]. Notably, viral strains that are resistant to zidovudine or 3TC can be sensitive to ABC [38]. However, ABC is associated with a dose dependent hypersensitivity response that may lead to death if therapy is not discontinued, and patients must be pre-screened for the HLA-B*5701 allele [39]. ABC can be used as an alternative to Truvada in pre-exposure prophylaxis (PrEP) drug regimens used in the management of HIV-1

transmission [40, 41]. Trizivir and other combination therapies lead to decreased viral resistance and improved long-term survival. Currently, ABC, 3TC, and dolutegravir are recommended as the most effective ART regimen [42]. However, the short half-lives of the current regimens and the intrinsic physicochemical properties of these antiretroviral drugs have limited their utilities and hence demonstrate the need for long acting delivery platforms that can improve patient adherence and facilitate drug entry into restricted anatomical reservoirs of HIV-1 persistence [15]. While progress has occurred towards developing long acting nanoformulations for protease and non-nucleoside RT inhibitors [16, 19, 20, 43] development of nanoformulations of hydrophilic drugs has remained elusive. Attempts have been made to encapsulate ABC into polymeric nanomedicines but poor loading and fast release kinetics have hampered their clinical applicability [44].

To overcome such challenges, a carboxylic acid ester prodrug approach has been widely used to improve lipophilicity and oral absorption of nucleoside analogs [23, 45]. In this approach, a carboxylic acid containing hydrophobic alkyl chain is reacted with the hydroxyl group located at the five membered ring moiety of the nucleoside analog. Even though the carboxylic acid ester prodrug approach has been used to modify a variety of anticancer compounds [46, 47] and antiviral drugs [48], development and nanoformulation of hydrophobic derivatives of antiretroviral drugs such as 3TC and ABC remain elusive. The goal of the present study was to improve the half-life and therapeutic efficacy of ABC through derivatization of the highly water soluble parent drug with a hydrophobic

fatty acid side chain to generate a myristoylated prodrug that would be easily encapsulated into polymer excipients and other surfactants to target macrophages. The 5-hydroxyl group on the cyclopentene moiety of ABC was esterified with myristic acid, a 14 carbon chain fatty acid. MABC was successfully synthesized at a final yield of 66% after purification and characterized using ¹H-NMR and FTIR spectroscopy. In the cell, MABC was converted to ABC by esterase cleavage followed by phosphorylation to produce the therapeutically active compound [30]. The success of such a strategy has been shown for CP-4126, a fatty acid prodrug of gemcitabine, which upon cleavage by esterases resulted in a 200-fold increase in therapeutic activity [46]. Our results demonstrated that prodrug synthesis does not impair the antiretroviral activity of parent ABC, as determined by RT activity.

Over the past decade, work from our laboratory has demonstrated the potential of targeted nanoART to produce sustained high plasma and tissue drug concentrations for weeks following a single IM administration that can suppress ongoing viral replication and mitigate dose associated viral resistance [17, 19]. In this context, nanoART was manufactured using folate-conjugated P407 that targets the FOLR2 expressed on activated macrophages [20]. Macrophage activation and subsequent overexpression of FOLR2 can be induced by folate-conjugated therapeutics [49]. Our results demonstrated that P407 and FA-P407 coating of MABC produced stable nanoformulations of similar physicochemical parameters. The drug loadings for both nanoformulations were high (62-65% w/w), which offers the advantage of administering a dose with less non-active

excipients. Since the geometry of nanoparticles plays an important role in determining attachment to the macrophage surface [50], the morphology of the MABC nanoformulations was analyzed using SEM. Our results demonstrated that the morphology for both NMABC and FA-NMABC nanoparticles was cylindrical rods, which is advantageous in terms of macrophages uptake. The mechanism reflects the preference of macrophages for engulfment of most bacteria that have a rod shaped geometry in nature [51].

In the case of folate targeting, receptor-mediated endocytosis occurs through interaction of folic acid moieties present on FA-nanoART with FOLR present on the macrophage surface [20]. Our results demonstrated that FA-NMABC nanoformulations showed a significantly increased macrophage uptake through binding to the FOLR compared to non-targeted NMABC. Indeed, folate-mediated uptake was cross validated by the inhibition of FA-NMABC uptake by blocking the FOLR with excess free folic acid (Figure 4A). When FOLR were blocked, the uptake of FA-NMABC by MDM was significantly decreased to a level similar to that for NMABC demonstrating that the superior uptake of folate nanoformulations occurred through engagement of the FOLR. Consequently, the amount of MABC that was retained in MDM using FA-NMABC was greater compared to that for NMABC nanoformulations (Figure 4B). MDM retained more than 2-fold greater levels of FA-NMABC than NMABC over a period of 15 days. As a consequence of enhanced uptake and retention of MABC, the FA-NMABC nanoformulations exhibited superior antiretroviral activity compared to NMABC nanoformulations as measured by RT activity and HIV-1 p24 antigen staining

(Figure 4C & D). The protection of MDM from HIV-1_{ADA} infection was observed for 15 days using folate-targeted nanoformulations, in contrast to reduction in protection by 5-10 days for non-targeted formulations and free drug. Thus, sustained drug delivery and improved antiretroviral activity of MABC might be expected *in vivo* using folate-coated nanoformulations. In addition, no cytotoxicity was observed in MDM at the nanoformulations concentration tested.

Our laboratory demonstrated previously that storage of nanoART in late or recycling endosomal compartments provides a protected environment for the encased cargo in the same subcellular organelles that harbors the pathogen and promotes slow release of the encapsulated drugs. Similar subcellular trafficking pathways for nanoparticles and HIV would enhance the antiretroviral response of the drugs [32, 52]. In this study, subcellular localization of MABC nanoformulations was investigated in MDM. Our results showed greater co-localization of the MABC nanoformulations in recycling endosomal compartments (Rab11 and Rab14) compared to late endosomes (Rab7) or lysosomes (LAMP1) (Figure 5). For each compartment, the uptake of folate-targeted nanoformulation was significantly higher compared to non-targeted nanoformulation. These results reflect the higher overall uptake and greater antiviral efficacy of FA-NMABC compared to NMABC. However, some nanoparticles were localized in the degrading lysosomal compartments. Therefore, future studies will focus on minimizing the amount of nanoparticles trafficked into the lysosomal compartments to further improve the antiretroviral outcomes.

To determine whether FA-NMABC compared to NMABC or free drug could provide sustained blood drug levels, mice were treated with 50 mg/kg of ABC as free drug or MABC nanoformulations. Blood drug levels of ABC were detectable over 14 days following treatment with nanoformulated MABC. The folate coating increased the blood levels of ABC by approximately 2.5-fold compared to non-coated formulations and up to 18-fold compared to native drug. Interestingly, no MABC was detected in the blood of mice treated with MABC nanoformulations. This suggests that following release from the nanoformulation, MABC was efficiently converted to ABC by blood and tissue esterases. Hence, folate coating of nanoformulated crystalline MABC could be an effective strategy to reduce HIV levels in its sanctuaries by maintaining sustained blood drug levels.

4.5. CONCLUSIONS

We demonstrate that a carboxylic acid ester prodrug of ABC has improved antiretroviral activities over the native hydrophilic compound. The improved lipophilicity facilitated the encasement of the prodrug into poloxamer nanoformulations with high drug loading. Notably, coating the prodrug with a folate-modified polymer directed to the folic acid receptor enhanced nanoformulation uptake, retention, and antiretroviral efficacy of the drug. MABC nanoformulations localized to recycling endosomal compartments in macrophages, as previously observed for nanoformulated atazanavir and ritonavir [32]. Of importance, following a single IM injection, blood concentrations of ABC were maintained over 14 days using decorated nanoformulations.

4.6. SUMMARY

4.6.1. MABC Synthesis

- Modified ABC (MABC) was synthesized by esterification of myristic acid to the 5-hydroxyl- cyclopentene moiety of the drug.
- MABC was recovered with 66% efficiency after purification.
- When compared to ABC, the antiretroviral activity of MABC, was increased 2–fold in MDM.

4.6.2. Synthesis of MABC Encased Nanoformulations

- MABC was readily incorporated into P407 (NMABC) nanoparticles with a size range of 150-200 nm and a monodispersed cylindrical morphology.
- The nanoformulations were stable at 4 °C and 25 °C for at least 8 weeks.

4.6.3. PK Evaluation of MABC Nanoformulations

- Folate-targeting of the nanoformulation facilitated human MDM uptake and retention, and improved antiretroviral efficacy when compared to NMABC and free MABC.
- Macrophage drug depots were localized in recycling endosomes (Rab11 and Rab14).
- Following a single IM injection of NMABC or FA-NMABC in mice, blood concentrations of ABC were maintained over 14 days.
- FA-NMABC enhanced blood drug levels in mice by 1.7-fold compared to non-targeted nanoformulation (NMABC).

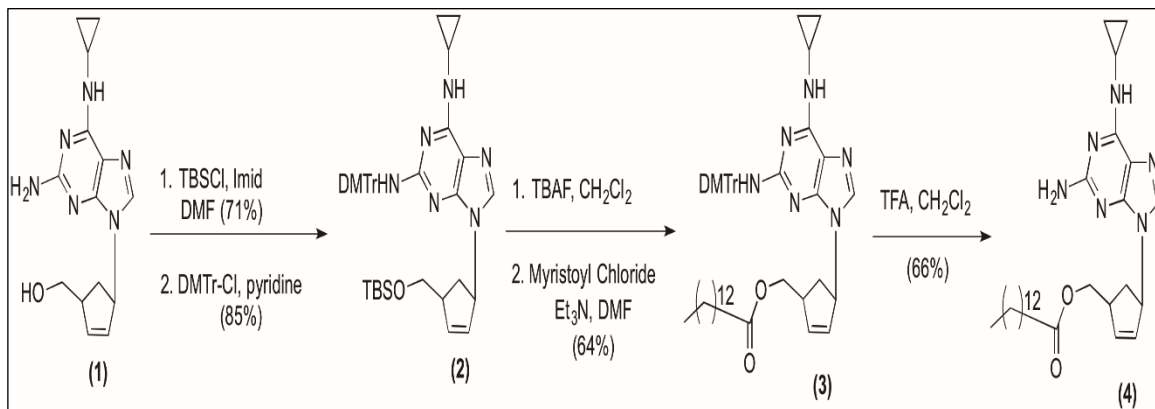


Figure 4.1. Synthesis of MABC. MABC was synthesized as illustrated at a final yield of 66%. The synthesis of MABC was accomplished through derivatization of the native compound with a cleavable fatty acid ester in four steps; (1) The hydroxyl and amino groups of ABC were protected using TBSCl, and DMTr-Cl respectively, (2, 3) the TBSCl group was selectively removed, followed by selective coupling of myristoyl chloride at 5-OH position of ABC, finally, (4) the DMTr-Cl protecting group was removed using TFA to yield final product. MABC was purified using silica chromatography.

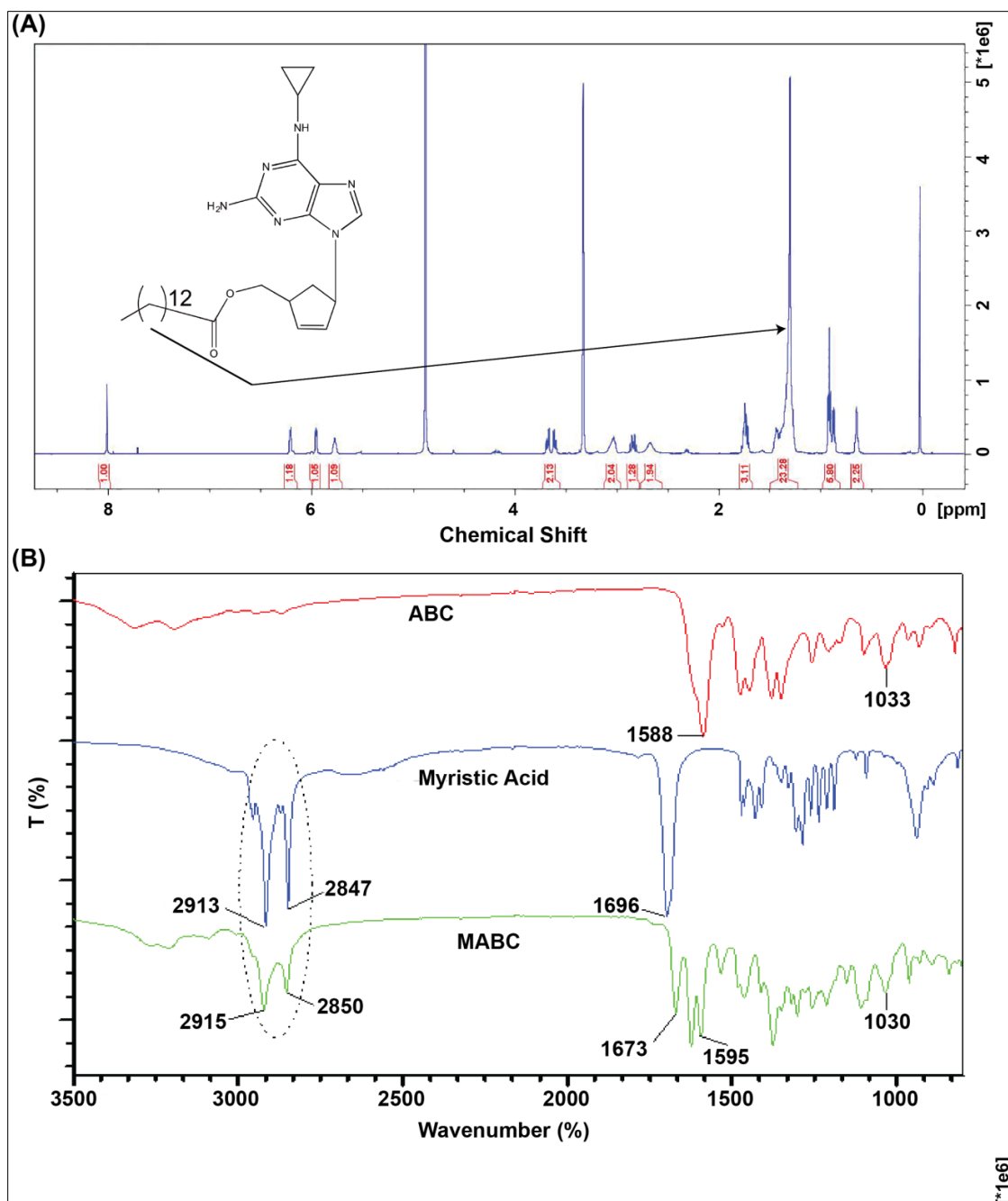


Figure 4.2. Characterization of MABC. Covalent linkage of myristic acid to the 5'-O-hydroxyl group of ABC was confirmed by nuclear magnetic resonance, Fourier transform infrared spectroscopy and tandem mass spectrometry (¹H-NMR, FTIR and MS/MS); (A) The ¹H-NMR spectrum of MABC showed the presence of an intense broad peak at 1.21-1.50 ppm. This peak corresponds to the aliphatic protons on the fatty acid moiety. (B) Peaks at 2915 cm⁻¹ and 2850 cm⁻¹ in MABC FTIR spectrum correspond to alkane (CH₂-CH₂) stretching of the myristic acid alkane.

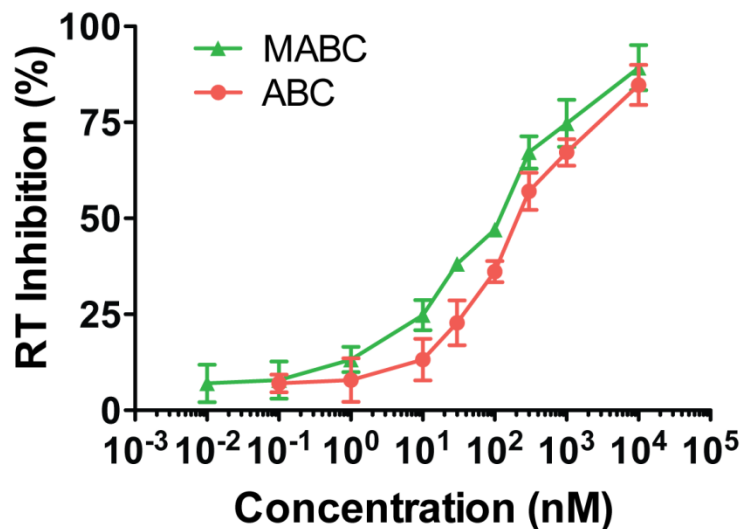


Figure 4.3. Antiviral activity of ABC and MABC in HIV-1ADA infected MDM. MDM were treated with various concentrations of ABC or MABC for 60 min and then challenged with HIV-1_{ADA} at a multiplicity of infection of 0.01 infectious viral particles/cell for 4 h. The cells were incubated for a further 10 days with MCSF-free media containing the same drug concentration. HIV RT activity was measured in the infectious supernatant on day 10 post-infection.

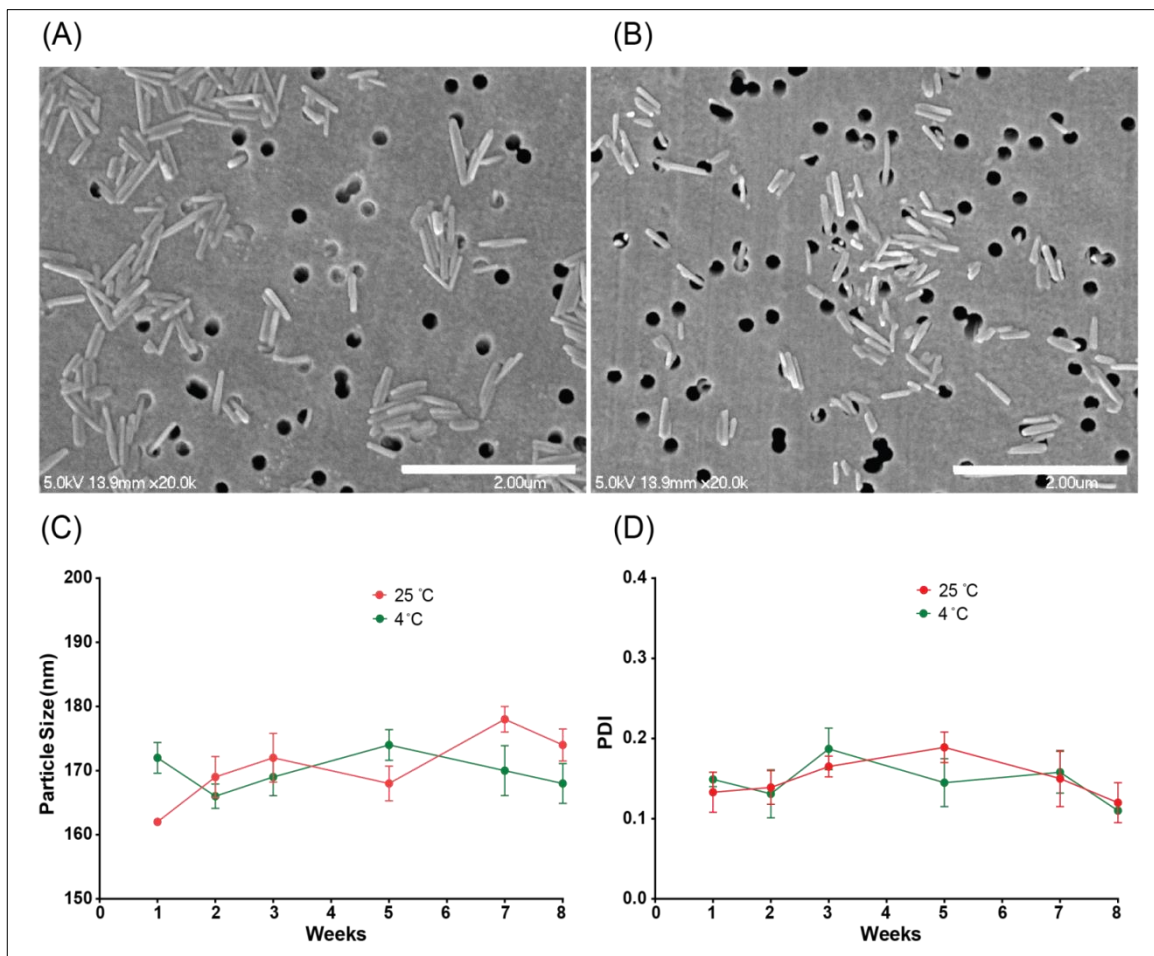


Figure 4.4. Morphology and stability of NMABC. SEM images of (A) NMABC and (B) FA-NMABC nanoformulations. Both formulations appeared as cylindrical monodispersed particles of ~200 nm. Stability of the NMABC nanoformulation was assessed by measuring (C) particle size and (D) PDI at 4 °C and 25 °C for 8 weeks.

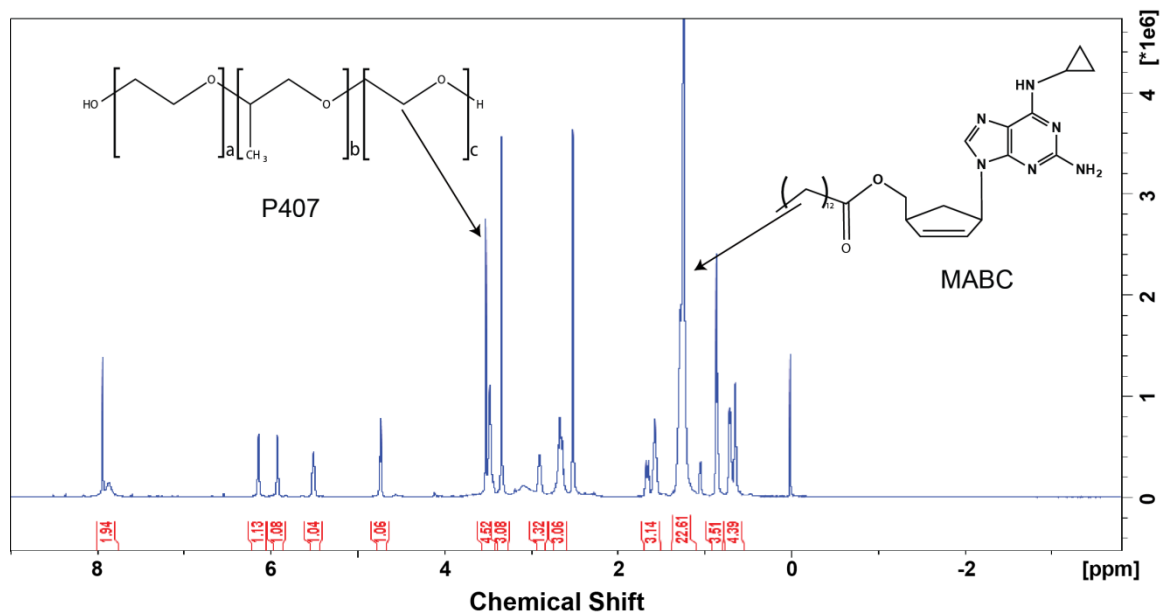


Figure 4.5. Characterization of nanoformulated MABC using $^1\text{H-NMR}$ spectroscopy. The $^1\text{H-NMR}$ spectrum of NMABC showed the presence of a singlet at 3.7 ppm that corresponds to the methylene-repeating unit of the polymer. Peaks corresponding to the myristoylated prodrug protons are also displayed on the formulation spectrum.

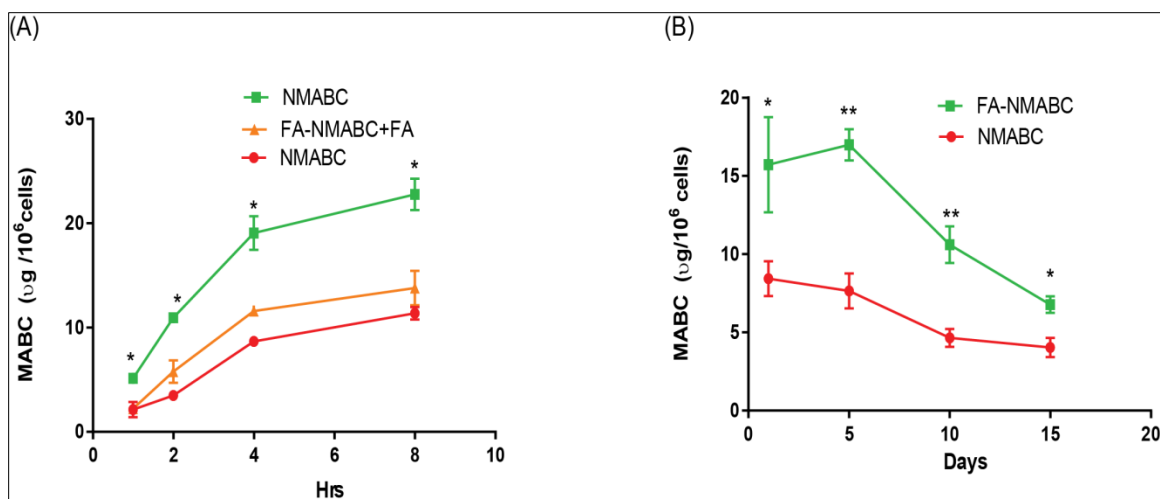


Figure 4.6. MDM uptake and retention of NMABC and FA-NMABC. (A) MDM uptake of 100 μM NMABC or FA-NMABC was determined over 8 h. For uptake studies, 50 μM free folic acid (FA) was added to MDM prior to treatment with FA-NMABC to block FOLR binding. (B) MDM retention of NMABC or FA-NMABC was determined over 15 days. For uptake studies, statistical differences were determined using one-way ANOVA among three groups; for retention studies statistical differences were determined using Student's t-test (** $P < 0.001$ and * $P < 0.05$).

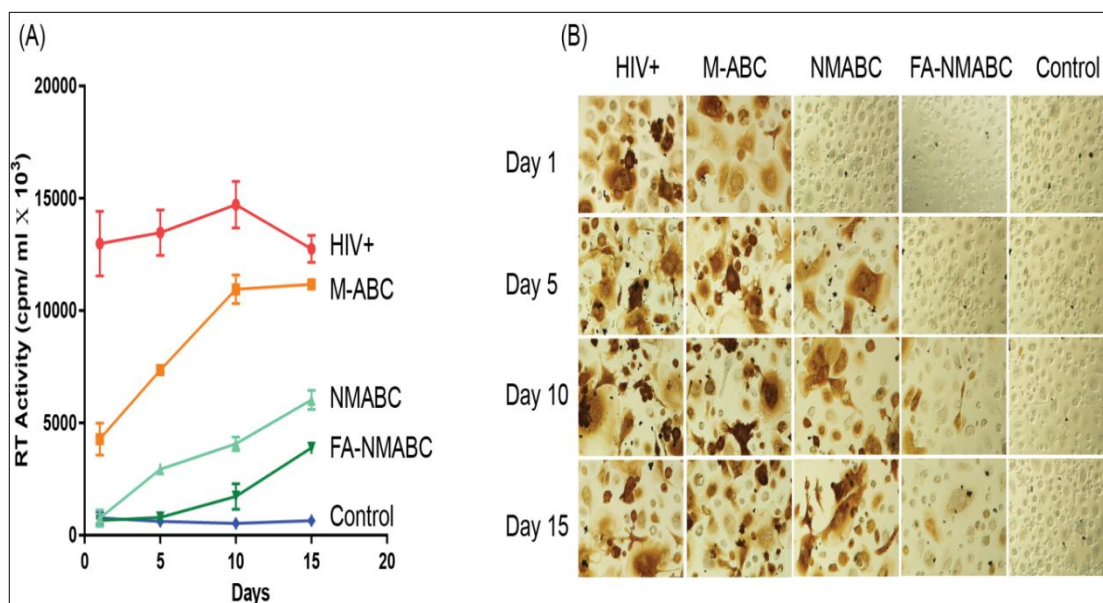


Figure 4.7. Antiretroviral activity of NMABC and FA-NMABC measured in MDM. Antiretroviral activity was determined in MDM treated for 8 h with 100 μ M free MABC or nanoformulated MABC and then infected with HIV-1_{ADA} at 1, 5, 10 or 15 days following drug loading. HIV replication was determined 10 days after infection by (A) HIV RT activity and (B) HIV p24 staining.

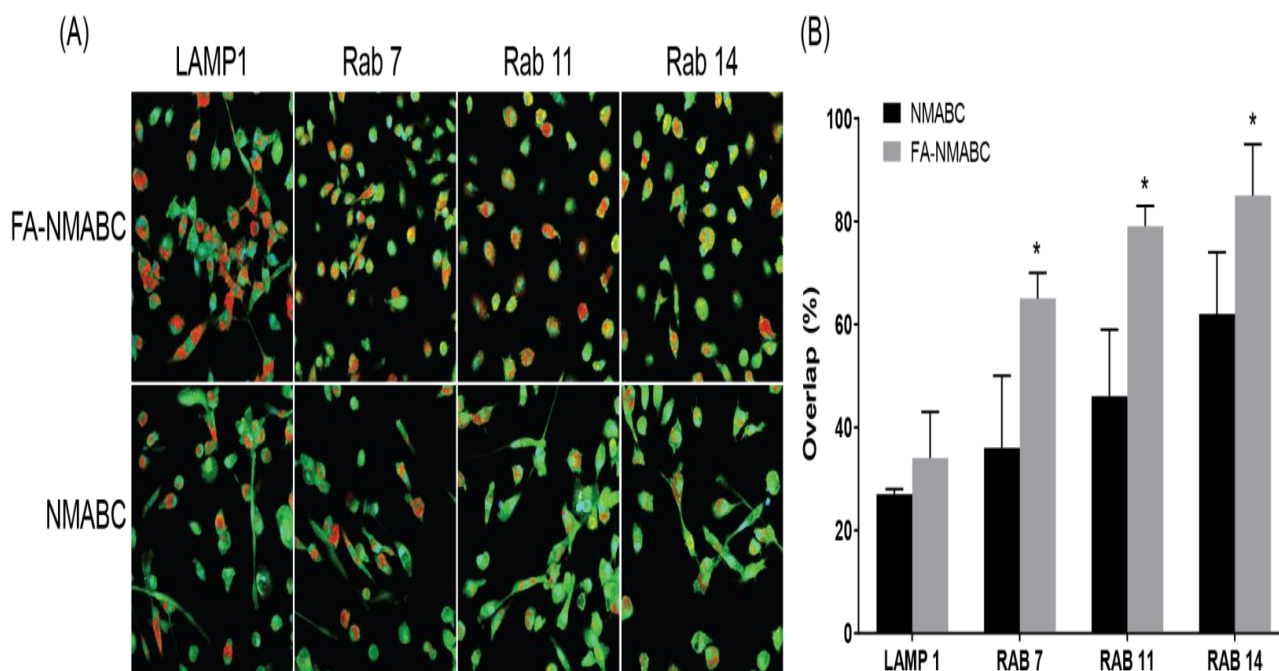


Figure 4.8. Subcellular localization of nanoformulated MABC in MDM. MDM cultured in 8 well Lab-Tek II CC² chamber slides were treated with 100 μ M CF633-labeled FA-NMABC or CF633-labeled NMABC for 8 h then fixed and stained with antibodies to Rab7, -11, -14, and LAMP1 as described [20]. (A) Co-localization is observed as a yellow punctate pattern throughout the cytoplasm and perinuclear cell regions in merged images of red nanoparticles and green subcellular compartments. (B) Percent fluorescence overlap was quantitated using ImageJ software, and JACoP plug-in. Statistical differences were determined using Student's t-test (* $P < 0.05$).

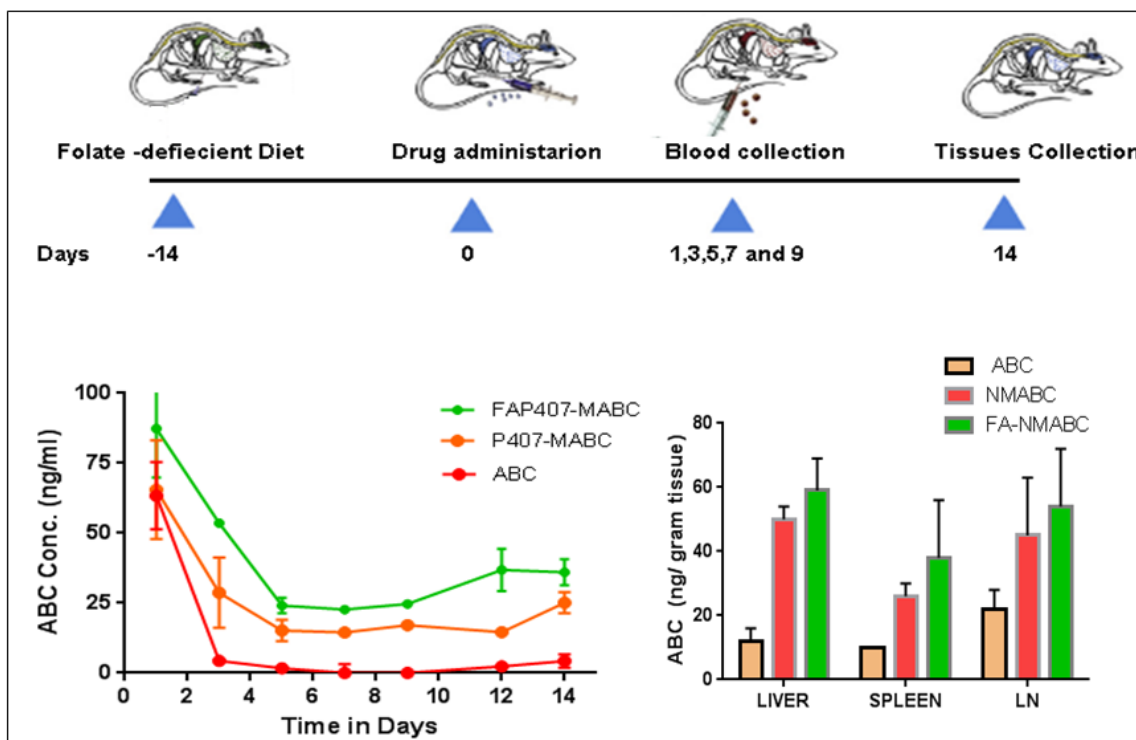


Figure 4.9. Plasma and tissue drug levels of nanoformulated MABC in mice. Balb/c mice were administered intramuscularly 50 mg /kg equivalents of ABC using free ABC, NMABC or FA-NMABC on day 0 and sacrificed on day 14. Whole blood was collected into acetonitrile for drug analysis on days 1, 3, 5, 7, 9, 12, and 14 after treatment. ABC levels were determined by UPLC-MS/MS. Data are expressed as mean \pm standard error of mean. *** ($P < 0.0001$), *($P < 0.05$) statistically different from ABC as determined by 2-way ANOVA and Bonferroni's Multiple Comparison tests

4.7. REFERENCES

1. Pirrone V, Thakkar N, Jacobson JM, Wigdahl B, Krebs FC: Combinatorial approaches to the prevention and treatment of HIV-1 infection. *Antimicrob Agents Chemother* 55(5), 1831-1842 (2011).
2. Chesney M: Adherence to HAART regimens. *AIDS Patient Care STDS* 17(4), 169-177 (2003).
3. Looney D, Ma A, Johns S: HIV therapy-the state of art. *Curr Top Microbiol Immunol* 389, 1-29 (2015).
4. Chun TW, Moir S, Fauci AS: HIV reservoirs as obstacles and opportunities for an HIV cure. *Nat Immunol* 16(6), 584-589 (2015).
5. Lorenzo-Redondo R, Fryer HR, Bedford T *et al.*: Persistent HIV-1 replication maintains the tissue reservoir during therapy. *Nature* 530(7588), 51-56 (2016).
6. Massanella M, Fromentin R, Chomont N: Residual inflammation and viral reservoirs: alliance against an HIV cure. *Curr Opin HIV AIDS* 11(2), 234-241 (2016).
7. Fois AF, Brew BJ: The Potential of the CNS as a Reservoir for HIV-1 Infection: Implications for HIV Eradication. *Current HIV/AIDS Reports* 12(2), 299-303 (2015).
8. Giacalone G, Hillaireau H, Fattal E: Improving bioavailability and biodistribution of anti-HIV chemotherapy. *Eur J Pharm Sci* 75, 40-53 (2015).

9. Li JZ, Paredes R, Ribaudó HJ *et al.*: Low-frequency HIV-1 drug resistance mutations and risk of NNRTI-based antiretroviral treatment failure: a systematic review and pooled analysis. *Jama* 305(13), 1327-1335 (2011).
10. Swenson LC, Min JE, Woods CK *et al.*: HIV drug resistance detected during low-level viraemia is associated with subsequent virologic failure. *Aids* 28(8), 1125-1134 (2014).
11. Vyas TK, Shah L, Amiji MM: Nanoparticulate drug carriers for delivery of HIV/AIDS therapy to viral reservoir sites. *Expert Opin Drug Deliv* 3(5), 613-628 (2006).
12. Kumar P, Lakshmi YS, C B, Golla K, Kondapi AK: Improved Safety, Bioavailability and Pharmacokinetics of Zidovudine through Lactoferrin Nanoparticles during Oral Administration in Rats. *PLoS One* 10(10), e0140399 (2015).
13. Shegokar R, Singh KK: Surface modified nevirapine nanosuspensions for viral reservoir targeting: In vitro and in vivo evaluation. *Int J Pharm* 421(2), 341-352 (2011).
14. Zhang T, Zhang C, Agrahari V, Murowchick JB, Oyler NA, Youan BB: Spray drying tenofovir loaded mucoadhesive and pH-sensitive microspheres intended for HIV prevention. *Antiviral Res* 97(3), 334-346 (2013).
15. Spreen WR, Margolis DA, Pottage JC, Jr.: Long-acting injectable antiretrovirals for HIV treatment and prevention. *Curr Opin HIV AIDS* 8(6), 565-571 (2013).

16. Nowacek AS, Miller RL, Mcmillan J *et al.*: NanoART synthesis, characterization, uptake, release and toxicology for human monocyte-macrophage drug delivery. *Nanomedicine (Lond)* 4(8), 903-917 (2009).
17. Dash PK, Gendelman HE, Roy U *et al.*: Long-acting nanoformulated antiretroviral therapy elicits potent antiretroviral and neuroprotective responses in HIV-1-infected humanized mice. *Aids* 26(17), 2135-2144 (2012).
18. Gautam N, Puligujja P, Balkundi S *et al.*: Pharmacokinetics, biodistribution, and toxicity of folic acid-coated antiretroviral nanoformulations. *Antimicrob Agents Chemother* 58(12), 7510-7519 (2014).
19. Puligujja P, Balkundi SS, Kendrick LM *et al.*: Pharmacodynamics of long-acting folic acid-receptor targeted ritonavir-boosted atazanavir nanoformulations. *Biomaterials* 41, 141-150 (2015).
20. Puligujja P, Mcmillan J, Kendrick L *et al.*: Macrophage folate receptor-targeted antiretroviral therapy facilitates drug entry, retention, antiretroviral activities and biodistribution for reduction of human immunodeficiency virus infections. *Nanomedicine* 9(8), 1263-1273 (2013).
21. Mahajan SD, Aalinkeel R, Law WC *et al.*: Anti-HIV-1 nanotherapeutics: promises and challenges for the future. *Int J Nanomedicine* 7, 5301-5314 (2012).
22. Nowacek AS, Balkundi S, Mcmillan J *et al.*: Analyses of nanoformulated antiretroviral drug charge, size, shape and content for uptake, drug release and antiviral activities in human monocyte-derived macrophages. *J Control Release* 150(2), 204-211 (2011).

23. Agarwal HK, Chhikara BS, Hanley MJ, Ye G, Doncel GF, Parang K: Synthesis and biological evaluation of fatty acyl ester derivatives of (-)-2',3'-dideoxy-3'-thiacytidine. *Journal of medicinal chemistry* 55(10), 4861-4871 (2012).
24. Farazi TA, Waksman G, Gordon JI: The biology and enzymology of protein N-myristoylation. *The Journal of biological chemistry* 276(43), 39501-39504 (2001).
25. Wu Z, Alexandratos J, Ericksen B, Lubkowski J, Gallo RC, Lu W: Total chemical synthesis of N-myristoylated HIV-1 matrix protein p17: structural and mechanistic implications of p17 myristoylation. *Proceedings of the National Academy of Sciences of the United States of America* 101(32), 11587-11592 (2004).
26. Ohta H, Takamune N, Kishimoto N, Shoji S, Misumi S: N-Myristoyltransferase 1 enhances human immunodeficiency virus replication through regulation of viral RNA expression level. *Biochem Biophys Res Commun* 463(4), 988-993 (2015).
27. Takamune N, Hamada H, Misumi S, Shoji S: Novel strategy for anti-HIV-1 action: selective cytotoxic effect of N-myristoyltransferase inhibitor on HIV-1-infected cells. *FEBS letters* 527(1-3), 138-142 (2002).
28. Meltzer MS, Gendelman HE: Effects of colony stimulating factors on the interaction of monocytes and the human immunodeficiency virus. *Immunol Lett* 19(3), 193-198 (1988).

29. Dou H, Destache CJ, Morehead JR *et al.*: Development of a macrophage-based nanoparticle platform for antiretroviral drug delivery. *Blood* 108(8), 2827-2835 (2006).
30. Balzarini J, Aquaro S, Hassan-Abdallah A, Daluge SM, Perno CF, Mcguigan C: Improved antiviral activity of the aryloxymethoxyalaninyl phosphoramidate (APA) prodrug of abacavir (ABC) is due to the formation of markedly increased carbovir 5'-triphosphate metabolite levels. *FEBS Lett* 573(1-3), 38-44 (2004).
31. Kalter SS, Heberling RL, Barry JD, Kuramoto IK, Holland PV, Sazama K: Detection of antibody to immunodeficiency viruses by dot immunobinding assay. *J Clin Microbiol* 30(4), 993-995 (1992).
32. Guo D, Zhang G, Wysocki TA *et al.*: Endosomal trafficking of nanoformulated antiretroviral therapy facilitates drug particle carriage and HIV clearance. *J Virol* 88(17), 9504-9513 (2014).
33. Balkundi S, Nowacek AS, Veerubhotla RS *et al.*: Comparative manufacture and cell-based delivery of antiretroviral nanoformulations. *Int J Nanomedicine* 6, 3393-3404 (2011).
34. Mcguigan C, Harris SA, Daluge SM *et al.*: Application of phosphoramidate pronucleotide technology to abacavir leads to a significant enhancement of antiviral potency. *J Med Chem* 48(10), 3504-3515 (2005).

35. Leamon CP, Reddy JA, Dorton R *et al.*: Impact of high and low folate diets on tissue folate receptor levels and antitumor responses toward folate-drug conjugates. *J Pharmacol Exp Ther* 327(3), 918-925 (2008).
36. Adetokunboh OO, Schoonees A, Balogun TA, Wiysonge CS: Efficacy and safety of abacavir-containing combination antiretroviral therapy as first-line treatment of HIV infected children and adolescents: a systematic review and meta-analysis. *BMC Infect Dis* 15, 469 (2015).
37. Ibbotson T, Perry CM: Lamivudine/zidovudine/abacavir: triple combination tablet. *Drugs* 63(11), 1089-1098; discussion 1099-1100 (2003).
38. Wang LH, Chittick GE, Mcdowell JA: Single-dose pharmacokinetics and safety of abacavir (1592U89), zidovudine, and lamivudine administered alone and in combination in adults with human immunodeficiency virus infection. *Antimicrob Agents Chemother* 43(7), 1708-1715 (1999).
39. Hughes CA, Foisy MM, Dewhurst N *et al.*: Abacavir hypersensitivity reaction: an update. *Ann Pharmacother* 42(3), 387-396 (2008).
40. Van Damme L, Corneli A, Ahmed K *et al.*: Preexposure prophylaxis for HIV infection among African women. *N Engl J Med* 367(5), 411-422 (2012).
41. Grant RM, Lama JR, Anderson PL *et al.*: Preexposure chemoprophylaxis for HIV prevention in men who have sex with men. *N Engl J Med* 363(27), 2587-2599 (2010).

42. Pialoux G, Marcelin A, Cawston H *et al.*: Cost-Effectiveness of Dolutegravir/Abacavir/Lamivudine in Hiv-1 Treatment Naive Patients in France. *Value Health* 18(7), A587 (2015).
43. Meng J, Zhang T, Agrahari V, Ezoulin MJ, Youan BB: Comparative biophysical properties of tenofovir-loaded, thiolated and nonthiolated chitosan nanoparticles intended for HIV prevention. *Nanomedicine (Lond)* 9(11), 1595-1612 (2014).
44. Wilson B, Paladugu L, Priyadarshini SR, Jenita JJ: Development of albumin-based nanoparticles for the delivery of abacavir. *Int J Biol Macromol* 81, 763-767 (2015).
45. Zhang Y, Gao Y, Wen X, Ma H: Current prodrug strategies for improving oral absorption of nucleoside analogues. *Asian Journal of Pharmaceutical Sciences* 9(2), 65-74 (2014).
46. Bergman AM, Adema AD, Balzarini J *et al.*: Antiproliferative activity, mechanism of action and oral antitumor activity of CP-4126, a fatty acid derivative of gemcitabine, in in vitro and in vivo tumor models. *Invest New Drugs* 29(3), 456-466 (2011).
47. Bergman AM, Kuiper CM, Voorn DA *et al.*: Antiproliferative activity and mechanism of action of fatty acid derivatives of arabinofuranosylcytosine in leukemia and solid tumor cell lines. *Biochem Pharmacol* 67(3), 503-511 (2004).
48. Steingrimsdottir H, Gruber A, Palm C, Grimfors G, Kalin M, Eksborg S: Bioavailability of aciclovir after oral administration of aciclovir and its prodrug

valaciclovir to patients with leukopenia after chemotherapy. *Antimicrob Agents Chemother* 44(1), 207-209 (2000).

49. Xia W, Hilgenbrink AR, Matteson EL, Lockwood MB, Cheng JX, Low PS: A functional folate receptor is induced during macrophage activation and can be used to target drugs to activated macrophages. *Blood* 113(2), 438-446 (2009).

50. Kumar S, Anselmo AC, Banerjee A, Zakrewsky M, Mitragotri S: Shape and size-dependent immune response to antigen-carrying nanoparticles. *J Control Release* 220(Pt A), 141-148 (2015).

51. Doshi N, Mitragotri S: Macrophages recognize size and shape of their targets. *PLoS One* 5(4), e10051 (2010).

52. Arainga M, Guo D, Wiederin J, Ciborowski P, Mcmillan J, Gendelman HE: Opposing regulation of endolysosomal pathways by long-acting nanoformulated antiretroviral therapy and HIV-1 in human macrophages. *Retrovirology* 12, 5 (2015).

Chapter 5

Challenges and Future direction

Even though the prodrugs synthesis, followed by its encapsulation into long acting PLGA and pluronic nanoformulations showed considerable improvement over poor efficacy and PK/PD profile of native drug, pitfall exists. Firstly, the manufacturing scheme was not optimized to clinical translation; moreover it was design for proof of concept studies. There is further need to generate more robust manufacturing process that generates particles with homogeneous physicochemical parameters. For instance, in current methods, purification of nanoformulation using centrifugation led to particles aggregation that poses a major challenge in resuspending the particles with initial size and size distribution. Secondly, robust lyophilization methods need to develop, if we chose to develop powder formulation for longer stability.

Therefore, future work should employ other alternative purification techniques such as tangential flow filtration (TFF) to circumvent the aggregation problem associated with conventional centrifugation. TFF is an efficient method of purification using membrane filtration to isolate nanoparticle and free polymers, and/or unencapsulated drugs.

The scope of this research limited to develop two separate prodrugs; phosphorylated pro-drug to bypass inefficient monophosphorylation conversion, and myristoylated prodrugs to improve hydrophobicity that encourages its encapsulation in to long acting nanoformulations. The probabilities of developing phosphorylated prodrugs with fatty acid end chain that ~~pese~~ improve phosphorylation and hydrophobicity concomitantly should be tested in future.

We can improve the PK of our nanoformulated MABC using a range of particle surface ligands or through the use of mixed lineage kinase inhibitors that can affect autophagy and prolong the nanoparticle storage capacities. If successful, this would improve antiretroviral activities and facilitate MABC's use as a component in a long-acting ART regimen. Such strategies are now being tested in relevant mouse models of HIV/AIDS. Parallel development of a nanoformulated hydrophobic prodrug of 3TC would provide a combination drug regimen with MABC and a long-acting formulation of the integrase inhibitor dolutegravir. Future development of a combination long acting prodrug-based delivery system would be a considerable benefit in the management of HIV infection.